Travail de Fin d'Etudes : Mass transfer (CO2) coefficients determination in airlift - HRAP

Auteur : Philippart de Foy, Marc
Promoteur(s) : Eppe, Gauthier; Toye, Dominique
Faculté : Faculté des Sciences appliquées
Diplôme : Master en ingénieur civil en chimie et science des matériaux, à finalité spécialisée
Année académique : 2019-2020
URI/URL : http://hdl.handle.net/2268.2/10780

UNIVERSITY OF LIEGE

FACULTY OF APPLIED SCIENCE

Mass transfer coefficients of CO_2 determination in airlift - HRAP

Marc Philippart de Foy

Graduation Studies conducted for obtaining the Master's degree in
Chemical and Materials Engineering

Supervisors: **Gauthier EPPE**
Dominique TOYE

Academic year *2019 - 2020*

Abstract

With regard to today's environmental challenges, there is a need to develop integrated technologies that provide concrete solutions. High rate algal ponds (HRAPs) are a good example: these ponds allow wastewater to be treated by cultivating algae or microalgae that can be harvested at the end and consume nutrients such as nitrogen, phosphorus and CO_2 for their growth.

In HRAPs, the algae consume nutrients contained in the wastewater and the produced biomass could be used in different sectors such as for biofuels production or in the food industry. Moreover, large-scale algae cultures require important carbon dioxide supply for the growth of the biomass so a sustainable use of the CO_2 captured in industrial waste gases can be considered.

Many HRAPs are currently in use, but some operating conditions are not fully optimised. For instance only a few studies have been carried out on the transfer of CO_2 between the water and the atmosphere in this type of basin. The present work proposes a methodology to quantify this transfer in order to optimise the CO_2 injection into the basin. The overall volumetric transfer coefficients $k_l a$ of different HRAPs are measured experimentally on small and large scales in Arlon, Belgium, and the results are compared with those of oxygen transfer in the same HRAPs to verify a correlation found in the literature.

This master thesis is part of the *Renewable* project (*REmoval of NutriEnts in Wastewater treatment via microAlgae and BiofueL/Biomass production for Environmental sustainability in Vietnam*). This project is funded by ARES (*Académie de Recherche et d'Enseignement Supérieur*) and is a collaboration between the University of Liège (ULiège) and the Industrial University of Ho Chi Minh (IUH) scheduled between May 2016 and December 2021. The *Renewable* project aims to develop a wastewater treatment system that uses microalgae in a HRAP in the Ninh Thuan province, in Vietnam.

The present work is a continuation of the master thesis of D. Royaux [1] and a scientific paper describing the methodology and the results of the tests will be submitted for publication.

Résumé

Au vu des challenges environnementaux rencontrés actuellement, il est nécessaire de développer des technologies intégrées qui apportent des solutions concrètes. Les chenaux algaux à haut rendement (CAHRs) sont un bon exemple: ils permettent de traiter des eaux usées tout en cultivant des algues ou des microalgues qui peuvent ensuite être récupérées et valorisées et qui consomment des nutriments tels que de l'azote, du phosphore et du CO_2 pour leur croissance.

Dans les CAHRs, les algues consomment des nutriments contenus dans les eaux usées et la biomasse produite peut être utilisée dans différents secteurs tels que la production de biocarburants ou l'industrie alimentaire. De plus, la culture d'algues à grande échelle demande un approvisionnement important en dioxyde de carbone pour la croissance de la biomasse, ce qui offre une possibilité d'utilisation durable du CO_2 récupéré dans les gaz de combustion industriels.

Un grand nombre de CAHRs sont déjà utilisés, mais certaines conditions opératoires ne sont pas entièrement optimisées. Par exemple, seules quelques études ont été menées sur le transfert de CO_2 entre l'eau et l'atmosphère dans ce type de bassin. Ce rapport propose une méthodologie pour quantifier ce transfert afin d'optimiser l'injection de CO_2 dans le bassin. Les coefficients volumétriques de transfert de masse globaux $k_l a$ de différents CAHR sont mesurés expérimentalement à petite et grande échelles à Arlon, en Belgique, et les résultats obtenus sont comparés à ceux du transfert d'oxygène dans les mêmes CAHRs afin de vérifier une corrélation provenant de la littérature.

Ce travail de fin d'étude fait partie du projet *Renewable* (*REmoval of NutriEnts in Wastewater treatment via microAlgae and BiofueL/Biomass production for Environmental sustainability in Vietnam*). Ce projet est financé par l'ARES (*Académie de Recherche et d'Enseignement Supérieur*) et résulte d'une collaboration entre l'Université de Liège (ULiège) et l'Université industrielle d'Ho Chi Minh (IUH) prévue de mai 2016 à décembre 2021. Le projet *Renewable* a pour but de développer un système de traitement des eaux usées qui utilise des microalgues dans un CAHR dans la province de Ninh Thuan, au Vietnam.

Ce travail est une continuation du travail de fin d'étude de D. Royaux [1] et un article scientifique décrivant la méthodologie et les résultats des tests doit être soumis pour une publication.

Acknowledgements

The completion of this master thesis would not have been possible without the help of many people.

First I would like to thank Pr. Jean-Luc Vasel who taught me so many things, who helped during all the test sessions and who was always there to answer to my many questions.

I also want to thank Pr. Eppe who gave me the opportunity to work on such an interesting project and who managed to found new plans B every time that plans A became impossible.

I also thank Pr. Dominique Toye and Pr. Grégoire Léonard for having accepted to be respectively my co-supervisor and in the jury of this master thesis.

Thanks to all the people in Vietnam that were ready to welcome me too, especially Pr. Anh for his advice regarding the organisation of the trip, Mrs. Thuy for all the help she was ready to give and Mrs. Phuong Khanh and Mr. Marc Pottier who were planning to take me everywhere in the country.

I also want to thank all the people who helped me during the test sessions, even if only by pouring a bucket of salty water into the pond. Special thanks to Mr. Sven Hanneteau for his help during the small-scale test sessions and his advice about the writing of my master thesis, and to Mr. Hugues Juspin for all he has done during the large-scale tests, and even before them to prepare the pond.

Thanks to Mr. Stéphane Lutz for having given me access to the laboratory and for the time he spent preparing the solutions, and even calibrating them in September when I had no more time left.

I would also like to thank Mr. Thierry Salmon who lent us the frequency alternator, which saved the large-scale test session from a disaster.

Then I want to thank all my friends and family, who have always been there for me during my five years of study, or even longer.

More specifically, thanks to Louis and François who have been my left foot in September, Rémi for his perfect titrations of January, Florian for having been there in my search of the new alternator, Sébastien and Adrien for the road trips and all the heavy stuff I made them carry and pour into the water, and Florence for the correction of so many tables.

I think that I cannot fail to mention Vincent and Quentin too, with whom I have spent most of my time during these studies, and Justin, Jean-Luc and Alexis for these great two years of master. And I need to thank Alexis again, without whom I would literally never have reached the second year of master and would still be hitchhiking on the side of the road. Thanks for these too many trips!

I want to deeply thank my grandparents too, for having taken such good care of me in the very beginning of my master thesis, and my physiotherapist Davy Gillet for having helped me to regain my abilities before my trip.

And finally, I would like to thank my parents, who helped me during all these years and who taught me so much things, even if not related to my studies...

Contents

Abstract **1**

Résumé **2**

Acknowledgements **3**

1 Introduction **10**
1.1 Objectives of the master thesis . . . 11

2 State of the art **12**
2.1 Algae cultivation . . . 12
2.1.1 Principles of algae cultivation . . . 12
2.1.2 Types of reactors . . . 13
2.2 High rate algal ponds . . . 15
2.3 Quantification of O_2 and CO_2 transfers in HRAPs . . . 17
2.4 Uses of algae . . . 18
2.4.1 Biofuels . . . 18
2.4.2 Food and feed . . . 20
2.4.3 Fertilisers . . . 21
2.4.4 Other uses . . . 22
2.5 Coupling algae production with wastewater treatment and CO_2 consumption . . . 22
2.5.1 Wastewater treatment . . . 22
2.5.2 CO_2 consumption . . . 23

3 Experimental design and tests presentation **25**
3.1 Tracer test . . . 26
3.2 O_2 transfer test . . . 27
3.2.1 Methodology of the test . . . 27
3.2.2 Calculation of the transfer coefficients . . . 29
3.3 CO_2 transfer test . . . 33
3.3.1 Different forms of CO_3 coordinates in water . . . 33
3.3.2 Methodology of the test . . . 34
3.3.3 Analysis of the samples . . . 36
3.3.4 Calculation of the concentration in CO_2 . . . 37
3.3.5 Calculation of the transfer coefficient . . . 43

4 Tests conducted on a small scale **45**
4.1 HRAP characteristics . . . 45
4.2 Tracer tests . . . 47
4.2.1 Test of September 2019 . . . 47
4.2.2 Test of January 2020 . . . 48
4.3 O_2 transfer tests . . . 48
4.3.1 Test of September 2019 . . . 48
4.3.2 Test of January 2020 . . . 50
4.4 CO_2 transfer tests . . . 51
4.4.1 Tests of September 2019 . . . 51
4.4.2 Tests of January 2020 . . . 52
4.5 Summary of the small-scale tests . . . 56

5 Tests conducted on a large scale **58**
5.1 Airlift with external circulation reactor characteristics . . . 58
5.2 Tracer test . . . 59
5.3 O_2 transfer test . . . 61
5.4 CO_2 transfer tests . . . 62
5.4.1 Large-scale CO_2 transfer test **A** . . . 63
5.4.2 Large-scale CO_2 transfer test **B** . . . 64
5.4.3 Comment about the titrations . . . 67

6 Results analysis **68**

7 Conclusion and perspectives **73**

References **75**

8 Appendices **81**
8.1 Glossary . . . 81
8.2 Dimensions of the HRAPs . . . 83
8.2.1 Small-scale ponds . . . 83
8.2.2 Large-scale pond . . . 85
8.3 Oxygen transfer tests . . . 86
8.3.1 September 2019 . . . 86
8.3.2 January 2020 . . . 86
8.3.3 June 2020 . . . 87
8.4 Small-scale CO_2 transfer tests . . . 88
8.4.1 September 2019 - test **A** . . . 88
8.4.2 September 2019 - test **B** . . . 91
8.4.3 January 2020 - test **B** . . . 95
8.5 Large-scale CO_2 transfer tests . . . 97
8.5.1 June 2020 - test **A** . . . 97
8.5.2 June 2020 - test **B** . . . 101
8.6 Summary of test conditions and results . . . 107

List of Figures

1 Logarithmic evolution of the number of algae cells during their cultivation [20]. . 13
2 Aerial view of the *Qualitas Health algae production facility* in New Mexico, US (Courtesy photo) [24]. 14
3 Example of a tubular reactor [28]. 15
4 Paddlewheels used in a raceway pond in St Helena and Hilmar California, US [31]. 15
5 Drawing of the airlift system used in the HRAP in the Ninh Thuan province, Vietnam [1]. 16
6 Examples of forms of algae used in industry [58]. 20
7 Examples of HRAP wastewater treatment plants. 23
8 Small-scale HRAP ("basin 1") used to perform the tests of September 2019, with the direction of the water flow in blue and the positions of the probes in red. . . 25
9 Evolution of the conductivity at 25°C at the outlet of the airlift during the small-scale tracer test of January 2020: $t_c = 393$ s. 27
10 Evolution of the DO concentration at the inlet (red) and outlet (blue) of the airlift during the small-scale oxygen transfer test of January 2020. 28
11 Curve of $\ln\left(D\left(t\right)/D_0\right)$ at the inlet of the airlift and linear regression in the relevant interval for the small-scale O_2 transfer test of January 2020: $\left(k_l a\right)_{\mathrm{R}} = 1.6 \times 10^{-3}$ s^{-1} ($\pm$ 1.5×10^{-5} s^{-1}) / conditions: water temperature = 16.2°C - $V_{\mathrm{R}} = 408.9$ L - water height = 7 cm - $t_{\mathrm{c}} = 393$ s - $C_{\mathrm{S}} = 9.97$ mg/L. 30
12 Evolution of the deficit at the outlet of the airlift: recorded by a probe (blue) and modelled on the basis of the data recorded at the inlet of the airlift (green) for the oxygen transfer test of January 2020; the green frame represents the zone in which the value of $\left(k_l a\right)_{\mathrm{A}}$ is adjusted to model the deficit: $\left(k_l a\right)_{\mathrm{A}} = 6.6 \times 10^{-3}$ s^{-1} / conditions: water temperature = 16.2°C - $V_{\mathrm{A}} = 70.9$ L - water height = 7 cm - $t_{\mathrm{A}} = 130$ s. 32
13 Fraction of CO_3 coordinates in water as a function of the pH at a temperature of 20°C and an electrical conductivity of 250 μs cm^{-1}: dissolved CO_2 (referred as $H_2CO_3^*$ in this work), bicarbonate ion (HCO_3^-) and carbonate ion (CO_3^{2-}) [80]. 33
14 Evolution of the pH at the outlet of the airlift and sampling moments during the small-scale CO_2 transfer test **B** of January 2020. 35
15 pH-curve of sample "B6" of 23.44 mL (conductivity of 9 400 μs/cm at 25°C) collected during the small-scale CO_2 transfer test **B** of January 2020, titrated at 25°C with a NaOH solution of 11.26 mmol/L. 36
16 Evolution of $[CO_{3_{\mathrm{tot}}}]$ and $[CO_2]$ at the outlet of the airlift during the small-scale CO_2 transfer test **B** of January 2020 / conditions: water temperature = 16.3°C - $V_{\mathrm{R}} = 408.9$ L - water height = 7 cm - $t_{\mathrm{c}} = 393$ s. 42
17 Curve of $\ln\left(D\left(t\right)/D_0\right)$ at the outlet of the airlift and linear regression for the small-scale CO_2 transfer test **B** of January 2020: $\left(k_l a\right)_{\mathrm{R}} = 1.2 \times 10^{-3}$ s^{-1} ($\pm$ 4.6×10^{-4} s^{-1}) / conditions: water temperature = 16.3°C - $V_{\mathrm{R}} = 408.9$ L - water height = 7 cm - $t_{\mathrm{c}} = 393$ s - $C_{\mathrm{S}} = 0.08$ mmol/L. 43
18 Small-scale HRAP ("basin 2") used to perform the tests of January 2020. 45
19 Airlift system used in basin 1 and direction of the water flow. 46
20 Curved wood sheets and cut plastic bottles used in the small-scale basins to mimic the shape of large-scale HRAPs [1]. 47
21 Evolution of the conductivity at 25°C at the outlet of the airlift during the small-scale tracer test of September 2019: $t_c = 227$ s. 47
22 Evolution of the DO concentration at the inlet (red) and outlet (blue) of the airlift during the small-scale oxygen transfer test of September 2019. 48

23 Curve of $\ln(D(t)/D_0)$ at the inlet of the airlift and linear regression in the relevant interval for the small-scale O_2 transfer test of September 2019: $(k_l a)_R = 1.9 \times 10^{-3}$ s^{-1} ($\pm$ 1.5×10^{-5} s^{-1}) / conditions: water temperature = 23.8°C - V_R = 267.1 L - water height = 9.8 cm - t_c = 227 s - C_S = 8.5 mg/L. 49
24 Evolution of the deficit at the outlet of the airlift: recorded by a probe (blue) and modelled on the basis of the data recorded at the inlet of the airlift (green) for the oxygen transfer test of September 2019; the green frame represents the zone in which the value of $(k_l a)_A$ is adjusted to model the deficit: $(k_l a)_A = 2.36 \times 10^{-2}$ s^{-1} / conditions: water temperature = 23.8°C - V_A = 22 L - water height = 9.8 cm - t_A = 24 s. 50
25 Evolution of the pH at the outlet of the airlift and sampling moments during the small-scale CO_2 transfer test **A** of January 2020. 55
26 Evolution of $[CO_{3_{tot}}]$ and $[CO_2]$ at the outlet of the airlift during the small-scale CO_2 transfer test **A** of January 2020 / conditions: water temperature = 17.1°C - V_R = 408.9 L - water height = 7 cm - t_c = 393 s. 55
27 Curve of $\ln(D(t)/D_0)$ at the outlet of the airlift and linear regression for the small-scale CO_2 transfer test **A** of January 2020: $(k_l a)_R = 1 \times 10^{-3}$ s^{-1} ($\pm$ 1.2×10^{-4} s^{-1}) / conditions: water temperature = 17.1°C - V_R = 408.9 L - water height = 7 cm - t_c = 393 s - C_S = 0.8 mmol/L. 56
28 Large-scale pond used to perform the tests of June 2020. 59
29 Evolution of the conductivity at 25°C at the outlet of the airlift during the large-scale tracer test of June 2020: $t_c \simeq 20$ s. 60
30 Evolution of the conductivity at 25°C at the inlet of the airlift during the large-scale tracer test of June 2020: $t_c \simeq 20$ s. 60
31 Evolution of the DO concentration at the inlet (red) and outlet (blue) of the airlift during the large-scale oxygen transfer test of June 2020. 61
32 Curve of $\ln(D(t)/D_0)$ at the inlet of the airlift and linear regression in the relevant interval for the large-scale O_2 transfer test of June 2020: $(k_l a)_R = 4.2 \times 10^{-4}$ s^{-1} ($\pm$ 2.8×10^{-6} s^{-1}) / conditions: 15.4°C - V_R = 78 400 L - water height = 150 cm - C_S = 10.2 mg/L. 62
33 Evolution of $[CO_{3_{tot}}]$ and $[CO_2]$ at the outlet of the airlift during the large-scale CO_2 transfer test **A** of June 2020 / conditions: water temperature = 16.1°C - V_R = 78 400 L - water height = 150 cm - $t_c \simeq 20$ s. 63
34 Evolution of $[CO_{3_{tot}}]$ and $[CO_2]$ at the outlet of the airlift during the large-scale CO_2 transfer test **B** of June 2020 / conditions: water temperature = 16.5°C - V_R = 78 400 L - water height = 150 cm - $t_c \simeq 20$ s. 64
35 Curves of $\ln(D(t)/D_0)$ at the outlet of the airlift and linear regressions for the large-scale CO_2 transfer test **B** of June 2020 for the three time intervals considered / conditions: water temperature = 16.5°C - V_R = 78 400 L - water height = 150 cm - $t_c \simeq 20$ s - C_S = 1.16 mmol/L. 66
36 pH-curve of sample "B24" of 24.46 mL (conductivity of 14 850 μs/cm at 25°C) collected during the large-scale CO_2 transfer test **B** of June 2020, titrated at 25°C with a NaOH solution of 28.29 mmol/L. 67
37 Actual and theoretical curves of the CO_2 concentration for test **B** of June 2020, for the three CO_2 transfer coefficients obtained with the different time intervals. 68
38 Actual and theoretical curves of the CO_2 concentration for test **B** of June 2020, for the three CO_2 transfer coefficients obtained with the different time intervals and for the optimum of these coefficients. 69
39 Actual and theoretical curves of the CO_2 concentration for test **B** of June 2020, for four CO_2 transfer coefficients obtained with different ratios $(k_l a)_{CO_2} / (k_l a)_{O_2}$ and with the O_2 transfer coefficient of June 2020. 71

40 Dimensions of the small-scale basin 1 used for the test session of September 2019. 83
41 Dimensions of the small-scale basin 2 used for the test session of January 2020. . 84
42 Dimensions of the large-scale basin used for the test session of June 2020. 85
43 Curve of $\ln(D(t)/D_0)$ at the outlet of the airlift and linear regression in the relevant interval for the small-scale O_2 transfer test of September 2019: $(k_l a)_R = 2.3 \times 10^{-3}$ s^{-1} ($\pm$ 1.3×10^{-5} s^{-1}) / conditions: water temperature = 23.8°C - $V_R = 267.1$ L - water height = 9.8 cm - $t_c = 227$ s - $C_S = 8.5$ mg/L. 86
44 Curve of $\ln(D(t)/D_0)$ at the outlet of the airlift and linear regression in the relevant interval for the small-scale O_2 transfer test of January 2020: $(k_l a)_R = 1.8 \times 10^{-3}$ s^{-1} ($\pm$ 1.2×10^{-5} s^{-1}) / conditions: water temperature = 16.2°C - $V_R = 408.9$ L - water height = 7 cm - $t_c = 393$ s - $C_S = 9.97$ mg/L. 86
45 Curve of $\ln(D(t)/D_0)$ at the outlet of the airlift and linear regression in the relevant interval for the large-scale O_2 transfer test of June 2020: $(k_l a)_R = 4.4 \times 10^{-4}$ s^{-1} ($\pm$ 1×10^{-6} s^{-1}) / conditions: water temperature = 15.4°C - $V_R = 78\,400$ L - water height = 150 cm - $t_c \simeq 20$ s - $C_S = 10.2$ mg/L. 87
46 Evolution of the pH at the outlet of the airlift and sampling moments during the small-scale CO_2 transfer test **A** of September 2019. 88
47 Evolution of $[CO_{3_{tot}}]$ and $[CO_2]$ at the outlet of the airlift during the small-scale CO_2 transfer test **A** of September 2019 / conditions: water temperature = 23.6°C - $V_R = 267.1$ L - water height = 9.8 cm - $t_c = 227$ s. 88
48 Evolution of the pH at the outlet of the airlift and sampling moments during the small-scale CO_2 transfer test **B** of September 2019. 91
49 Evolution of $[CO_{3_{tot}}]$ and $[CO_2]$ at the outlet of the airlift during the small-scale CO_2 transfer test **B** of September 2019 / conditions: water temperature = 23.6°C - $V_R = 267.1$ L - water height = 9.8 cm - $t_c = 227$ s. 94
50 Curve of $\ln(D(t)/D_0)$ at the outlet of the airlift and linear regression for the small-scale CO_2 transfer test **B** of September 2019: $(k_l a)_R = 1.3 \times 10^{-3}$ s^{-1} ($\pm$ 2.1×10^{-4} s^{-1}) / conditions: water temperature = 23.6°C - $V_R = 267.1$ L - water height = 9.8 cm - $t_c = 227$ s - $C_S = 0.16$ mmol/L. 94
51 Evolution of the pH at the outlet of the airlift during the large-scale CO_2 transfer test **A** of June 2020. 97
52 Evolution of the pH at the outlet of the airlift during the large-scale CO_2 transfer test **B** of June 2020. 101

List of Tables

1 Height and volumes of water in the two small-scale HRAPs used for the test sessions of September 2019 and January 2020. 46
2 Volumetric mass transfer coefficients of oxygen for the small-scale test of September 2019 in basin 1 / conditions: water temperature = 23.8°C - water height = 9.8 cm. 50
3 Volumetric mass transfer coefficients of oxygen for the small-scale test of January 2020 in basin 2 / conditions: water temperature = 16.2°C - water height = 7 cm. 51
4 Values of the different variables used for the determination of the CO_2 concentration in the HRAP for the small-scale test **A** of January 2020. 53
5 Summary of the conditions and results of the small-scale tests. 57
6 Height and volumes of water in the large-scale basin used for the test session of June 2020. 59

7 Values of the CO_2 transfer coefficient of the large-scale test **B** of June 2020 for the different time intervals used for its calculation / conditions: water temperature = 16.5°C - V_R = 78 400 L - water height = 150 cm - $t_c \simeq$ 20 s. 65
8 Summary of the O_2 and CO_2 transfer coefficients of the whole HRAP for all the transfer tests conducted and ratios of the transfer and diffusion coefficients. . . . 70
9 Values of the different variables used for the determination of the CO_2 concentration in the HRAP for the small-scale test **A** of September 2019. 89
10 Values of the different variables used for the determination of the CO_2 concentration in the HRAP for the small-scale test **B** of September 2019. 92
11 Values of the different variables used for the determination of the CO_2 concentration in the HRAP for the small-scale test **B** of January 2020. 95
12 Values of the different variables used for the determination of the CO_2 concentration in the HRAP for the large-scale test **A** of June 2020. 98
13 Values of the different variables used for the determination of the CO_2 concentration in the HRAP for the large-scale test **B** of June 2020. 102
14 Summary of the conditions and results of all the tests. 107

1 Introduction

The Earth is facing many changes due to anthropogenic actions. Climate change and sea pollution are two examples of the consequences of human behaviour. Solutions to these issues must be found to preserve life and ecosystems.

Several technologies are being developed and used to find answers to these challenges, and this work focuses on an example of integrated technology that addresses different issues simultaneously: high rate algal ponds (HRAPs). These ponds are dedicated to wastewater treatment through the growth of algae or microalgae. The nutrients in the water are consumed by the algae and the water can be released into the environment with minimum risk of eutrophication [2, 3].

In addition to the water treatment, HRAPs allow the production of algal biomass. Once harvested, algae can be sold as a raw material for the production of biofuels, in the food and pharmaceutical industries, as pigments, as fertiliser, or for many other applications [2, 4, 5].

The use of algae as a biofuel source reduces the greenhouse gas emissions compared to fossil fuels. Indeed, the biomass production step consumes CO_2 through photosynthesis [6]. This CO_2 consumption can be coupled to industrial plants that emit carbon dioxide: once purified, the waste exhaust gases of the plant can be injected into the algae culture in order to reduce the plant's environmental impact [7].

The present work focuses on the transfer of CO_2 between the water and the atmosphere in HRAPs. The carbon is a limiting factor for the growth of algae and the performances of HRAPs can be improved by injecting CO_2 into the pond. However, few studies are devoted to CO_2 transfer and the lack of suitable probes for measuring the concentration of dissolved CO_2 in the range corresponding to HRAPs prevents the optimisation of CO_2 injection in this type of pond [8].

This master thesis intends to propose a methodology for the quantification of CO_2 transfer in HRAPs, based on a theoretical background developed by J. Hissel [9] and on an experimental procedure tested on small and large scales in the course of this work. The main purpose is to quantify the volumetric transfer coefficient, $k_l a$, of CO_2 for the studied application.

Three types of tests are conducted: first, tracer tests are used to determine the circulation time in the HRAP, then an oxygen transfer test is performed to estimate the oxygen transfer coefficients and to compare them to a previous work conducted in the same basins. The last type of test is the carbon dioxide transfer test: its experimental procedure is described, as well as the calculations required to evaluate the CO_2 concentration in the pond based on the samples collected during the test. The calculation of the transfer coefficient of CO_2 is also detailed.

This work is a part of the *Renewable* project (*REmoval of NutriEnts in Wastewater treatment via microAlgae and BiofueL/Biomass production for Environmental sustainability in Vietnam*), in collaboration with the University of Liège (ULiège) and the Industrial University of Ho Chi Minh (IUH). It is an ARES (*Académie de Recherche et d'Enseignement Supérieur*) project coordinated by both Professor Gauthier Eppe (ULiège) and Professor Le Hungh Anh (IUH) scheduled between May 2016 and December 2021.

The aim of this project is to promote a sustainable development of the aquaculture in Vietnam. A HRAP prototype has been built in the Ninh Thuan province in Vietnam in order to remove the nutrients from the wastewater of shrimp aquaculture before its discharge into the sea and with the objective to convert the algal biomass into valorisation products such as biofuel or animal feed.

The present work is the continuation of the work of D. Royaux, [1], that focused on the hydrodynamics and oxygen transfer of the HRAP built in the Ninh Thuan province. However, due to the international situation in the first half of the year 2020 by the Covid-19 pandemic,

the large-scale tests that were supposed to take place in the HRAP of the Ninh Thuan province have been replaced by tests in a basin situated in Arlon, Belgium, which has some similarities with the pond built in the Ninh Thuan province.

The knowledge of the transfer coefficients of oxygen and carbon dioxide is an important step in the design of the HRAPs as it allows to calculate the surface area required to treat the wastewaters in Vietnam. The algae activity can be evaluated too if these coefficients are known and with further studies on the photosynthetic and respiratory capacities of the algae. This master thesis intends thus to provide results that will be used in the scope of the *Renewable* project while proposing a general methodology for the quantification of the CO_2 transfer in HRAPs.

This report is separated into different sections. First, a literature review describes the characteristics of algae cultivation and HRAPs, summarises the knowledge about the oxygen and carbon dioxide transfers in this type of pond, lists the different uses of algae and shows the advantages of coupling wastewater treatment to CO_2 consumption.

The three types of tests conducted in the course of this work are then detailed. The experimental procedures are explained and the methodologies followed for the calculation of the CO_2 concentration and the transfer coefficients are described.

The small and large-scale tests conducted are then presented and the results of the different tests are analysed. Potential analogies with a correlation found in the literature are also described.

All the calculations and graphs presented in this master thesis were made in *Excel*.

1.1 Objectives of the master thesis

The main objective of this master thesis is to describe in details a methodology to quantify the volumetric mass transfer coefficient of CO_2 in open ponds such as HRAPs and to show that this method allows to provide reliable results.

The first purpose is the application of the theoretical works of J. Hissel [9] and J.-L. Vasel [10] and the definition of clear experimental procedures for the studied application of HRAPs. The second objective is to describe the tests carried out while following the developed methodology and to analyse the obtained results in order to verify a correlation found in the literature.

Finally, this master thesis intends to provide results for the quantification of CO_2 transfer in HRAPs that can be used in the design of large-scale basins and to propose a method that may enable industrial players to optimise their operating conditions, which could play a role, however modest, in the effort made against sea pollution and greenhouse gas emissions.

2 State of the art

The present section proposes an overview of the existing technologies for algae production, focusing on high rate algal ponds (HRAPs) as it is the type of reactor used in the *Renewable* project. The current situation regarding the quantification of oxygen and carbon dioxide transfers in HRAPs between the water and the atmosphere is also detailed. Uses of algae are then presented. The interest of algae cultures for wastewater treatment and in the carbon economy is eventually studied to understand the benefits they can bring in the current context of climate change.

2.1 Algae cultivation

Algae are chlorophyll-containing photosynthetic organisms living in aquatic environments. Their photosynthetic property is due to the presence of cyanobacteria, an oxygenic phototroph species of bacteria present in plants and algae [2, 11, 12, 13, 14].

Micro and macro algae can be differentiated. Macroalgae are multicellular and plant-like species with roots while microalgae are unicellular and do not have roots. It was estimated that there are between 1 to 10 million species of algae on Earth, most of them being microalgae [11]. In the present work, algae in general are considered, without specifying whether they are macro or microalgae, even if in HRAPs, microalgae are most commonly used.

Algae live through photosynthesis. When exposed to light, they convert the solar energy into chemical energy and consume carbon dioxide and water to produce organic matter and oxygen. The general equation of photosynthesis is

$$\mathrm{n\ CO_2\ + n\ H_2O\ +\ light\ energy\ \rightarrow\ (CH_2O)_n\ +\ n\ O_2} \tag{2.1}$$

where carbohydrates are produced. Photosynthesis is thus the reduction of carbon dioxide into carbohydrate and oxygen [15]. This phenomenon occurs during the day, when light is available. At night, algae live through normal respiration, emitting CO_2 while consuming O_2. The respiratory losses can significantly impact the biomass production capacity of algae cultures [16]. Several studies have shown that more than 30% of the biomass fixed during the day can be lost at night, depending on the algae species [17, 18]. However, algae production results in a net positive CO_2 uptake [19].

When the concentration in algae has reached a satisfying level, they can be harvested and used in several ways, such as for biofuel production, as food, as biofertilisers, as pigments or as protein source.

2.1.1 Principles of algae cultivation

During the process of algae cultivation, the organisms pass through different physiological states, presented in Figure 1. First a lag phase occurs before the growth of the algae. Then algae consume nutrients and expand exponentially until the growth phase is replaced by a stationary phase during which algae still consume nutrients but do not expand, before reaching the decreasing phase [20, 21].

Algae cultures are started on a laboratory scale. A few algal strains are added to a small volume of water and the adequate nutrients amounts are supplied. The algae expand in this volume and this volume of water is then added into a larger water volume where algae will keep growing. To optimise the process and avoid excessive nutrient consumption, the passage is made at the end of the growth phase, before entering in the stationary phase during which algae consume nutrients without expanding [21].

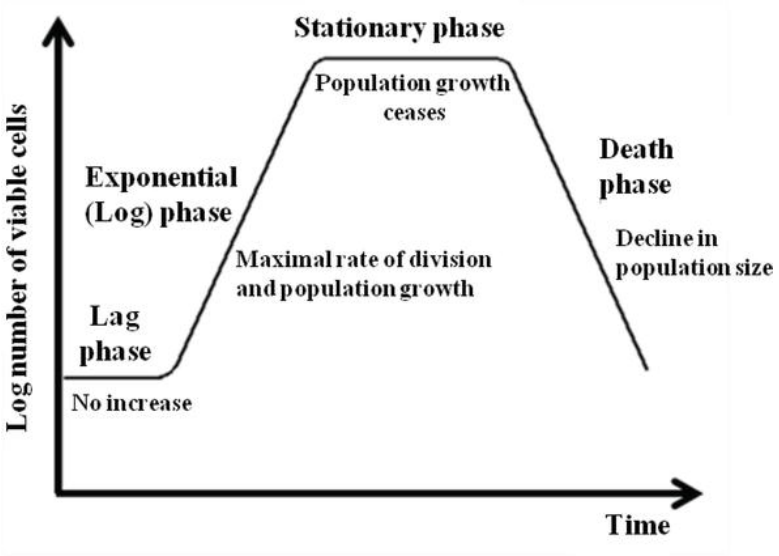

Figure 1: Logarithmic evolution of the number of algae cells during their cultivation [20].

The volume of water containing algae is increased similarly until it reaches a sufficient scale to be added into the continuous reactor.

During their growth, algae have to be fed with several nutrients. First, carbon is the source of energy for different cellular events such as metabolite production and reproduction, and it is part of the physical structure of the cell. This carbon can either come from organic or inorganic sources, respectively heterotrophic substrates and CO_2 for instance [22].

The two other major nutrients required for algae growth are nitrogen and phosphorus. The former contributes to the production of protein, chlorophyll and amino acids and the second takes part in the energy transfer and in the photosynthesis. Other nutrients are required to obtain an effective cultivation, such as calcium, potassium, magnesium, iron and manganese. [22, 23].

2.1.2 Types of reactors

Many types of reactors exist to grow algae, each having specific characteristics and drawbacks. They are divided into two main branches: open and closed systems.

Open systems usually consist in large shallow ponds in which water containing algae circulates, enlightened by solar rays or artificial ones and in contact with the atmosphere. An example is presented in Figure 2. The present work focuses on this type of reactor and the following section describes more precisely their characteristics.

The main advantages of open ponds are their small capital and operating costs. Indeed, the structure can be made of concrete or fiberglass [25] and the operations required for the cultivation are really simple as they mainly consist in setting the water into motion with an airlift system or a paddlewheel. Open ponds can operate in a continuous mode and algae can be harvested at the end of the lap after their growth.

Open ponds are reactors used on a large scale as their production costs are low. However, this type of reactor has several drawbacks. The poor mixing of the water induces bad light utilisation as the cells pass through dark zones and might stay at the bottom of the channel during their circulation. The level of water inside the pond is thus limited, which decreases the productivity. There is no real control of the operating conditions as temperature and lightning depend on the weather if the pond is situated outside. Moreover, the evaporation of water and the transfer of CO_2 to the atmosphere are non-negligible. Open ponds are also subjected to contamination by other organisms and require an important land use compared to closed

Figure 2: Aerial view of the *Qualitas Health algae production facility* in New Mexico, US (Courtesy photo) [24].

reactors [25, 26, 27].

There exist many different closed systems that allow to avoid the drawbacks of open ponds. For instance, adding a transparent barrier made of plexiglass on the open pond keeps the CO_2 trapped in the pond and allows to better control the environment, creating a greenhouse [26].

Other closed systems are used and called photobioreactors. They consist in enclosed and illuminated vessels of different forms and shapes. Stirred tanks illuminated by fluorescent lamps and agitated mechanically allow the batch production of specific biological components in controlled and nearly sterilised conditions. Their productivity is however limited as the tanks need to be emptied, washed and refilled between each utilisation [21].

The most common closed systems for algae culture are tubular photobioreactors. The water containing algae flows inside transparent tubes in which nutrients and CO_2 are injected and photosynthesis occurs inside the tubes with the light provided by solar rays. Fluorescent lamps can also be used if the environment is poor in solar radiations. Different configurations exist to optimise the illumination: vertical, horizontal, inclined or helical, depending on the light radiation used to supply the light required for the photosynthesis [26]. An example of a horizontal tubular photobioreactor is presented in Figure 3.

Tubular photobioreactors are characterised by a large illuminated surface area and allow to avoid the drawbacks of open ponds, but they have more important costs. Their use and maintenance is more complex too as the accumulation of oxygen can inhibit the photosynthesis and solid algae can stick on the walls of the tubes, causing fouling and preventing the light to enter into the tubes [25, 26, 27].

Other types of closed reactors exist too, such as bubble columns or flat plates. The former give good mass transfer with low energy consumption but requires sophisticated material and can not be scaled-up easily while the latter is relatively cheap with good biomass productivity but needs to be duplicated many times to be scaled-up [26, 27].

Figure 3: Example of a tubular reactor [28].

2.2 High rate algal ponds

The present work focuses on the transfer of oxygen and carbon dioxide between the water and the atmosphere in high rate algal ponds. A more detailed presentation of this type of basin is thus presented below.

As described previously, high rate algal ponds are open shallow raceway ponds in which water circulates. This type of pond was first developed in the 1950's in California [29, 30]. The configuration of the pond can consist in a single loop or several walls can be built alongside to increase the length crossed by the water and thus the hyrdaulic retention time.

The motion of the water is usually created by a paddlewheel or an airlift, or both. The picture of a paddlewheel is presented in Figure 4. The rotation of the wheel is induced by mechanical energy and the water is pushed forward.

Figure 4: Paddlewheels used in a raceway pond in St Helena and Hilmar California, US [31].

In airlifts, no mechanical energy is required. The water is set into motion with the injection of gas that pushes the water to the outlet of the airlift. The drawing of the airlift system from Ninh Thuan is presented in Figure 5.

Different parameters can be modified to optimise the algae culture: the depth of water, the velocity of the water and its retention time, the flow regime, the mixing, the oxygen injection

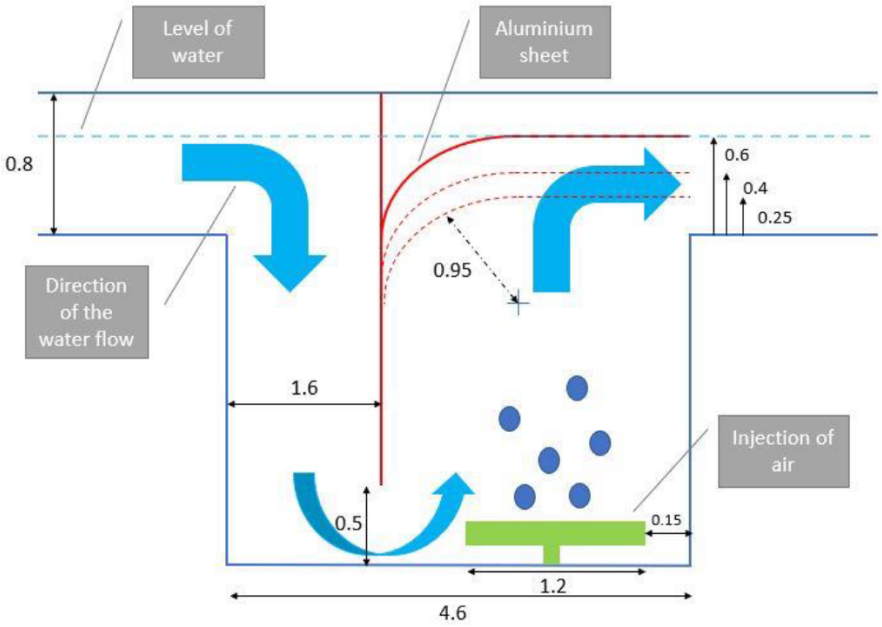

Figure 5: Drawing of the airlift system used in the HRAP in the Ninh Thuan province, Vietnam [1].

in the airlift, the nutrient supply, the potential CO_2 injection, the light intensity, etc [1, 32]. Many studies have been conducted to optimise most of those parameters, but the CO_2 injection has not been studied in detail. It is a common knowledge that injecting CO_2 inside the pond improves the performances as algal growth is often carbon limited [31, 33], but only few studies quantify the CO_2 assimilation by algae and its transfer to the atmosphere [10, 34], so the operating conditions are not optimised in general.

HRAPs are mainly used for wastewater treatment. Compared with conventional wastewater treatment technologies, HRAPs have smaller capital and operating costs. Indeed, more than 50% of the electrical energy consumption of conventional mechanical wastewater treatment technologies can be saved by the capture of solar energy through photosynthesis [35]. Moreover, the wastewater treatment can be coupled with algae harvesting by gravity settling for instance, producing a valuable product. In 2016, around 98% of the commercial algae biomass production came from open ponds as it seemed to be the most economical way to cultivate them [2].

However, a major drawback of HRAPs is their land use. Indeed, this type of pond requires large land plots in order to obtain long retention times and increase the treated volume as the ponds are usually shallow. Moreover, the pond should be situated in places with great sun exposure during the year to avoid the use of lamps that would increase the operating costs, so the choice of the pond's location can be limited. Contamination by other organisms and bad weather conditions are risks too for the operation of HRAPs. [25, 36].

Algae are generally harvested before the paddlewheel or airlift, after having crossed one lap of the pond. The harvesting part of algae culture represents an important cost of the process as it accounts for 20 to 30% of the total production costs [22, 37]. The most common harvesting methods are detailed in [1] and in [38].

2.3 Quantification of O_2 and CO_2 transfers in HRAPs

The supply of carbon dioxide to algae is essential in algae culture. A lack of CO_2 could indeed lead to a dramatic decrease in the production of biomass, or even cause the death of the microorganisms. It has been shown that CO_2 addition enhances algal productivity in wastewater treatment HRAPs [36, 39, 40] and it is standard practice in all commercial algal production HRAP systems [23].

However, if oxygen accumulates because a too important photosynthetic rate occurs due to a too high CO_2 concentration, it can act as an inhibitor of hydrogenases, the enzymes that catalyse the transformation of protons into hydrogen, and thus decrease the production of lipids that are required to produce biofuels from the obtained algae [20].

For these reasons, the operating conditions need to be adapted to reach an optimal situation for the algae development. The quantification of the transfer phenomena between the water and the atmosphere plays a part in this process and can be done through the evaluation of the volumetric transfer coefficients $k_l a$.

Several studies have already been conducted on these subjects and the transfer of O_2 is relatively easy to evaluate experimentally [8, 41]. However, the transfer of CO_2 is more complex to describe. Indeed, only few models of probes measuring the CO_2 concentration in water are available for the studied range of concentrations [10]. Methodologies to evaluate the transfer coefficient of CO_2 based on the transfer of O_2 or on the pH are also developed, but the results obtained with the different paths are sometimes incoherent [8, 34].

The evaluation of the CO_2 transfer is thus less developed. Experiments have been conducted to study the impact of CO_2 injections into specific ponds [8, 42, 43] and numerical modellings based on CFD can be done to simulate the phenomena occurring [8], but experimentally, the evaluation of the CO_2 transfer is not easily performed. Different techniques have been used but none has become a reference. Commonly, the value used for the kla of CO_2 is based on the value calculated for the oxygen transfer. Equation (2.2) is used in many cases [8, 34, 44, 45], where D_{CO_2} and D_{O_2} are the diffusion coefficients in water of CO_2 and O_2 respectively:

$$(k_l a)_{CO_2} = (k_l a)_{O_2} \sqrt{\frac{D_{CO_2}}{D_{O_2}}} \tag{2.2}$$

The overall volumetric gas-liquid mass transfer coefficient of CO_2 is thus expected to be smaller than the $k_l a$ of oxygen as the diffusion coefficient in water is smaller for CO_2 than for O_2.

Probes can also be used to perform a direct measurement of the transfer coefficients [8, 34], but these probes usually operate in concentration ranges too high for the present application. Indeed, most of these probes measure the concentration in dissolved CO_2 based on the variation of the pH in buffer solutions. For too small concentrations in dissolved CO_2, the variation of the pH is not important enough to give precise results [10].

Following the pH during the experiment combined with alkalinity titrations can also lead to the evaluation of the $k_l a$. This is the method developed in this work. Some studies are based on the pH evolution too but do not focus on HRAPs. For instance in [43], an empirical correlation based on the pH is developed but it is specific to well-mixed baffled reactors and the correlation involves other parameters of the reactor.

However, the results obtained with the different methods can be contradictory [8] and few studies have been conducted for HRAPs. The method proposed in this work intends thus to characterise the transfer of CO_2 in the specific case of HRAPs in order to optimise the conditions for the algae culture.

2.4 Uses of algae

Algae can be used for several applications. Their high lipid content allows to produce biofuels once harvested, they can be used as food as they are rich in proteins, many vitamins and minerals, or they can serve as biofertilisers to fix the atmospheric nitrogen [46]. A brief overview of the main applications of algae is presented below.

2.4.1 Biofuels

To face the current issues due to climate change, alternatives to fossil fuels need to be used in order to decrease the greenhouse gases emissions. The production of biofuels is a possibility to replace, at least partially, conventional fuels based on fossil resources.

Using biofuels made of algae allows to decrease drastically the CO_2 emissions compared to fossil fuels. Even if in the end, both biofuels and fossil fuels are consumed and emit similar amounts of CO_2, the difference lies in the fact that the production of algae is CO_2-consuming as algae need carbon dioxide for photosynthesis. This CO_2 can come from exhaust gases of industrial sites for instance and is injected into the basin where algae are grown. As the production process of algae-based fuels does not require the consumption of fossil fuels, except for small steps such as potential transportation, the only significant CO_2-emitting step is the combustion of the biofuel itself. It is thus the whole production line that needs to be studied to see the benefits of algae-based fuels [6].

Several studies have focused on the possibility of using algae for the production of biofuels [2, 36, 47]. Algae are an interesting raw material for the production of fuels as many species can accumulate substantial amounts of lipids. The lipid content depends essentially on the algae used and, in average, can vary between 1 and 70% of the dry weight. However, under certain conditions, some species can reach 90% of their dry weight [32, 48].

Algae biofuels have many advantages. As other biofuels, their consumption of CO_2 during their growth reduce their impact on climate change. As approximately half of the dry weight of algal biomass is carbon, around 1.8 g of CO_2 is required per gram of microalgae produced [2, 6, 49].

Compared to other biofuels, algae-based fuels have the huge advantage of not being in competition with the production of food and feed. Even if algae can be used as food, as explained afterward, it is not their main application nowadays, while soybeans or rapeseed represent important feed stocks for agriculture. Moreover, algae cultivation is characterised by high growth rates and productivity and the yield of biodiesel production from algae is 5 to 20 times higher than that of rapeseed and more than 20 times higher than that of soybean [12, 50].

Algae can also be grown in a wide range of climate conditions and, most importantly, on non-arable lands. Indeed, algae can be grown in already existing water plants or artificial basins can be built in places where appropriate conditions for their cultivation are encountered. It stretches the limits of terrestrial agriculture and nearly infinite possibilities can thus be considered for their production. Algae also need much less land for their cultivation than terrestrial crops [2]. The fresh water consumption drastically decreases too as algae can be grown in saline water while terrestrial crops require huge quantities of fresh water [4].

Another interest of biofuels is that if a country manages to produce them on a large scale, it reduces its dependency on foreign oil imports and can thus modify its geopolitical situation [2].

A broad spectrum of biofuels can be produced from algae and microalgae, including biodiesel, biomethane, bioethanol or biobutanol, hydrocarbon gases and bio-crude oil. Each type of biofuel can be obtained with a specific method. For instance, biodiesel is produced through the transesterification of lipid triglycerides extracted from the algae into fatty acid methyl esters (FAMEs), which are the main component of biodiesel. Bioethanol is produced with yeast fermentation of the carbohydrates followed by a distillation to separate it from the other products.

Biomethane is obtained through anaerobic digestion, gasification or pyrolysis of the organic residues of algae after the lipid extraction [4, 12, 47].

An important advantage of biodiesel is its miscibility with petrodiesel at all blend levels. Its fatty acid profile, which determines many of its fuel properties, is really similar to that of its parent oil. However, biodiesel is characterised by poor cold flow properties compared to traditional diesel. The fatty acid profile of the biodiesel is thus studied and the properties of the obtained fuel can be accurately predicted, allowing to adapt the product to cope with this limitation [51].

The combustion of the biofuels are also characterised by a reduction of most of the regulated exhaust emissions other than CO_2 and NO_x as they contain only little or no sulfur and aromatics for instance [51].

Using algae as a source of biofuels has however several disadvantages. First, their high production costs and low cost efficiency compared to conventional fossil fuels, due to the cultivation, harvesting, separation and processing of the final product, prevent them from being widely cultivated for the production of fuels [2].

Another issue related to algae culture is the anthropogenic eutrophication. To improve the production yields of algae, it is essential to supply them with sufficient nutrient amounts. However, if a too large excess of nutrient is added into the system, accumulation of the nutrient will occur and algae risk to reproduce excessively under aerobic metabolism, using large quantities of the dissolved oxygen contained in the water [52]. If, for instance, too much macroalgae or plants lay on the surface of the water, less sunbeams will pass through the surface and plants at the bottom will not be able to partake in photosynthesis. Moreover, once the excess algae dies, it decomposes at the bottom of the water and this process consumes important amounts of oxygen that are not available any more for fishes or other aquatic animals which could suffocate [2, 53].

This issue needs to be considered when algae are cultivated in natural ecosystems whose balance risks to be disturbed. The complete life cycle of the algae needs thus to be considered when assessing the benefits for the environment, and native water ecosystems should remain undisturbed to a maximum extend in order to keep the sustainable characteristic of the biofuel production [2]. The waste products of the algae growth and biofuel production also need to be treated.

Algae requiring 50 to 100 times more nitrogen nutrients than rapeseed, the fertilisers quantities need to be used wisely as they could damage the environment as well as limit the economic viability of the process [12]. Recycling the nitrogen and phosphorus accumulated in algal wastes of the biofuel production process is a way to decrease the costs of the fertilisers [54].

The lack of policies over algae cultivation in the world, as well as the absence of clear sustainable criteria for biofuel production are other drawbacks that restrain the development of algae-based biofuel production to a larger scale [2, 13].

Currently, the production of algae-based biofuels is technologically feasible but economically non-viable [4, 11, 47]. Each step of the process needs to be optimised to decrease its costs. The yields of the large-scale cultivation need to be improved and the harvesting methods used for the recovery of the algae and the extraction of the valuable components consume too much energy, inducing high operating costs [11, 50].

A way to produce economically feasible algae-based biofuels could be to couple the process with the production of high value co-products or the creation of beneficial functions [47]. As HRAPs are primarily used for wastewater treatment, the most suitable possibility is to produce biofuels with algae grown in wastewater. Recent studies have shown that HRAPs dedicated only to the production of algae for biofuel production are not economically viable but that, coupled with wastewater treatment, algae production in HRAPs could become a profitable process [29, 36]. Existing HRAPs used for wastewater treatment can serve as "testing ground"

to develop and optimise this biofuel production process in order to be available when it becomes competitive due to higher fossil fuel costs [47].

Modifications of the algal biology will also be required to improve the production yields. Even if these yields are much higher than those of seed crops, they can still be increased through genetic and metabolic engineering to modify the algae's composition and properties [2, 11, 50].

Even if algae-based fuels have several major drawbacks, algae are considered as the most sustainable renewable energy source that has the capacity to meet the global demand for fuels in the long term [2]. Indeed, the technological feasibility of the large-scale production of algae and the environmental benefits that it can bring appear to compensate the current limitations and may lead to the development of the processes to a competitive position on the fuel market. Studies still need to be conducted to reach maturity and the plausible rise of the fossil fuel costs would increase the interest in algae-based business [47].

2.4.2 Food and feed

Algae can be used in the food industry too in different forms, as shown in Figure 6. In many Asian countries, algae are already used as a source of food due to their high nutritional value. Algae are rich in vitamins, proteins, minerals, carbohydrates, enzymes, polyunsaturated fatty acids (PUFAs), antioxidants, etc [46, 55]. However, in the food industry, algae are essentially used as nutritional supplement or health food [5]. They can be added to drinks, pasta or snacks for instance, to improve their nutritional value. They can also serve as natural colorant.

Several species of algae have high potential as healthy human food and can be sold as nutritional supplements: *Chlorella* contains more vitamins than many plants [55] and is mostly sold in "healthy food" stores [56] and *Spirulina* is an excellent source of PUFAs and vitamins too and, as *Dunaliella salina*, it is rich in β-carotene, an orange-dye pigment converted by the human body into Vitamin A [5]. Those three algae species are major producers of high value compounds such as proteins and lipids and the two former rule the microalgae market due to their ease of growing [57].

Figure 6: Examples of forms of algae used in industry [58].

As explained previously, the main advantage of algae over classical food production is the ability to grow them on non-arable lands. Indeed, provided the supply in nutrients and good conditions such as good light exposure and appropriate temperature, algae can be cultivated anywhere while agricultural crops require fertile soil for their production.

Algae can also serve as animal feed. They can be fed to fishes, larvae or shrimps as these aquatic animals naturally eat them, but they can also be added in the diet of cows, pigs, sheeps or poultry.

As for humans, they are not used as a primary source of food most of the time: they are added as supplement. However, even when present in small amounts, algae can improve the immune system of animals, increase their weight and fertility and reduce their cholesterol levels. The production yields of meat and eggs can thus be enhanced by the addition of algae in the animal feed. The milk produced by milk cattle can also be enriched in iodine by feeding the animals with algae as they are an important source of iodine [55, 59].

A huge advantage of algae dedicated to animal feed is that the animals can convert the low-quality proteins contained in algae into proteins of higher quality. The quality of the meat obtained for human consumption increases thus, without the need of extensive processing of the algae fed to the cattle [59].

2.4.3 Fertilisers

Another use of algae is as biofertilisers in agriculture. Even if no study has provided a clear evidence that the use of algae is the only reason why improvements are encountered, many beneficial effects occur when algae-based biofertilisers are used. These effects can be observed on vegetables, fruits or flower crops and include higher production yields, improved vigor and seed germination, increased uptake of soil nutrients and resistance to diseases or enhanced defense against abiotic stresses. Algae biofertilisers are also responsible for the increase of the chlorophyll content in plants, due to the reduction of its degradation, inducing a higher photosynthetic rate [59].

Adding algae into soils improves their fertility. Some characteristics of algae that allow their use as fertilisers are their high mineral content and their ability to fix the atmospheric nitrogen. This latter characteristic allows to replace N-rich fertilisers by biological nitrogen fixation: the nitrogen fixed by the algae is liberated and re-assimilated by the plants [46].

Another benefit of algae as fertilisers is the increased uptake of phosphorus and nitrogen. P and N are often the primary limiting nutrients, so adding algae in soils allows to increase their availability for the plants.

Once dead, the decay of the organisms provides organic matter to the soil too. It acts as binding agent for the soil texture and increases its humus content, creating a more fertile place for future plants in the following years [60].

Algae can also be used in the form of liquid biofertiliser. In this case, it is not added into the soil but directly sprayed on the plant instead. The nutrients are then quickly absorbed through leaf openings, within 10 to 15 minutes [59].

Another advantage of algae biofertilisers is their biodegradability. They are also non-polluting and non-hazardous to humans, animals and birds, while chemical fertilizers risk to degrade the fertility of the soil by modifying its pH, resulting in the dissolution of the oil crumbs that are essential for drainage and air circulation and thus rendering it unsuitable for raising crops [61, 62]. Moreover, chemical fertilisers don't bring the decaying matter that will improve the soil structure and may result in a toxic build-up of chemicals such as arsenic, cadmium and uranium which can eventually make their way into the fruits and vegetables [63].

2.4.4 Other uses

There exist several other possibilities to use harvested algae. For instance, the pharmaceutical industry is interested in the exploitation of PUFAs, vitamins and antioxidants contained in algae. Indeed, the human and animal bodies lack the enzymes necessary to synthesize long ω-3 PUFAs and need to obtain them from external sources such as pharmaceuticals or food supplements that can be derived from algae [4, 5, 13].

As mentioned previously, algae can also serve to grow pigments such as carotenoids, which can be converted by the body into vitamin A and protect the cells and tissues from free radicals and singlet oxygen, in addition to their colouring role. Pigments and other components found in algae can also serve in the cosmetic industry as thickening agents, water-binding agents and antioxidants [2, 4].

Algae can also serve as source of biomass for direct combustion to generate heat or electricity. However, this application is not efficient as algae have a high moisture content, leading to a decrease of the calorific value and of the combustion temperature compared to terrestrial biomass. The combustion efficiency of algae is thus lower [2]. Moreover, their ash chemistry restricts their use for direct combustion and gasification as algae ashes contain a large percentage of potassium, which can lead to problems such as deposition of salts and fouling [64, 65].

Microalgae biotechnology is a promising field too. Microalgae are currently used as an important source of valuable natural active molecules and, via genetic engineering, new products such as vaccines, antibodies, enzymes, immunoregulators or hormones can be synthesised [11].

Algae are thus really versatile crops that can be used in many fields, growing appropriate species for the desired application. Other sectors such as textile production, paper industry or metallurgy can also consider algae for some applications [2].

2.5 Coupling algae production with wastewater treatment and CO_2 consumption

In addition to all the possible applications of algae once harvested, their cultivation offers two major contributions: wastewater treatment (WWT) and CO_2 consumption. These couplings add value to the final product, improving its competitiveness compared to that of other products, which can be essential to obtain competitive biofuels for instance.

2.5.1 Wastewater treatment

Algae requiring nutrients to grow, using wastewater as their cultivation medium is relevant as the majority of wastewaters already contain high concentrations in nutrients, especially in total N and total P [37]. Using HRAPs in the WWT process allows the removal of nitrogen and phosphorus from the effluents, which would cause eutrophication if the water was released in the nature without treatment. Their removal efficiency is high due to the long hydraulic retention time of the wastewater in the pond [3].

As mentioned previously, this is one of the objectives of the *Renewable* project: the wastewater of shrimp cultivation has a rather high concentration in nutrients and needs to be purified before being discharged into the sea.

Many thousands of HRAPs of various sizes are dedicated to wastewater treatment around the world [23], such as those in Waikato, New-Zealand, and in Arizona, US, shown in Figure 7.

In common WWT processes, the nitrogen removal is performed by nitrification-denitrification, a costly electromechanical process that requires additional aeration energy [47]. The corresponding energy requirements in biological treatments are lower and biological processes are

(a) Waikato, New Zealand [31].

(b) Arizona, US [66].

Figure 7: Examples of HRAP wastewater treatment plants.

considered to be the least expensive WWT method [67, 68].

Moreover, algae are also able to uptake heavy metals present in the wastewater. Indeed, cyanobacteria contained in algae are able to concentrate metal ions present in their environment [60]. This accumulation of heavy metals can occur by different phenomena, such as physical adsorption, ion exchange or covalent bonding [69]. As indicated by [69], "algae also enhance the deactivation of pathogens by raising the pH value, the temperature and the dissolved oxygen concentration of the treated effluent".

2.5.2 CO_2 consumption

Carbon accounts for 40 to 50% of algae dry weight [2, 5]. There are two types of carbon sources: inorganic, *i.e.* CO_2 and organic, *i.e.* heterotrophic organisms. In most cases, it is the gaseous CO_2 present in the atmosphere that serves as source of carbon for natural algae plants and concentrated CO_2 can be injected in commercial algal reactors [5, 23, 70].

In the current global warming context, the development of technologies consuming greenhouse gases that would be emitted into the atmosphere otherwise should be a priority. International policy measures have been taken to limit the rise of temperature, mainly based on the cut of greenhouse gases emissions, but even if all CO_2 emissions were immediately cut to zero, climate change would still continue in the future due to the long residence time of CO_2 in the atmosphere. It is observed that currently, the atmospheric CO_2 concentration is rising of about 2 ppm per year [49].

Algae have a huge potential in the efforts against global warming. Indeed, they need to consume CO_2 to grow. Two possibilities exist: algae can directly draw CO_2 from the atmosphere or gaseous CO_2 can be injected in the pond, so algae offer a direct use of fossil CO_2 from industrial plants flue gases. As mentioned previously, it is estimated that 1.8 g of CO_2 can be fixed via the cultivation of 1 g of microalgae [2, 6, 49] and that algae are able to mitigate 10 to 50 times more CO_2 than terrestrial plants [71]. The CO_2 fixation efficiency also depends on the algae species used [19].

As explained previously, one of the major advantages of algae is the possibility to reach very high biomass productivities. They have thus the potential to be grown on a very large scale and thus play an important role in the CO_2 mitigation [23]. Moreover, injecting CO_2 in the cultivation process allows to increase the productivity [36, 39, 40].

To obtain the required amount of CO_2 to inject in the ponds, carbon capture and storage (CCS) processes are required. They include the CO_2 capture from the flue gases of the industrial plant, its purification to remove sulfur dioxide and hydrogen sulfide that are toxic for algae and can kill the culture in less than two days for instance [72], its compression and its transportation

to the plant. The resulting production of bioenergy is named BECCS [49].

The possibility of growing algae directly in the industrial CO_2-emitting plant can also be considered. For instance, the Israel Electric Corporation-IEC in Ashkelon or the Niederaussem power station in Germany have used desulphurised flue gas for algal growth to consume a part of the emitted CO_2 [7]. However, due to climatic, land and water restrictions, it may be impracticable to grow algae directly on site [19]. The captured CO_2 needs thus to be concentrated and transported to a more convenient place for the culture. In this case, the greenhouse gases emissions related to the transportation stage need to be considered for the life cycle assessment of the technology.

As explained in this section, algae can remove CO_2 from the atmosphere, so their cultivation enters in the category of negative emission technologies (NETs). Life cycle analyses of algae-based products need thus to consider the entire algae growth stage to truly assess the advantages of algae cultivation [73].

3 Experimental design and tests presentation

As explained in the introduction, this master thesis has several objectives. This section focuses on the development of the methodology for the quantification of the CO_2 transfer. Its application to HRAPs and the potential limitations encountered are detailed in Sections 4 and 5 and the analysis of the results and the comparison with information found in the literature are in Section 6.

Usually, high rate algal ponds are operated continuously. Water enters at the outlet of the airlift or paddlewheel and a part of it is removed at the entrance of the airlift, after its circulation inside the pond [12]. In the present work, a batch system is considered: the experiments are designed for a defined volume of water with total recirculation in the pond. No paddlewheel is used and the water motion is induced by an airlift.

The tests are conducted in clear water, *i.e.* without algae, in order to avoid the production of oxygen and the consumption of carbon dioxide, as well as to characterise the transfer in a base case without a certain type of algae that could influence the results. Indeed, as mentioned previously, there is a species dependence of the CO_2 fixation efficiency [19].

Different probes are used during each test and are placed at two points of the pond to measure the temperature, the conductivity, the pH or the oxygen concentration, depending on the type of test conducted. The most relevant positions of the probes are at the outlet and at the inlet of the airlift, so at the points A and B in Figure 8 that shows one of the small-scale ponds used to conduct the tests. The probes allow to divide the pond into two parts: the channel "A→B" in which the water circulates, guided by the transparent walls, and the airlift "B→A" at the front of the picture, in which air is injected by diffusers to mix and expel the water into the channel. The direction of the water flow is also shown in blue in Figure 8.

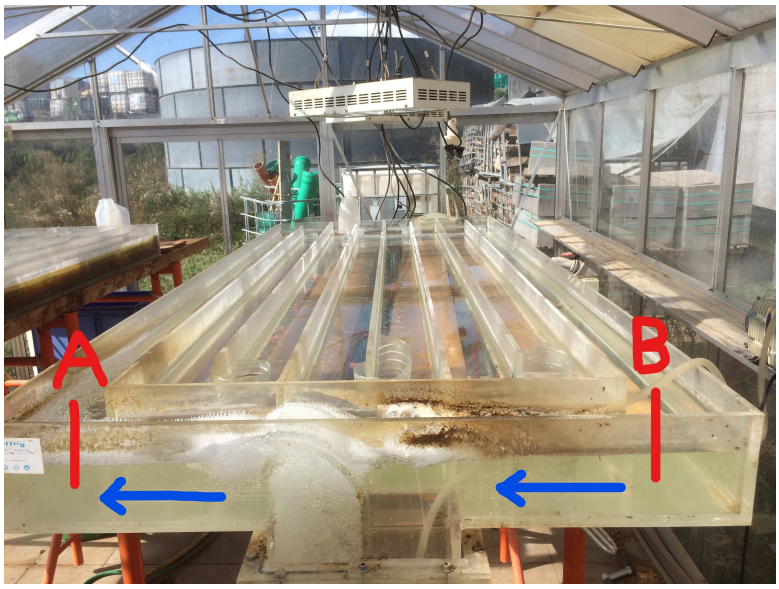

Figure 8: Small-scale HRAP ("basin 1") used to perform the tests of September 2019, with the direction of the water flow in blue and the positions of the probes in red.

The different tests are presented in the following sections. Tracer tests are first required to evaluate the circulation time in the basin, then the tests of oxygen and carbon dioxide transfers are conducted, following the methodologies detailed below.

3.1 Tracer test

The first parameter to measure is the circulation time t_c. It is the time required by a particle inside the pond to cross an entire lap of the basin, driven by the flow created by the airlift. The circulation time is a key parameter for the further experiments because the reactants have to be injected homogeneously into the pond and because the studied phenomena are evaluated per lap.

The tracer test consists in injecting a tracer and measuring its concentration in the pond during a certain lapse of time. The tracer used is a saline solution that is injected at the outlet of the airlift and the conductivity is measured with two probes situated at both sides of the airlift. Each passage of the saline solution in front of a probe is characterised by a peak as the salt increases the conductivity of the water. The saline solution is added at the outlet of the airlift, just before the probe A.

Theoretically, the salt is supposed to be injected as a Dirac function in order to obtain one discrete value for the time corresponding to the injection. However, the saline solution being denser than the water circulating in the pond, it is not optimal to add the solution in its entirety at once as a part of it would sink to the bottom of the basin without being carried away by the flow. The salt that would settle at the bottom of pond at the injection point would detach afterwards and be detected by the probe, leading to undesired peaks in the conductivity measurements. The saline solution is thus injected as quickly as possible while being careful to avoid the fall of the dense solution to the bottom of the pond. It has been shown by other authors that an injection time of less than 1 or 2% of the circulation time is a good compromise [1, 10, 74].

If no dispersion occurred in the flow, the peaks measured at each lap should be similar to the peak corresponding to the injection [75]. In that case, no mixing would be encountered by the saline solution during the test and thus its concentration would be similar at each lap. In reality, the concentration of the saline solution is diluted along the pond due to dispersion. The intensity of the peaks of the conductivity curve decreases thus at each lap, until the saline solution is completely mixed in the pond.

The evolution of the tracer concentration over time can be modelled with Voncken's equation. This equation represents the impulse response of a plug flow reactor with dispersion and recirculation. Two variables have to be adjusted to fit the curve: the Péclet number for the amplitude of the peaks and the dimensionless time for their spread [1, 76]. This equation can be used to describe the hydrodynamics of HRAPs, as detailed in [1].

An example of the evolution of the conductivity during a tracer test is presented in Figure 9. The circulation time is measured graphically as it is the average time gap between the top of two consecutive peaks.

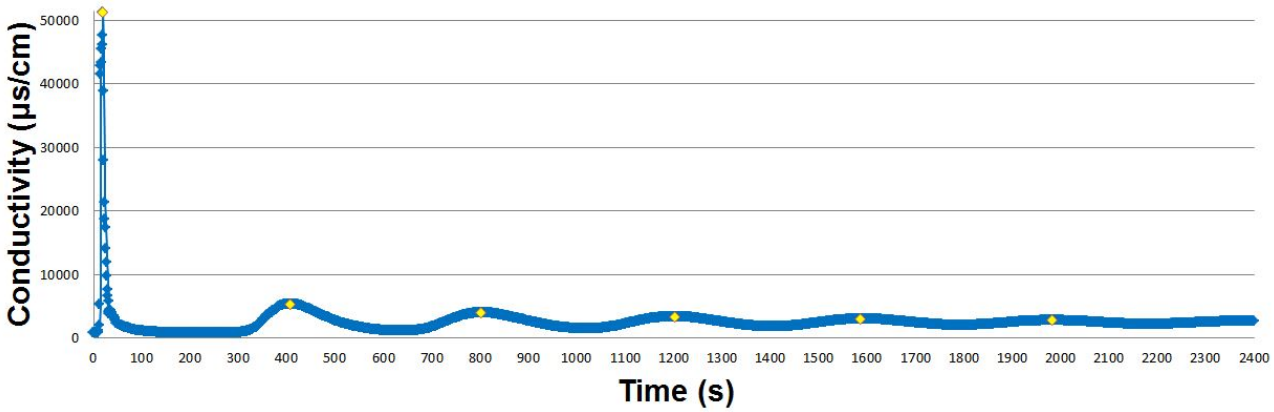

Figure 9: Evolution of the conductivity at 25°C at the outlet of the airlift during the small-scale tracer test of January 2020: $t_c = 393$ s.

3.2 O_2 transfer test

Once the circulation time is known, the transfer tests can be conducted. Those tests intend to quantify the transfer of oxygen and carbon dioxide between water and the atmosphere along the pond by calculating the value of the corresponding volumetric mass transfer coefficients $k_l a$ of O_2 and CO_2.

In order to quantify the mass transfer of O_2 and CO_2 between the water and the atmosphere, the concentration of the component of interest dissolved in the water has to be followed during the test, to be able to see how fast it is transferred to the atmosphere. All the transfer tests are conducted with clear water, without algae, such that there is no oxygen production and CO_2 consumption.

3.2.1 Methodology of the test

The concentration in dissolved oxygen (DO) in the water is assumed to be at its saturation value, which depends on the temperature. At 25°C for instance, it is equal to 8.3 mg/L [77]. If algae are present in the basin, the DO concentration can be superior to this saturation value as oxygen is produced by photosynthesis.

In order to observe a transfer, the concentration in DO is first lowered, then the transfer of oxygen from the atmosphere to the water occurs and the increase of the DO concentration is recorded to calculate the transfer coefficients.

The decrease of the DO concentration is obtained with the addition of anhydrous sodium sulfite in the pond. The sulfite consumes the oxygen present in the water and the concentration of DO decreases drastically. The reactions that occur are

$$Na_2SO_3 \rightarrow 2\ Na^+ + SO_3^{2-} \tag{3.1}$$

$$2\ SO_3^{2-} + O_2 \rightarrow 2\ SO_4^{2-} \tag{3.2}$$

The second reaction is catalysed by cobalt. The catalyst is added in the pond before the addition of the sulfite and a concentration of around 1 mg/L of cobalt is required to obtain an effective action.

Once the catalyst is well homogenised in the HRAP, after around five times the circulation time, the sulfite is added. The amount of sulfite is calculated to reach a concentration of 0 mg/L in oxygen in the basin. Regarding reactions (3.1) and (3.2), it is deduced that around 7.9 g of Na_2SO_3 are required per gram of O_2. The amount of oxygen present in the pond is the

product of the DO concentration at saturation measured with a probe before the test with the volume of liquid phase in the reactor.

The addition is performed continuously at one point of the reactor during a time few seconds shorter than the circulation time. Adding the reactant during this defined lapse of time allows to inject homogeneously the sulfite in the reactor and to consume the majority of the oxygen present in the pond as nearly all the water is in contact with the sulfite. It is thus essential to have conducted a tracer test previously to know precisely the circulation time in the pond and thus be able to add the sulfite optimally.

During the test, the evolution of the DO concentration is recorded with probes at both sides of the airlift. An example of the obtained graph is shown in Figure 10. The sulfite solution is added at time $t = 0$ at the outlet of the airlift, just before the position of the probe. The peaks at the beginning of the blue curve are due to the fact that the injection is done manually, thus not continuously, for practical issues, but the global effect is that the concentration in DO becomes null. This is indeed the case when the water reaches the inlet of the airlift after having crossed the channel, as it can be seen on the red curve: the sulfite has consumed all the oxygen initially present.

The beginning of the oxygen transfer is observed after a second lap and it can be seen that the oxygen is transferred from the atmosphere to the water step by step. Each peak is due to the passage of the water through the airlift, where the transfer is higher because of the important mixing of the water and the direct air injection. The peaks are followed by nearly horizontal stages corresponding to the flow of the water in the channel, where the transfer with the atmosphere is less important because of the poorer mixing and the absence of direct air injection.

An unexpected slight decrease of the DO concentration occurs after the first peak in Figure 10. This is certainly due to residual sulfite still present in the pond that had not reacted during the first lap as no more oxygen was available at that time. The intensity of the peaks decreases over time as the DO concentration approaches saturation, until the transfer becomes nearly monotonic and C_S is reached.

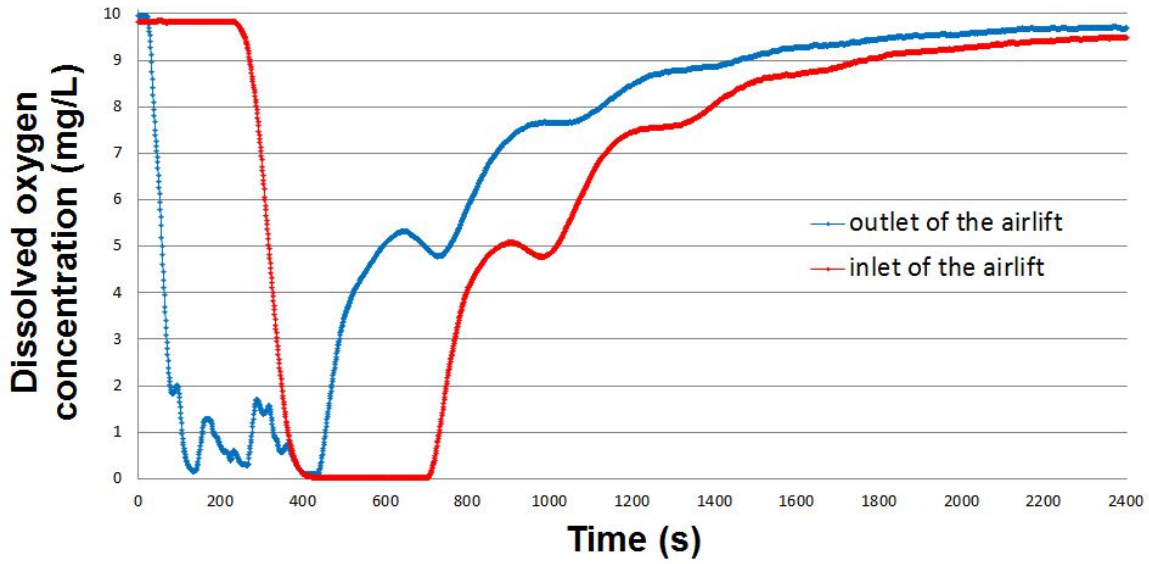

Figure 10: Evolution of the DO concentration at the inlet (red) and outlet (blue) of the airlift during the small-scale oxygen transfer test of January 2020.

The test is conducted until the DO concentration becomes close to its saturation value and the data recorded by both probes is used to calculate the values of the transfer coefficients of oxygen, as explained below.

3.2.2 Calculation of the transfer coefficients

To evaluate the mass transfer coefficient of oxygen between the liquid that flows inside the pond and the atmosphere, a mass balance on this component is applied. A Lagrangian description is used here, taking as control volume a fluid packet in the HRAP that is followed over time. Assuming that no O_2 is produced or consumed, the mass balance is

$$V \frac{dC}{dt} = k_l a \; V \; (C_S - C(t)) \tag{3.3}$$

where V is the volume of the water packet, C is the concentration of dissolved O_2 in water, t is the time and C_S is the concentration of dissolved O_2 at saturation that is measured with a probe before the beginning of the test. The two terms of the mass balance can be divided by the volume of the water packet as it is constant by definition.

To simplify the notations, the deficit D is used. It is defined as $D(t) = C_S - C(t)$, leading to

$$-\frac{dD}{dt} = k_l a \; D(t) \tag{3.4}$$

This equation can be integrated such that

$$D(t) = D_0 \exp(-k_l a \; t) \tag{3.5}$$

where $D_0 = C_S - C_0$, C_0 being the initial concentration in oxygen for the considered lapse of time. This equation can also be written as

$$\ln\left(\frac{D(t)}{D_0}\right) = -k_l a \; t \tag{3.6}$$

The test conducted in the HRAP allows to calculate the values of different $k_l a$. Three volumetric transfer coefficients are defined. The transfer along the whole HRAP is described with $(k_l a)_R$. The coefficients related to the two parts of the reactor can also be evaluated: $(k_l a)_A$ for the transfer in the airlift and $(k_l a)_{channel}$ for the transfer in the channel. Those coefficients are evaluated in s^{-1}.

Different methods exist to calculate the value of those coefficients. Those methods are described more precisely in [1], only a brief review is presented here.

whole reactor - $(k_l a)_R$

To evaluate the volumetric mass transfer coefficient of the entire pond, the assumption that the basin is a perfectly mixed tank is done. The curve of $\ln(D(t)/D_0)$ is drawn and, regarding Equation (3.6), it can be seen that the slope of this curve is supposed to be equal to $-(k_l a)_R$.

This equation is only valid from the moment when O_2 is no longer consumed until the DO saturation is reached. C_0 is the concentration in DO at the beginning of this interval.

The data recorded by the probes during the test is used to draw the curve and a linear regression in the range of validity of Equation (3.6) allows to find the value of $(k_l a)_R$. The range of validity of the equation starts when the oxygen consumption ends, so for the curve in Figure 10 recorded at the inlet of the airlift, it starts at around 1 000 s.

An example of the calculation of $(k_l a)_R$ with this method is presented in Figure 11.

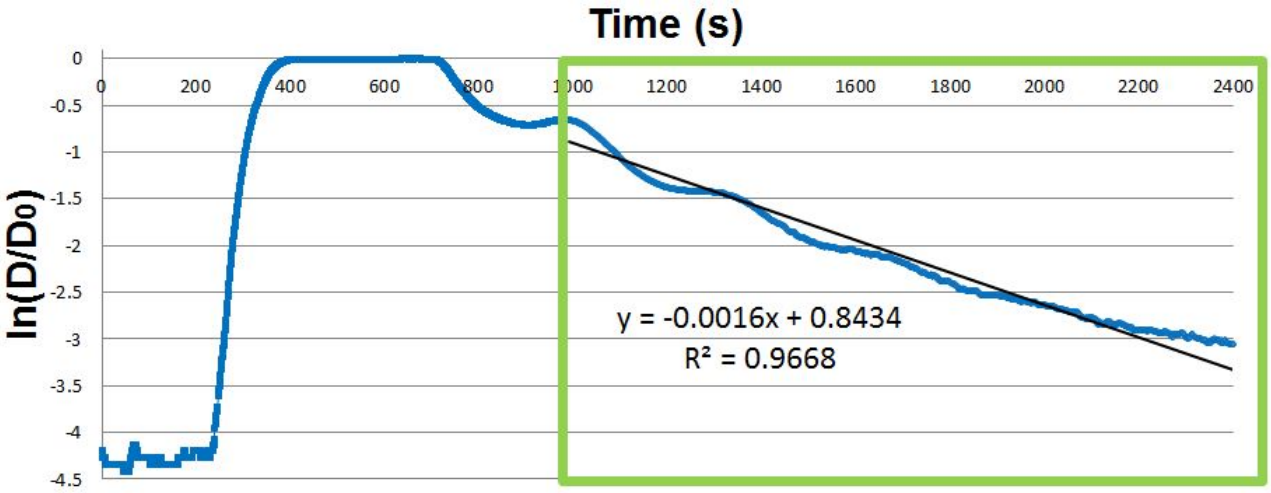

Figure 11: Curve of $\ln\left(D\left(t\right)/D_0\right)$ at the inlet of the airlift and linear regression in the relevant interval for the small-scale O_2 transfer test of January 2020: $\left(k_l a\right)_{\mathrm{R}} = 1.6{\times}10^{-3}$ s^{-1} ($\pm$ $1.5{\times}10^{-5}$ s^{-1}) / conditions: water temperature = 16.2°C - $V_{\mathrm{R}} = 408.9$ L - water height = 7 cm - $t_{\mathrm{c}} = 393$ s - $C_{\mathrm{S}} = 9.97$ mg/L.

The value obtained for the slope of the linear regression is always accompanied by its standard deviation, called s_m, which is the square root of the variance of the slope s_m^2. The standard deviation of the slope is defined as follows, with equations and notations from [78].

For an experimental curve composed of n points $y_i(x_i)$, the linear regression is of the form of

$$\widehat{y} = \widehat{m}x + \widehat{b} \tag{3.7}$$

The variance of the slope of the linear regression is defined as

$$s_m^2 = \frac{s_{y,x}^2}{S_{xx}} \tag{3.8}$$

where $s_{y,x}^2$ is the variance of $y(x)$ and is equal to

$$s_{y,x}^2 = \frac{1}{(n-2)} \sum_{i=1}^{n} \left(y_i - \widehat{y}_i\right)^2 \tag{3.9}$$

and where S_{xx} is defined as

$$S_{xx} = \sum_{i=1}^{n} \left(x_i - \bar{x}\right)^2 \tag{3.10}$$

with the mean $\bar{x}$ of the x_i experimental values, calculated with

$$\bar{x} = \frac{\sum_{i=1}^{n} \left(x_i\right)}{n} \tag{3.11}$$

All the values of the transfer coefficients calculated with linear regressions are given with their 95% confidence interval. According to [78], this interval can be approximated by

$$\left[\widehat{m} - 2s_m \ ; \ \widehat{m} + 2s_m\right] \tag{3.12}$$

if $n \geq 6$, which is the case for all the linear regressions built in this work. Each transfer coefficient calculated with this method is given in the form "$\widehat{m}$ ($\pm$ $2s_m$)" in this master thesis.

The linear regression method is applied similarly with the data of several probes measuring the O_2 concentration at different positions in the pond and the value of $(k_l a)_{\mathrm{R}}$ is the mean of all the obtained coefficients, $\widehat{m}_{\mathrm{mean}}$.

In this case, the standard deviation of the mean value of k slopes, $s_{m_{\mathrm{mean}}}$, is calculated based on [79] with the equation

$$s_{m_{\mathrm{mean}}} = \sqrt{\sum_{i=1}^{k} \left(s_{m_i}^2\right)} \tag{3.13}$$

and the 95% confidence interval is

$$[\widehat{m}_{\mathrm{mean}} - 2s_{m_{\mathrm{mean}}} \ ; \ \widehat{m}_{\mathrm{mean}} + 2s_{m_{\mathrm{mean}}}] \tag{3.14}$$

airlift - $(k_l a)_{\mathbf{A}}$

To evaluate the volumetric transfer coefficient of the airlift, two probes are required, one at the entrance and the other at the outlet of the airlift. The transfer coefficient of the airlift is calculated by isolating $k_l a$ in Equation (3.6):

$$(k_l a)_{\mathrm{A}} = \frac{-\ln\left(\frac{D(t+t_{\mathrm{A}})}{D_0(t)}\right)}{t_{\mathrm{A}}} \tag{3.15}$$

where t_{A} is the time for the water to cross the airlift, between the two probes. The value of $(k_l a)_{\mathrm{A}}$ is calculated continuously, between the end of the consumption of the oxygen by the sulfite and the moment when the saturation in DO is reached, and it is the mean of all the values obtained with (3.15) during this lapse of time that is taken as the actual value of $(k_l a)_{\mathrm{A}}$.

In (3.15), $D_0(t) = C_{\mathrm{S}} - C_0(t)$ and $D(t + t_{\mathrm{A}}) = C_{\mathrm{S}} - C(t + t_{\mathrm{A}})$, where C_{S} is the concentration of dissolved O_2 at saturation.

The studied transfer in the present case is the one occurring inside the airlift. To quantify it, a Lagrangian description of the water is used and the DO concentrations at the two ends of the airlift are compared: $C_0(t)$ is the concentration in DO at time t recorded with the probe B at the entrance of the airlift and $C(t + t_{\mathrm{A}})$ is the concentration in DO at time $(t + t_{\mathrm{A}})$ recorded with the probe A at the exit of the airlift. The transfer of oxygen from the injected air to the water inside the airlift can thus be quantified as it is the only source of DO concentration increase in this section of the HRAP.

Another possibility to evaluate the mass transfer coefficient of the airlift is by modelling the evolution of the deficit at the outlet of the airlift, based on the concentration recorded at its inlet. Equation (3.16) is used:

$$D(t + t_{\mathrm{A}}) = D_0 \exp\left((-k_l a)_{\mathrm{A}} \ t_{\mathrm{A}}\right) \tag{3.16}$$

where D is the deficit at the outlet of the airlift and D_0 is the deficit at the inlet of the airlift. The deficit at the outlet of the airlift is thus calculated with this equation, where t_{A} is fixed and $(k_l a)_{\mathrm{A}}$ is adjusted to minimise the sum of the squared residuals.

An example of the use of this model is presented in Figure 12. The model is compared to the actual deficit calculated with the data recorded by the probe at the outlet of the airlift. As explained previously, this model is only valid when there is no oxygen consumption, so inside the green frame, and the value of $(k_l a)_{\mathrm{A}}$ is calculated to fit the curve in this interval only. The validity interval starts when the O_2 consumption ends at the inlet of the airlift as it is the data with which the deficit at the outlet of the airlift is modelled. The validity interval starts thus after around 1 000 s.

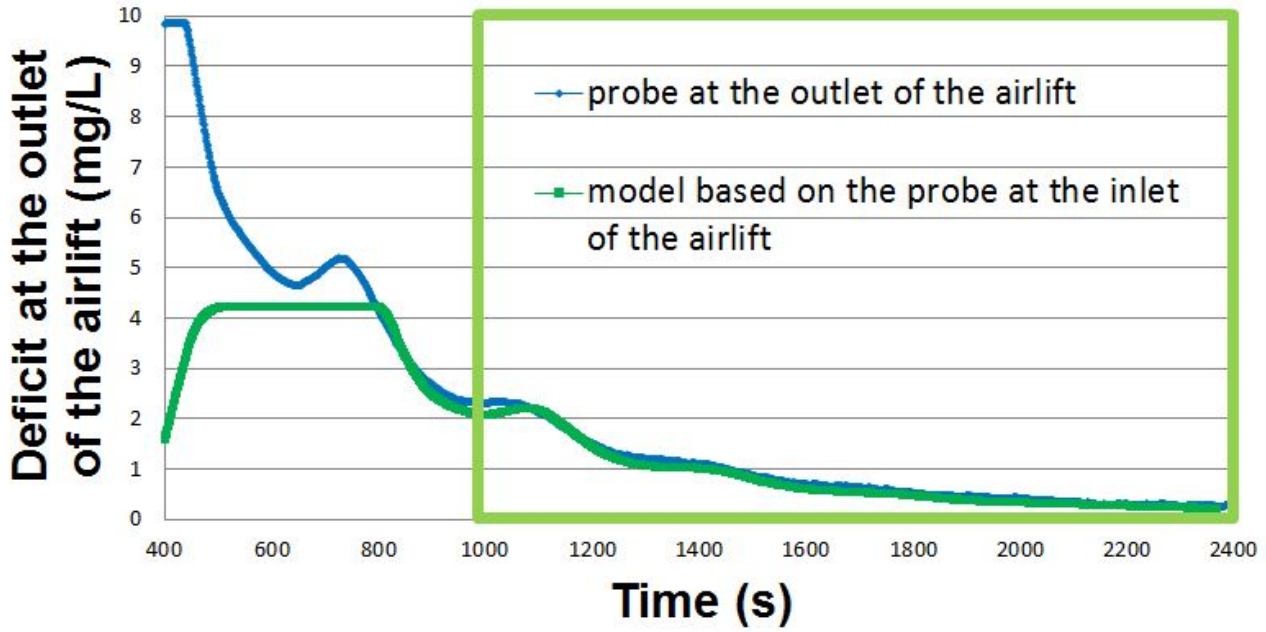

Figure 12: Evolution of the deficit at the outlet of the airlift: recorded by a probe (blue) and modelled on the basis of the data recorded at the inlet of the airlift (green) for the oxygen transfer test of January 2020; the green frame represents the zone in which the value of $(k_l a)_{\mathrm{A}}$ is adjusted to model the deficit: $(k_l a)_{\mathrm{A}} = 6.6 \times 10^{-3}$ s^{-1} / conditions: water temperature = 16.2°C - $V_{\mathrm{A}} = 70.9$ L - water height = 7 cm - $t_{\mathrm{A}} = 130$ s.

Both methods are used to calculate the transfer coefficient. Using Equation (3.15) with the data corresponding to Figure 12 gives a transfer coefficient of $(k_l a)_{\mathrm{A}} = 6.2 \times 10^{-3}$ s^{-1}, which is close to the value obtained with the model of $(k_l a)_{\mathrm{A}} = 6.6 \times 10^{-3}$ s^{-1}.

channel - $(k_l a)_{\mathbf{channel}}$

The transfer in the channel is calculated considering the fact that the total mass transferred along the whole reactor is the sum of the transfers in the channel and in the airlift. The value of $(k_l a)_{\mathrm{channel}}$ is thus calculated as follows:

$$(k_l a)_{\mathrm{R}} \ (C_{\mathrm{S}} - C_0) \ V_{\mathrm{R}} = (k_l a)_{\mathrm{A}} \ (C_{\mathrm{S}} - C_0) \ V_{\mathrm{A}} + (k_l a)_{\mathrm{channel}} \ (C_{\mathrm{S}} - C_0) \ V_{\mathrm{channel}} \tag{3.17}$$

$$(k_l a)_{\mathrm{channel}} = \frac{(k_l a)_{\mathrm{R}} \ V_{\mathrm{R}} - (k_l a)_{\mathrm{A}} \ V_{\mathrm{A}}}{V_{\mathrm{channel}}} \tag{3.18}$$

where V_{R} is the total volume of water in the HRAP, V_{A} is the volume of water in the airlift and V_{channel} is the volume of water in the channel. V_{channel} is thus equal to $V_{\mathrm{R}} - V_{\mathrm{A}}$.

It should be noted that the two methods detailed above used to calculate $(k_l a)_{\mathrm{A}}$ can be applied to estimate $(k_l a)_{\mathrm{channel}}$, and vice versa.

3.3 CO_2 transfer test

The test conducted to calculate the transfer coefficients of CO_2 in the HRAP is based on the same principle as for the oxygen transfer test. An important variation of the concentration in CO_2 dissolved in the pond is generated, then the evolution of the concentration is recorded until the steady state is reached. The transfer coefficients are then calculated with the obtained graphs.

Unfortunately, probes measuring the concentration of dissolved CO_2 in water are designed for larger concentration ranges than for that in the water used in HRAPs [10], so the concentration cannot be followed continuously for the CO_2. An alternative needs thus to be found to draw the evolution of the concentration of CO_2 in the water over time in order to calculate the value of the transfer coefficient.

The methodology proposed in this work is to take several samples during the test and to evaluate their concentration in dissolved CO_2, enabling to draw a discrete curve of the concentration in the HRAP over time, and then to calculate the transfer coefficient similarly to the O_2 transfer test. Only the transfer coefficient of the whole HRAP, $(k_l a)_{\mathrm{R}}$, is calculated in the CO_2 transfer tests, as explained afterwards.

3.3.1 Different forms of CO_3 coordinates in water

A first important remark concerning the quantification of the CO_2 transfer is that the CO_3 coordinate can be present in different forms in water. The following equations describe the acid-base pairs that are present:

$$\mathrm{CO_3^{2-}} + \mathrm{H^+} \rightleftharpoons \mathrm{HCO_3^-} \tag{3.19}$$

$$\mathrm{HCO_3^-} + \mathrm{H^+} \rightleftharpoons \mathrm{H_2CO_3} \tag{3.20}$$

The most present form depends on the pH of the water, as presented in Figure 13.

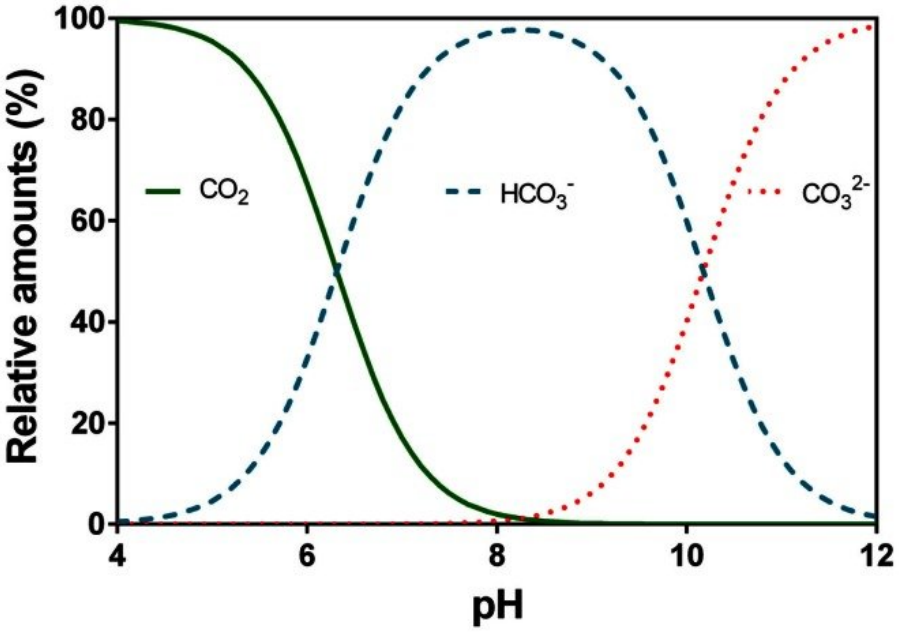

Figure 13: Fraction of CO_3 coordinates in water as a function of the pH at a temperature of 20°C and an electrical conductivity of 250 μs cm^{-1}: dissolved CO_2 (referred as $H_2CO_3^*$ in this work), bicarbonate ion (HCO_3^-) and carbonate ion (CO_3^{2-}) [80].

In water, the gaseous carbon dioxide is partially hydrated into carbonic acid H_2CO_3, following the equilibrium

$$CO_2 \ + \ H_2O \ \rightleftharpoons H_2CO_3 \tag{3.21}$$

The hydration reaction is fast and it is assumed that the equilibrium between the two forms is reached. The distinction between the gaseous and hydrated forms is often overlooked and the form $H_2CO_3^*$ is used to describe the sum of the CO_2 and the "actual" H_2CO_3 present in the water [81]. This form will be used in the developments.

Biologically, algae can easily assimilate CO_2 and bicarbonate but can hardly use carbonate [22].

3.3.2 Methodology of the test

Unlike in the O_2 transfer test, the concentration in CO_2 dissolved in the water is increased by the addition of an external product and it is its stripping that is studied during the test, so the transfer from the water to the atmosphere. However, as the same equations apply to the absorption and the stripping processes, the principle of the calculation of the CO_2 transfer coefficient is the same for the oxygen transfer test.

As explained in the previous section, the carbon dioxide is in the form of CO_3 coordinates when dissolved in water and it is the pH that defines which form is dominant.

To increase the concentration of CO_3 coordinates in the water, sodium bicarbonate is added into the HRAP to reach a concentration of around 2 g/L in $NaHCO_3$, so a concentration of around 17 mmol/L in CO_3 coordinates. The sodium bicarbonate is first dissolved in water and then added into the pond to avoid deposits at the bottom of the basin. The solution can be added simultaneously at different positions of the pond, the purpose being that the bicarbonate is equally distributed in the HRAP before the beginning of the test.

Once the CO_3 concentration is homogeneous in the basin, the test can start. As the objective is to measure the CO_2 transfer to the atmosphere, the CO_3 coordinates have to be in the form of $H_2CO_3^*$. The water being at a high pH, acid is added to decrease the pH and transform quantitatively all the CO_3 coordinates into $H_2CO_3^*$. The acid used in the present work is HCl and the amount added into the pond is such that all the bicarbonate will react to give carbonic acid. A little more than the stoichiometric requirement is thus injected to make sure that all the CO_3 coordinates end up as $H_2CO_3^*$. This stoichiometric amount is of around 0.62 g of HCl per gram of $NaHCO_3$ added into the pond.

The acid injection is similar to the sulfite injection of the oxygen transfer test: the liquid HCl is added continuously at the outlet of the airlift during a lapse of time few seconds shorter than the circulation time. Most of the CO_3 present in the water is thus in contact with the acid and passes in the form of $H_2CO_3^*$.

The transfer of the CO_2 to the atmosphere occurs then along the channel and in the airlift. The evolution of the concentration is expected to be comparable to that of the oxygen in the O_2 transfer test, except that here it is stripping that occurs: the concentration in dissolved CO_2 decreases over time as it is removed from the liquid. There are peaks in the curve when the liquid passes through the airlift and the transfer in the airlift is more important than along the channel due to higher mixing, so more dissolved CO_2 is removed from the water in that part of the HRAP.

As explained previously, no performing probe is available to record continuously the concentration in dissolved CO_2 [10]. To draw the curve and calculate the transfer coefficients, samples of around 25 mL are collected during the test in order to measure the CO_2 concentration at

different moments and draw a discrete curve. The samples are taken at the outlet of the airlift at regular times. A sample is first collected before the bicarbonate injection to have a reference value of the concentration in CO_2 at equilibrium. The second sample is taken just before the acid injection, then a sample is taken at the same position every lap, starting at the moment of the acid injection. Again, the knowledge of the circulation time is essential to take samples at relevant times. The samples of water should be such that no air is present in the flask to avoid CO_2 transfer between the liquid and the gas phase inside the flask.

To measure the concentration in CO_2 in each sample, manipulations are carried out and calculations lead to the desired value, as explained in the following sections. Those calculations require the knowledge of the temperature, the conductivity and the pH of each sample. Probes measuring those variables are thus placed at the sampling position during the test.

An example of the pH evolution during a test is presented in Figure 14. During this test, the initial pH was around 8, then the addition of acid lowered it. The evolution recorded before the first peak of the graph is supposed to be flat but some disturbances occurred due to the manual acid injection that was not perfectly continuous. After the injection period, peaks occurred at each lap of the water because the acid had been injected in a time few seconds shorter than the circulation time, so part of the water had not been in contact with the acid. Those peaks softened over time due to dispersion and transfer. It can be seen in Figure 14 that most of the time, the water was at a low pH, meaning that the CO_3 coordinates were in the form of $H_2CO_3^*$ and that it was indeed the CO_2 transfer between water and atmosphere that was observed. The periodic sampling moments are also highlighted in Figure 14.

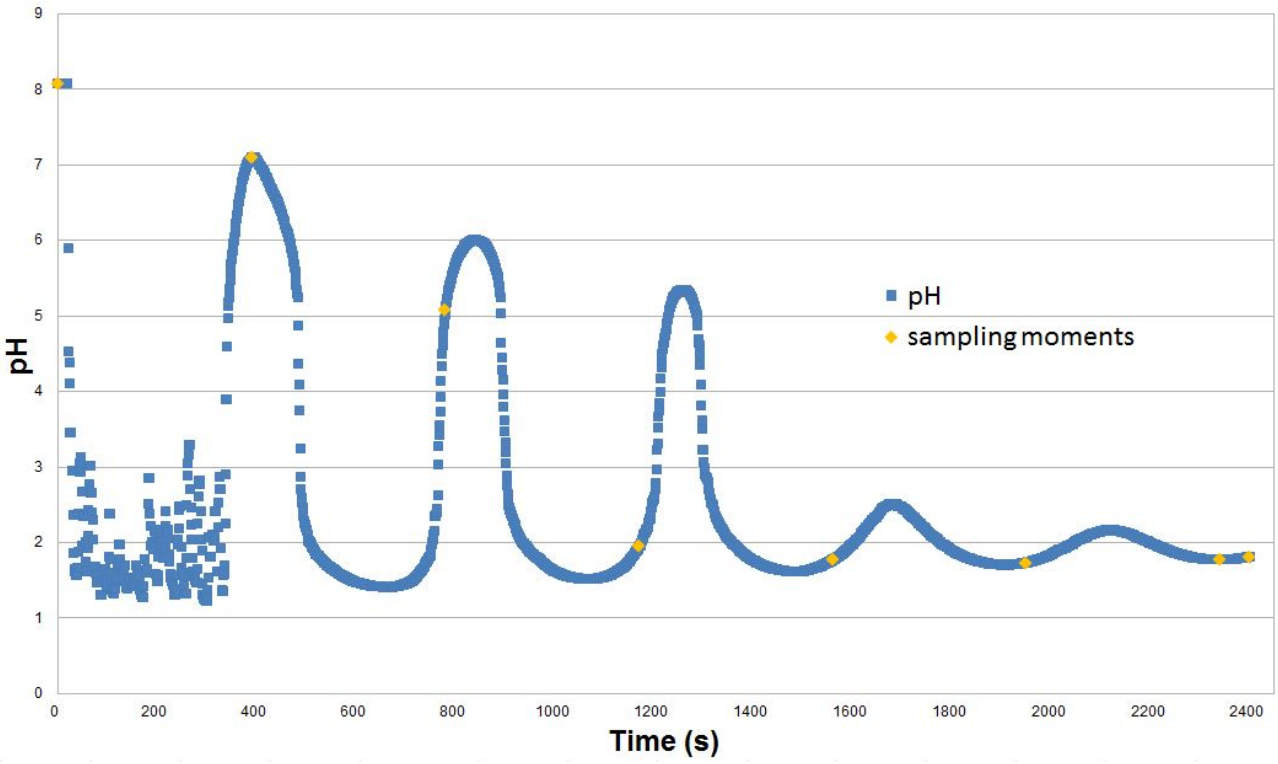

Figure 14: Evolution of the pH at the outlet of the airlift and sampling moments during the small-scale CO_2 transfer test **B** of January 2020.

3.3.3 Analysis of the samples

To evaluate the CO_2 concentration in the samples, a method developed by Hissel [9] is used. This method is described in details in [9] and its application on the present case is proposed in the next section.

Before developing the calculations that will lead to the CO_2 concentrations in the samples, some manipulations have to be carried out on each sample. The theory developed by Hissel [9] is based on the calculation of the total CO_3 coordinates concentration in the water, $[CO_{3_{tot}}]$. If this value is known, the amount of CO_2 present in the water can be deduced using a distribution function depending on the pH, the temperature and the ionic force of the water.

To measure the concentration in $CO_{3_{tot}}$, titrations are carried out on the samples with a pH-probe to draw the pH-curve. The pH-curve of carbonates contains two equivalent points at pH = 4.5 and pH = 8.3. An example of a pH-curve obtained with the titration of a sample with NaOH is presented in Figure 15.

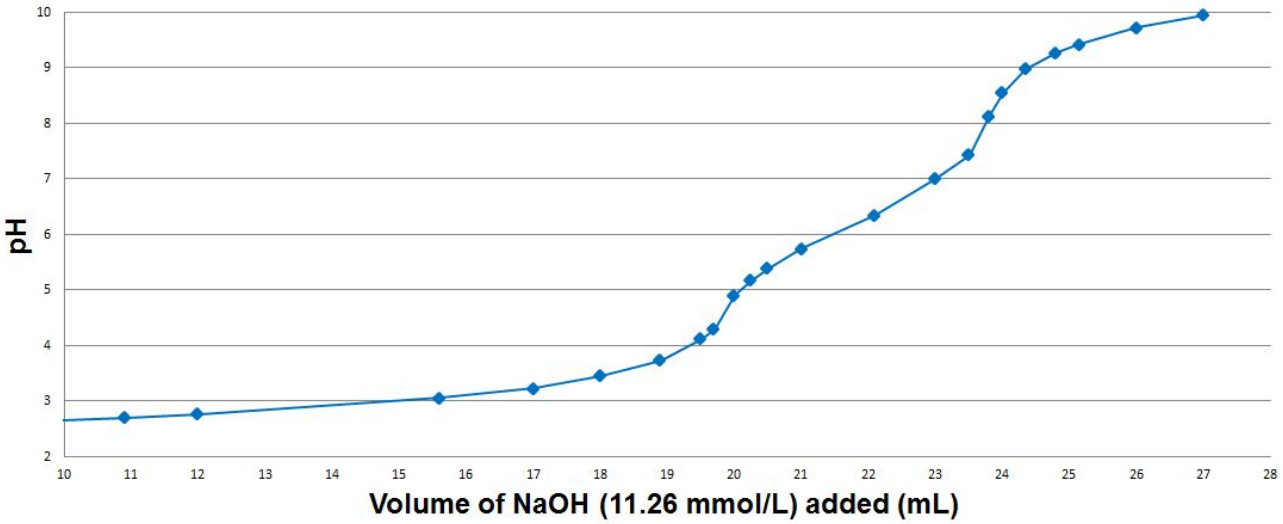

Figure 15: pH-curve of sample "B6" of 23.44 mL (conductivity of 9 400 μs/cm at 25°C) collected during the small-scale CO_2 transfer test **B** of January 2020, titrated at 25°C with a NaOH solution of 11.26 mmol/L.

The titrant used depends on the pH of the sample. If the pH is higher than 8.3, an acid solution is used as titrant, HCl for instance, and the pH-curve is drawn until around 3. In the case of a sample with a pH lower than 4.5, it is a basic solution such as NaOH that allows to draw the curve until a pH above 9, such that both equivalent points are passed through. When the pH of the sample is between the two equivalent points, the type of titrant is chosen to cover the largest pH-range possible between these two points.

To minimise the impact of experimental errors on the results, the amount of titrant that is used in the calculations is the amount required to go from the first equivalent point to the second one, if the pH curve passes through these two points [9]. In Figure 15 for instance, the corresponding volume of titrant is equal to $23.9 - 19.8 = 4.1$ mL. If the pH of the sample is between the two equivalent points, *i.e.* between 4.5 and 8.3, the volume considered is the volume that allows to reach the appropriate equivalent point starting with the pH of the sample.

3.3.4 Calculation of the concentration in CO_2

The data obtained with the titration serves to the evaluation of the concentration in CO_2 in the sample. The method developed by Hissel [9] is applied for the present case. One must pay attention to the fact that in this theory, the temperatures are evaluated in °C unless explicitly stated otherwise.

This method is based on the calculation of the concentration in $CO_{3_{tot}}$ in the sample. Once this value is known, the amount of CO_2 present is deduced, regarding the pH and other variables.

The notations used for the calculations are the same as in [9].

$[CO_{3_{tot}}]$ in the sample

The first step in the estimation of the CO_2 concentration in the HRAP is the calculation of the concentration in $CO_{3_{tot}}$ in each sample. This estimation in based on the data obtained during the titration, so the temperature at which the different variables are evaluated is the temperature of the sample during the titration. Some adaptations will thus be required while using the data, as explained later in the developments.

To calculate the amount of $CO_{3_{tot}}$ present in the sample, the concept of Total Potential Acidity (TPA) is used. The TPA, also named $[H^+_{tot}]$, is defined as the concentration of all the coordinates that could release protons in solution, including H_2O. In the case of pure water for instance, the TPA is

$$[H^+_{tot}] = [H^+] + [H_2O] \tag{3.22}$$

as the H^+ particles can either be in the form of free H^+ particles or be linked to OH^- groups to form H_2O.

To evaluate the amount of $CO_{3_{tot}}$ present in the sample, two formulas are used, depending on the type of titrant added. If the titration is conducted with an acid, the TPA varies because acid is added into the solution. The added H^+ particles are either engaged in the acidic molecules present in the water, such as H_2CO_3, HCO_3^- or H_2O, or stay as free H^+. The amount of H^+ added during the titration is equal to the variation of the TPA and this variation takes into account the contributions of all the coordinates present in the water. The equation developed in [9] that corresponds to the TPA variation between the initial and final pH of the titration is

$$[H^+_{added}] = \Delta\,(1 - f_{11})\ \ [OH_{tot}] + \Delta f_{12}\ [CO_{3_{tot}}] + \Delta\left(\frac{10^{-pH}}{\gamma_1}\right) \tag{3.23}$$

If the sample is titrated with a base, the TPA is not impacted as no H^+ is added into the medium. However, the concentration in OH coordinates increases due to the addition of OH^- groups, and expressing the fact that the TPA remains constant while $[OH_{tot}]$ increases leads to the equation

$$[OH^-_{added}] = \frac{\Delta\,(f_{11})\ \ [OH_{tot}] + \Delta f_{12}\ [CO_{3_{tot}}] + \Delta\left(\frac{10^{-pH}}{\gamma_1}\right)}{-f_{11_{final}}} \tag{3.24}$$

The obtainment of those two equations is described in details in [9].

For each sample, one of those two equations is used to evaluate $[CO_{3_{tot}}]$ after having calculated all the other terms of the formula as explained below. In both equations, the concentrations are evaluated in mol/L, γ_i is the activity coefficient of the CO_3 coordinate form i and the variables f_{11} and f_{12} are functions of the pH, the activity coefficients and the equilibrium constants of the equilibria between the different CO_3 coordinate forms.

It should be noted that the titration induces an increase of the volume of the solution in the container in which the sample is titrated, so the concentration $[CO_{3_{tot}}]$ obtained with the previous equations is the concentration in the total final volume of the titration, *i.e.* the sum of the sample and titrant volumes. A correction will thus be required in the end to evaluate the concentration in $CO_{3_{tot}}$ in the sample itself, assuming that the added titrant does not contain any CO_3 coordinate.

As explained above, $[H^+_{added}]$ and $[OH^-_{added}]$ are respectively the concentrations in added H^+ and in added OH^-. They are equal to the amount of titrant added between the two equivalent points of the pH-curve divided by the final total volume in the container in which the titration is conducted, so the sum of the sample and the added titrant volumes. The titrant solutions need thus to be calibrated to know exactly the amounts of H^+ and OH^- added to the sample.

$[OH_{tot}]$ is a rather unusual concept: it represents the concentration of water in water. Knowing that the density of water is equal to 1 000 g/L at 4°C, $[OH_{tot}]$ equals

$$[OH_{tot}\,(4°C)] = \frac{\text{density}}{\text{molar mass}} = \frac{1\ 000\ \text{g/L}}{18.015\ \text{g/mol}} = 55.51\ \text{mol/L} \tag{3.25}$$

However, the volume of water varies with the temperature. If the temperature is higher than 4°C, the volume will increase and thus the concentration $[OH_{tot}]$ will decrease. In order to take that effect into account, the variable g is used.

g is defined as the relative volume of water. A reference volume is chosen, corresponding to a reference temperature t_{ref}, and the ratio between this volume and the volume at the temperature of interest t is defined as

$$g\,(t) = \frac{V\,(t_{ref})}{V\,(t)} \tag{3.26}$$

The value of g is thus smaller than 1 if the operating temperature is higher than the reference temperature.

There exist different relations that give the value of g at a given temperature, depending on which reference temperature is chosen. A reference temperature close to the operating temperature should be considered to use the most appropriate correlation of $g\,(t)$. In the present case, the reference temperature is chosen at 20°C as the manipulations are conducted in conditions close to this temperature. The relative volume of water at 20°C compared to that at 4°C is equal to 1.00177 [9], so

$$[OH_{tot}\,(20°C)] = \frac{[OH_{tot}\,(4°C)]}{1.00177} = 55.41\ \text{mol/L} \tag{3.27}$$

The correlation that gives $g\,(t)$ with a reference temperature of 20°C is

$$g\,(t) = \frac{1.0021387}{0.000003882\ t^2 + 0.000055796\ t + 0.99947}\ ,\ t \text{ in °C [10]} \tag{3.28}$$

It can be verified that 20°C is the reference temperature in (3.28) as $g = 1$ if $t = 20$°C.

The value of $[OH_{tot}]$ at the titration temperature is thus calculated as follows:

$$[OH_{tot}\,(t_{titration})] = 55.41\ g\,(t_{titration}) \tag{3.29}$$

The next variables to evaluate in Equations (3.23) and (3.24) are the activity coefficients γ_i. For the component i, the activity coefficient is found with the equation

$$log\left(\gamma_i\right) = -A\ z_i^2\ \sqrt{J}\ ,\ \text{if } J \leq 0.02 \tag{3.30}$$

or

$$log\left(\gamma_i\right) = \frac{-A\ z_i^2\ \sqrt{J}}{1+\sqrt{2J}}\ ,\ \text{if } J > 0.02 \tag{3.31}$$

In these equations, A is a function of the temperature t defined as

$$A = \frac{1.826 \times 10^6}{\left(\epsilon\left(t+273.15\right)\right)^{1.5}} \tag{3.32}$$

with the dielectric constant ϵ of the water

$$\epsilon = 78.54\left(1 - 0.0046\left(t-25\right) + 0.0000088\left(t-25\right)^2\right) \tag{3.33}$$

z_i is the valence of the component i. γ_1 corresponds to the ion HCO_3^- so $z_1 = -1$ while γ_2 is related to CO_3^{2-} so $z_2 = -2$.

The last parameter required to calculate the activity coefficients is the ionic force J of the water. It is defined in [9] as a function of the concentrations m_i and valences z_i of all the components present in the water:

$$J = \frac{1}{2}\sum_i m_i\ z_i^2 \tag{3.34}$$

However, it is complicated to use this definition practically, so a satisfactory approximation based on empirical correlations is used instead to calculate the value of J at the reference temperature of 20°C:

$$J\left(20°\text{C}\right) = \frac{\exp\left(10.243 - 1.157\ \ln\left(\rho\left(20°\text{C}\right)\right)\right)0.0015 + \frac{16.5}{\rho(20°\text{C})}}{2}\ [10] \tag{3.35}$$

where ρ is the resistivity measured in ohm.cm, which is equal to the inverse of the conductivity, in μs/cm. The conductivity is measured during the test. Depending on the probe, the conductivity can either be given at the temperature of the test or at a standard temperature. In both cases, a correction needs to be applied to obtain the value of the resistivity at 20°C and use Equation (3.35). For a probe giving the conductivity at t_{probe}, the correction is

$$\rho\left(20°\text{C}\right) = \frac{\rho\left(t_{\text{probe}}\right)}{g\left(t_{\text{probe}}\right)} \tag{3.36}$$

as the reference temperature in the definition of g is 20°C.

The value of the ionic force at the titration temperature is then obtained with

$$J\left(t_{\text{titration}}\right) = J\left(20°\text{C}\right)\ \ g\left(t_{\text{titration}}\right) \tag{3.37}$$

All the required data is now available to calculate the activity coefficients of the different forms of carbonate in the water at the titration temperature.

The last variables that are required in Equations (3.23) and (3.24) to evaluate the concentration in $CO_{3_{tot}}$ are f_{11} and f_{12}. Those coefficients are distribution functions calculated for real solutions. They depend on several parameters such as the pH of the sample, the conductivity and the temperature. They are defined as follows:

$$f_{11} = \frac{1}{1 + \frac{K_0}{\gamma_1\ 10^{-\mathrm{pH}}}} \tag{3.38}$$

$$f_{12} = \frac{2\ \gamma_2\ 10^{-2\mathrm{pH}} + \frac{\gamma_2}{\gamma_1}\ K_1\ 10^{-\mathrm{pH}}}{\gamma_2\ 10^{-2\mathrm{pH}} + \frac{\gamma_2}{\gamma_1}\ K_1\ 10^{-\mathrm{pH}} + K_1\ K_2} \tag{3.39}$$

where K_0 is the equilibrium constant of water dissociation and K_1 and K_2 are the equilibrium constants of the CO_3 coordinates forms:

$$K_0 = \frac{[H^+]\ [OH^-]}{[H_2O]} = 1.825 \times 10^{-16} \text{ at } 25°C \text{ [9]} \tag{3.40}$$

$$K_1 = \frac{[H^+]\ [HCO_3^-]}{[H_2CO_3^*]} = 4.31 \times 10^{-7} \text{ at } 25°C \text{ [9]} \tag{3.41}$$

$$K_2 = \frac{[H^+]\ [CO_3^{2-}]}{[HCO_3^-]} = 5.61 \times 10^{-11} \text{ at } 25°C \text{ [9]} \tag{3.42}$$

It should be noted that the equilibrium constant of the water dissociation is often defined as the product of K_0 and $[H_2O]$ but it is not the case in [9]. The correlations used to calculate this product need thus to be divided by $[H_2O]$, which is in fact the concentration $[OH_{tot}]$ defined previously and calculated with Equation (3.29).

The values of the three equilibrium constants depend on the temperature T, in K here. They are calculated with the following equations adjusted from their values at different temperatures:

$$\ln\left(K_0\ [OH_{tot}\ (T - 273.15)]\right) = 148.9802 - \frac{13847.26}{T} - 23.6521\ \ln(T)\ \text{ [10]} \tag{3.43}$$

$$\ln(K_1) = 290.9097 - \frac{14554.21}{T} - 45,0575\ \ln(T)\ \text{ [10]} \tag{3.44}$$

$$\ln(K_2) = 207.6548 - \frac{11843.79}{T} - 33,6485\ \ln(T)\ \text{ [10]} \tag{3.45}$$

All the terms of Equations (3.23) and (3.24) are now known and the concentration in $CO_{3_{tot}}$ in the container can be found. In the case of an acid titrant, it is equal to

$$[CO_{3_{tot}}]_{\text{container}} = \frac{[H^+_{\text{added}}] - \Delta\,(1 - f_{11})\ [OH_{tot}] - \Delta\left(\frac{10^{-\mathrm{pH}}}{\gamma_1}\right)}{\Delta f_{12}} \tag{3.46}$$

and for a titration with a base, it is

$$[CO_{3_{tot}}]_{\text{container}} = \frac{-f_{11_{\text{final}}}\ [OH^-_{\text{added}}] - \Delta\,(f_{11})\ [OH_{tot}] - \Delta\left(\frac{10^{-\mathrm{pH}}}{\gamma_1}\right)}{\Delta f_{12}} \tag{3.47}$$

In those equations, the Δ corresponds to the difference between the initial and final points of the range of pH of interest and $f_{11_{\text{final}}}$ is the value of f_{11} evaluated at the final pH. If the pH of the sample, is smaller than 4.5 or greater than 8.3, the range of pH is between 4.5 and 8.3 as

both equivalent points are passed through during the titration. The initial and final pH values are thus 4.5 and 8.3 in this case, and vice versa, depending on whether the titration is carried out with an acid or a base. In the case of a sample with an intermediate pH, the initial pH is the pH of the sample and the final pH is the pH of the equivalent point reached during the titration.

The concentration in $CO_{3_{tot}}$ in the sample is obtained with Equation (3.48), assuming that the added titrant does not contain any CO_3 coordinate. $V_{container}$ is the volume of liquid in the container at the end of the titration and V_{sample} is the initial volume of water in the sample.

$$[CO_{3_{tot}}]_{sample} = [CO_{3_{tot}}]_{container} \frac{V_{container}}{V_{sample}} \tag{3.48}$$

$[CO_{3_{tot}}]$ in the HRAP

The concentration in $CO_{3_{tot}}$ in the samples being known, it is possible to calculate the concentration in $CO_{3_{tot}}$ in the HRAP with the variable g. Indeed, the temperature of the test being different from the temperature during the titrations, the volumes of water are not similar in the two situations.

The formula is obtained as follows:

$$[CO_{3_{tot}}(t_{test})] = \frac{n(CO_{3_{tot}})}{V(t_{test})} \tag{3.49}$$

$$[CO_{3_{tot}}(t_{test})] = \frac{n(CO_{3_{tot}})}{V(t_{titration})} \frac{V(t_{titration})}{V(t_{test})} \tag{3.50}$$

$$[CO_{3_{tot}}(t_{test})] = \frac{n(CO_{3_{tot}})}{V(t_{titration})} \frac{V(t_{titration})}{V(t_{ref})} \frac{V(t_{ref})}{V(t_{test})} \tag{3.51}$$

$$[CO_{3_{tot}}(t_{test})] = \frac{n(CO_{3_{tot}})}{V(t_{titration})} \frac{1}{g(t_{titration})} g(t_{test}) \tag{3.52}$$

$$[CO_{3_{tot}}(t_{test})] = [CO_{3_{tot}}(t_{titration})] \frac{g(t_{test})}{g(t_{titration})} \tag{3.53}$$

$[CO_2]$ in the HRAP

The concentration in CO_2 in the HRAP can finally be calculated at every sampling moment. As explained previously and shown in Figure 13, the ratio of $H_2CO_3^*$ compared to the total amount of carbonate depends on the pH. In [9], this ratio is named d_{32} and is defined as

$$[H_2CO_3^*] = d_{32}\ [CO_{3_{tot}}] \tag{3.54}$$

The distribution function defining d_{32} provided in [9] is

$$d_{32} = \frac{\gamma_2\ 10^{-2pH}}{\gamma_2\ 10^{-2pH} + \frac{\gamma_2}{\gamma_1}\ K_1\ 10^{-pH} + K_1\ K_2} \tag{3.55}$$

where all the variables are evaluated in the conditions of the test. The variables required to calculate d_{32} are ϵ, A, J, γ_1, γ_2, K_1 and K_2. The temperature and conductivity recorded by the probe at the corresponding sampling moment are used.

The pH recorded during the test might be different from the pH of the sample measured before the titration because some carbon dioxide may leave as gas when the sample is opened to be titrated or because the buffers used to calibrate the pH probe of the titrations might be a little different from those used for the probe of the test for instance. The pH recorded by the

probe is used in Equation (3.55) to consider the conditions of the test and thus decrease the risk of error.

The equilibrium constant of the reaction (3.21) being of the order of 10^{-3} [82], it is assumed that the concentration in dissolved CO_2 is equal to the concentration in $H_2CO_3^*$.

The method presented above is used to calculate the concentration in dissolved CO_2 in the HRAP at each sampling moment and the discrete curve of its evolution is drawn.

An example of the curves of $[CO_{3_{tot}}]$ and $[CO_2]$ in the HRAP over time is presented in Figure 16. This graph can be analysed along with Figure 14 where the sampling moments are highlighted.

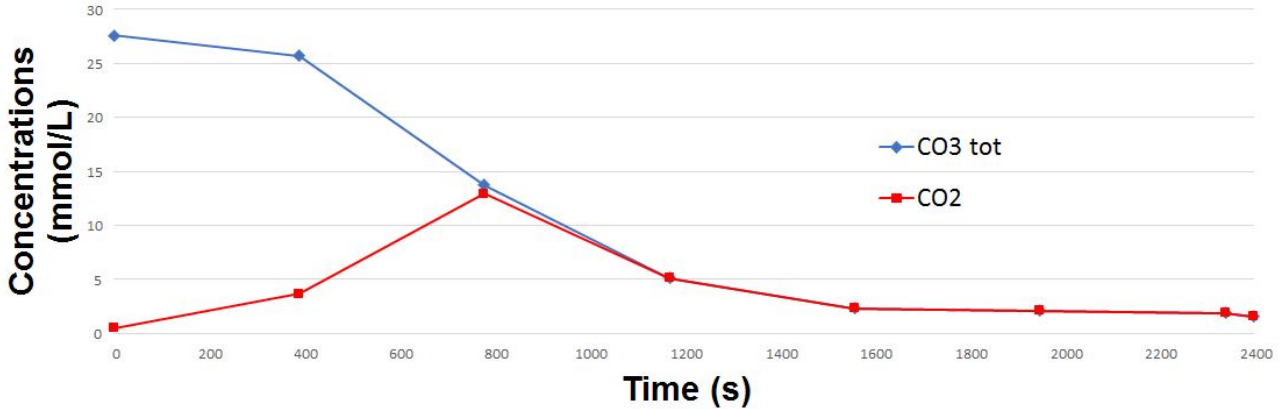

Figure 16: Evolution of $[CO_{3_{tot}}]$ and $[CO_2]$ at the outlet of the airlift during the small-scale CO_2 transfer test **B** of January 2020 / conditions: water temperature = 16.3°C - V_R = 408.9 L - water height = 7 cm - t_c = 393 s.

The first sample in the graph shown in Figure 16 is collected at time $t = 0$ s just before the beginning of the acid injection. The concentration in $CO_{3_{tot}}$ is high due to the sodium bicarbonate added in the basin before the test, while the concentration in CO_2 is close to zero because of the high pH of the water. It can be seen in Figure 14 that the second sample still has a high pH, close to 7, so the second point of the $[CO_2]$ curve is still small compared to the concentration in $CO_{3_{tot}}$. Afterwards, the concentration in CO_2 and $CO_{3_{tot}}$ are nearly equal as the pH of the samples is lower than 5 and both concentrations decrease over time due to the transfer from the water to the atmosphere.

Unlike in the O_2 transfer test, no peak is observed at each passage of the water through the airlift. The actual evolution of the concentration in CO_2 is expected to encounter those peaks but the methodology followed to characterise it does not allow to see them. However, these peaks could be easily detected by collecting more samples per lap, but more manipulations would be required as all these samples would have to be titrated.

Another possibility for the quantification of the CO_2 transfer in HRAPs would be to measure the CO_2 concentration in the headspace of the airlift, *i.e.* above the water level at the top of the airlift. This would allow to use devices measuring the CO_2 concentration in gas phase, or even to work with gas chromatography, which may be an easier method to implement than the one described in the present work.

A similar method is already followed for the oxygen transfer in gas injection systems: the "off-gas" method. The difference between the oxygen concentrations in the injected gas and in the gas leaving the water after having crossed it inside the airlift indicates how much oxygen is transferred to the liquid phase [83, 84].

Adapting this method to the CO_2 transfer would thus be a possibility for its quantification.

3.3.5 Calculation of the transfer coefficient

The curve of the evolution of the CO_2 concentration over time allows to calculate the transfer coefficient of CO_2 between the water and the atmosphere, with a method similar to that of the oxygen transfer. However, only the transfer coefficient along the whole HRAP $(k_l a)_R$ can be evaluated here as the curve is drawn at one point of the pond only. If the transfers along the channel and inside the airlift need to be quantified too, samples at the entrance of the airlift have to be taken too and the same analysis method can be followed to draw a second curve. In this case, the samples at the outlet of the airlift should be collected at each lap, as described previously, while those at the entrance of the airlift should be taken at each lap too, but shifted in time by the time required to cross the channel in order to apply Equation (3.15) as for the oxygen transfer.

Similarly to the calculation of $(k_l a)_R$ for the oxygen, a mass balance is applied on the dissolved CO_2 in the water of the whole basin. Assuming that no CO_2 is produced or consumed, the relations (3.3) to (3.6) are obtained and the curve $\ln(D(t)/D_0)$ is drawn.

In this development, $D(t) = C_S - C(t)$ and $D_0 = C_S - C_0$, where $C(t)$ is the concentration of dissolved CO_2 in the water at time t, C_S is the concentration of dissolved CO_2 at equilibrium, so corresponding to the sample collected before the bicarbonate injection, and C_0 is the concentration of the first sample of the interval in which the linear regression is built.

The curve of $\ln(D(t)/D_0)$ is drawn in the time interval in which the concentration in CO_2 decreases and the slope of its linear regression gives the value of $-(k_l a)_R$. An example of this graph is presented in Figure 17 and the definition of this time interval is explained more precisely in Section 4.4.2.

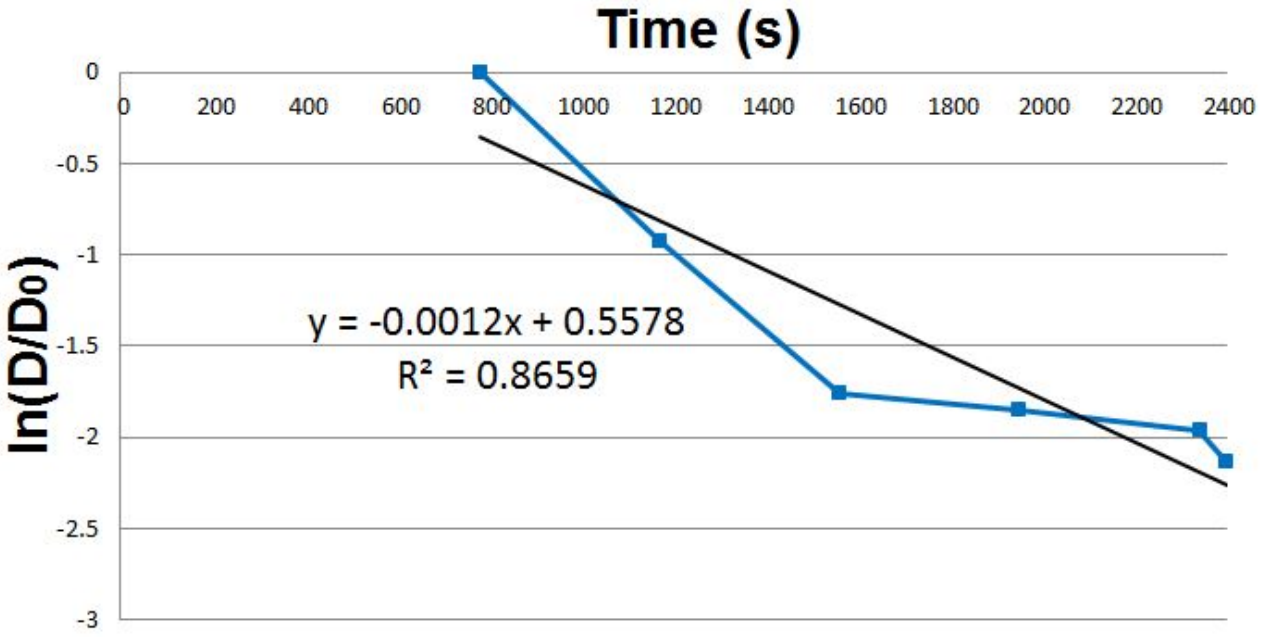

Figure 17: Curve of $\ln(D(t)/D_0)$ at the outlet of the airlift and linear regression for the small-scale CO_2 transfer test **B** of January 2020: $(k_l a)_R = 1.2 \times 10^{-3}$ s^{-1} ($\pm$ 4.6×10^{-4} s^{-1}) / conditions: water temperature = 16.3°C - V_R = 408.9 L - water height = 7 cm - t_c = 393 s - C_S = 0.08 mmol/L.

The method proposed for the evaluation of the volumetric transfer coefficient of CO_2 in the HRAP is less precise than for the O_2 transfer because manipulations are required, leading to possible errors in the results, and because the curve on which the calculation of $k_l a$ is based is discrete as only a finite number of samples are taken. Moreover, the time required to analyse the samples can be consequent as the pH-curve of the titration needs to be drawn for each sample collected. This method presents thus some drawbacks, but it allows to quantify the transfer of CO_2 to the atmosphere in a HRAP. The value of the volumetric mass transfer coefficient of CO_2 in this type of basin is not easily obtained due to the lack of appropriate probes [10] and a method such as the one proposed in this work can help for the optimisation of the operating conditions in HRAPs.

4 Tests conducted on a small scale

The tests presented in the previous section were first conducted on a small scale, in order to have reference values of the mass transfer coefficients and to optimise the manipulations before carrying them on a large scale. Those tests were performed on two small-scale pilots situated in the "Ferme du Faascht", Kessler SCRL, in Arlon, Belgium, which is a partner of an *Interreg* project called *Persephone*.

Two batteries of small-scale tests were conducted in the scope of this work. The first session took place on 4 and 5 September 2019 and the second on 29 and 30 January 2020. During each session, the volume of water and its flow rate were kept constant for all the tests to compare the results of the different types of tests.

As mentioned previously, the HRAPs operated with total recirculation and the water did not contain algae in order to characterise the transfer in a base case and avoid production of O_2 and consumption of CO_2.

4.1 HRAP characteristics

The three types of tests were conducted in two small-scale HRAPs. A picture of the smallest basin, "basin 1", can be seen in Figure 8 and the largest basin, "basin 2", is shown in Figure 18. The first test session, in September 2019, was carried out in the smallest pond, basin 1, and the second test session, in January 2020, was conducted in basin 2, as were the tests performed in [1].

It should be noted that in other works conducted in the scope of the *Renewable* project that involve these basins, the small basin is called "basin 3" and the large one is called "basin 1". However, in order to simplify the reading of this report, a chronological numbering is used such that the first test session is performed in "basin 1" and the second in "basin 2".

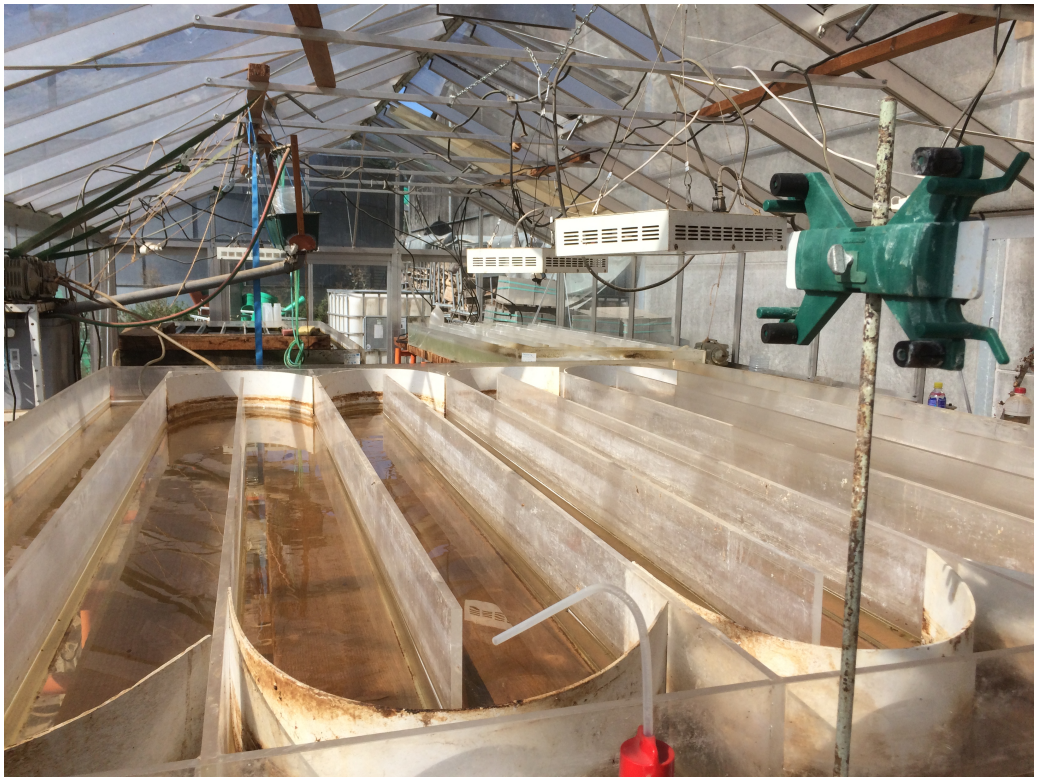

Figure 18: Small-scale HRAP ("basin 2") used to perform the tests of January 2020.

The two basins contain several rectangular walls that define the path followed by the water. The water circulates inside the channel and is set into motion in the airlift, where diffusers add air and push the water inside the channel.

The dimensions of the two basins are shown in Figures 40 and 41 in Appendix 8.2.1. The volumes of water in the basins and in their respective channel and airlift are gathered in Table 1.

Table 1: Height and volumes of water in the two small-scale HRAPs used for the test sessions of September 2019 and January 2020.

Height and volume	September 2019 (basin 1)	January 2020 (basin 2)
water height (cm)	9.8	7
V_{R} (L)	267.1	408.9
V_{A} (L)	22	70.9
V_{channel} (L)	245.1	338

A picture of the airlift system of basin 1 is presented in Figure 19. A similar system is used in basin 2. The water enters in the airlift, flows to the bottom and is pushed by the air injected through the diffusers. The water leaves then the airlift and starts to circulate inside the channel.

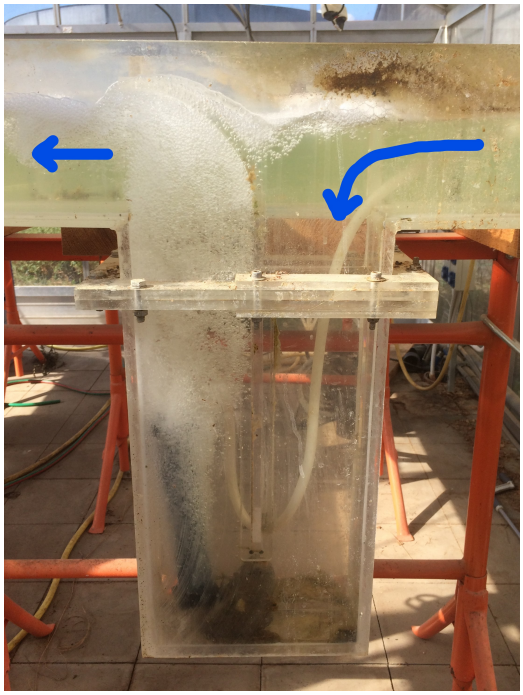

Figure 19: Airlift system used in basin 1 and direction of the water flow.

The last characteristic of the small-scale basins is the presence of curved wood sheets at the edges of the rectangular walls. Those curves are placed to decrease the energy losses of the flow and to copy more precisely the configuration of the tests conducted in [1] and of large-scale HRAPs in general.

For the tests conducted in basin 1, cut plastic bottles have also been used to mimic the shape of large-scale HRAPs. Both wood sheets and plastic bottles can be seen in Figure 20.

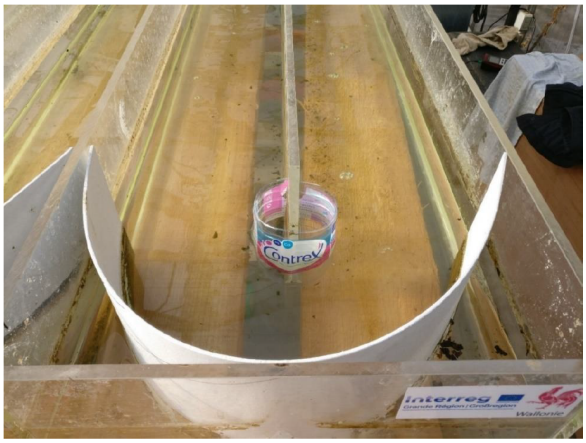

Figure 20: Curved wood sheets and cut plastic bottles used in the small-scale basins to mimic the shape of large-scale HRAPs [1].

4.2 Tracer tests

For each test session, the first type of test conducted is the tracer test. As explained in the test presentation, tracer tests are essential for the evaluation of transfer coefficients as they allow to determine the value of the circulation time t_c.

The ideal situation would have been to have water velocities close to those in [1] in order to compare the results. However, even if the ceramic diffusers available for the tests were those used in [1], they had got partially clogged during the two years separating the tests. They have thus been soaked in acid for cleaning and to improve their performances, but they never reached their initial performances of [1]. The water velocities in the two test sessions conducted in this work are thus smaller than that in [1].

4.2.1 Test of September 2019

The test session of September 2019 took place nearly two years after the work of [1]. During the first test session, all the tests were performed in basin 1 with a height of water of 9.8 cm.

At the beginning of the tracer test, 201 g of NaCl were injected. The conductivity curve obtained is presented in Figure 21. This curve was recorded at the outlet of the airlift. The circulation time corresponding to the tests of September 2019 is of 227 s.

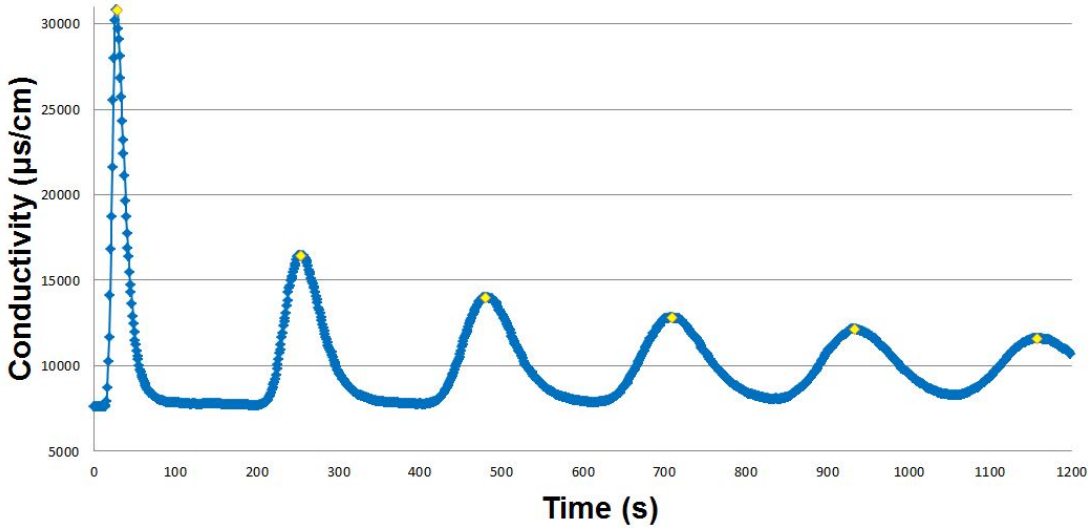

Figure 21: Evolution of the conductivity at 25°C at the outlet of the airlift during the small-scale tracer test of September 2019: $t_c = 227$ s.

4.2.2 Test of January 2020

In January 2020, the largest HRAP was used, basin 2, with a height of water of 7 cm and 348 g of NaCl.

The curve recorded at the outlet of the airlift is presented in Figure 9 and the measured circulation time is $t_c = 393$ s.

4.3 O_2 transfer tests

During each test session, an oxygen transfer test was carried out to compare the oxygen transfer coefficients with those obtained in [1] and to try to verify Equation (2.2).

4.3.1 Test of September 2019

The oxygen transfer test was conducted during 45 minutes and 65 g of anhydrous sodium sulfite were injected following the method described in Section 3.2. The curves of the concentration in dissolved oxygen recorded by the probes at the inlet and outlet of the airlift are presented in Figure 22. Comparing these two curves allows to find the times spent by the water to cross the airlift and the channel. Their values are respectively $t_A = 24$ s and $t_{channel} = 203$ s, the circulation time in the whole pond being of 227 s.

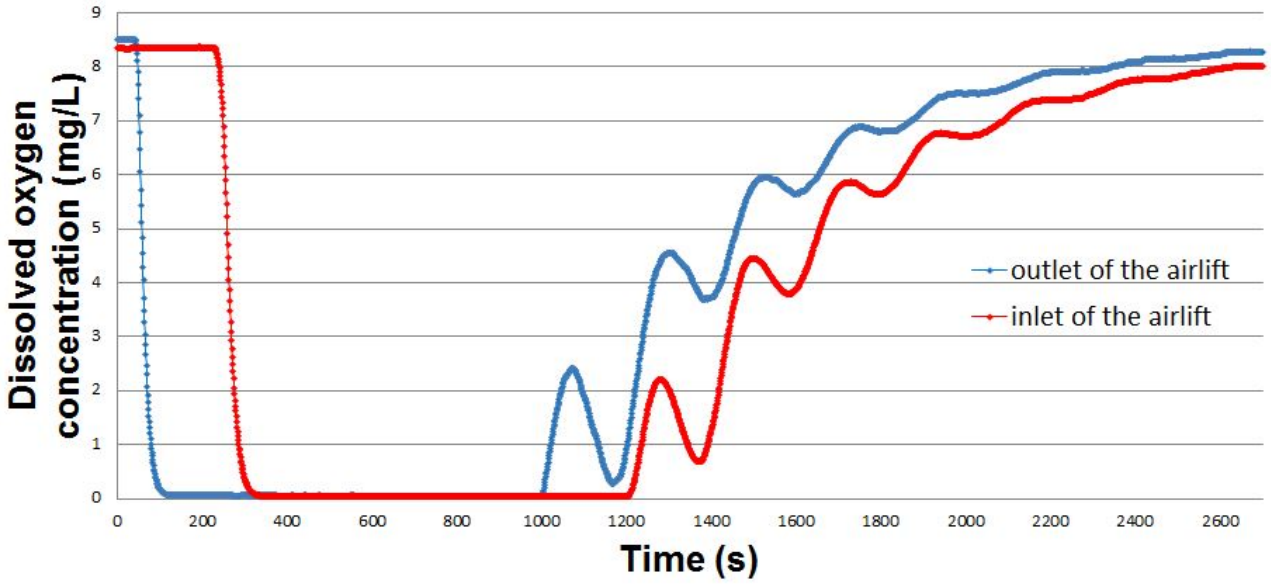

Figure 22: Evolution of the DO concentration at the inlet (red) and outlet (blue) of the airlift during the small-scale oxygen transfer test of September 2019.

First, the addition of sulfite occurs and the DO concentration decreases until it becomes null.

After the sulfite injection phase, the curves present some unexpected behaviours. First the oxygen transfer is only observed at the outlet of the airlift after around 1 000 s while the circulation time is only of 227 s. This time shift is probably due to the fact that the quantity of sulfite added into the pond exceeded largely the stoichiometric requirement for the total consumption of the oxygen initially present in the water. Indeed, 65 g of Na_2SO_3 were added while less than 20 g were theoretically required. The oxygen kept being consumed rapidly by the sulfite during a long time and this consumption entirely compensated the transfer from the atmosphere as the recorded DO concentration stayed null during this rather long time.

When the oxygen transfer began to prevail over its consumption by sulfites, peaks were observed at each passage through the airlift. The concentration in DO increased when the water passed through the airlift due to the air injection, then the oxygen was partially consumed in the channel as the reaction with the sulfite was competing with the transfer from the atmosphere. These decreases indicated the presence of remaining sulfite even after 75% of the test's duration, proving that the amount of sulfite added into the pond was too high.

The different transfer coefficients of oxygen are calculated following the methodologies explained in Section 3.2.2.

First the transfer coefficient of the whole HRAP is calculated. The graph of the linear regression whose slope is equal to $-(k_l a)_{\mathrm{R}}$ is presented in Figure 23, for the data recorded by the probe placed at the inlet of the airlift. As the equations used to find the value of $(k_l a)_{\mathrm{R}}$ are only valid when there is no O_2 consumption, the interval in which the linear regression is made starts at 1 800 s for the probe at the outlet of the airlift and 1 600 s for the probe at its inlet. It is indeed considered that the oxygen consumption can be neglected after this moment seen the curves shown in Figure 22: no more DO concentration decrease occurs after these moments, depending on the position of the probe.

In Figure 23, the slope of the linear regression, equal to $-(k_l a)_{\mathrm{R}}$, is of -1.9×10^{-3} s^{-1}. As explained in Section 3.2.2, the slope of the linear regression is always given with its 95% confidence interval. In this case, this interval is of $\pm$ 1.5 $\times$ 10^{-5} s^{-1} around the value of the slope. This is referred as "$(k_l a)_{\mathrm{R}} = 1.9 \times 10^{-3}$ s^{-1} ($\pm$ 1.5×10^{-5} s^{-1})" in the rest of this master thesis.

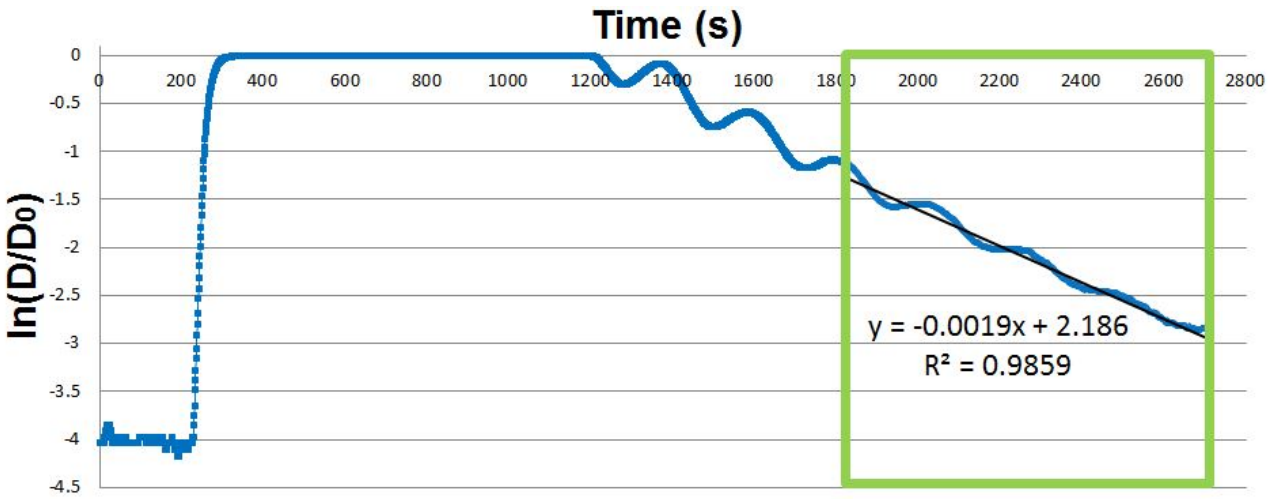

Figure 23: Curve of $\ln(D(t)/D_0)$ at the inlet of the airlift and linear regression in the relevant interval for the small-scale O_2 transfer test of September 2019: $(k_l a)_{\mathrm{R}} = 1.9 \times 10^{-3}$ s^{-1} ($\pm$ 1.5×10^{-5} s^{-1}) / conditions: water temperature = 23.8°C - V_{R} = 267.1 L - water height = 9.8 cm - t_c = 227 s - C_{S} = 8.5 mg/L.

The linear regression based on the data recorded at the outlet of the airlift is shown in Figure 43 in Appendix 8.3. The obtained transfer coefficient is $(k_l a)_{\mathrm{R}} = 2.3 \times 10^{-3}$ s^{-1} ($\pm$ 1.3×10^{-5} s^{-1}). The mean of these two values is the oxygen transfer coefficient of the whole HRAP: $(k_l a)_{\mathrm{R}} = 2.1 \times 10^{-3}$ s^{-1} ($\pm$ 2×10^{-5} s^{-1}).

The model of the deficit at the outlet of the airlift that is fitted to compute the value of $(k_l a)_{\mathrm{A}}$ is compared to the actual deficit recorded by the probe in Figure 24. Again, the validity interval starts at the end of the oxygen consumption at the inlet of the airlift, at 1 800 s, and the value of $(k_l a)_{\mathrm{A}}$ is fitted only in this interval.

The value of $(k_l a)_A$ is also computed with the first method described in Section 3.2.2 and a transfer coefficient of $(k_l a)_A = 2.65 \times 10^{-2}$ s^{-1} is obtained. The mean of the two obtained values is taken as the actual value: $(k_l a)_A = 2.5 \times 10^{-2}$ s^{-1}.

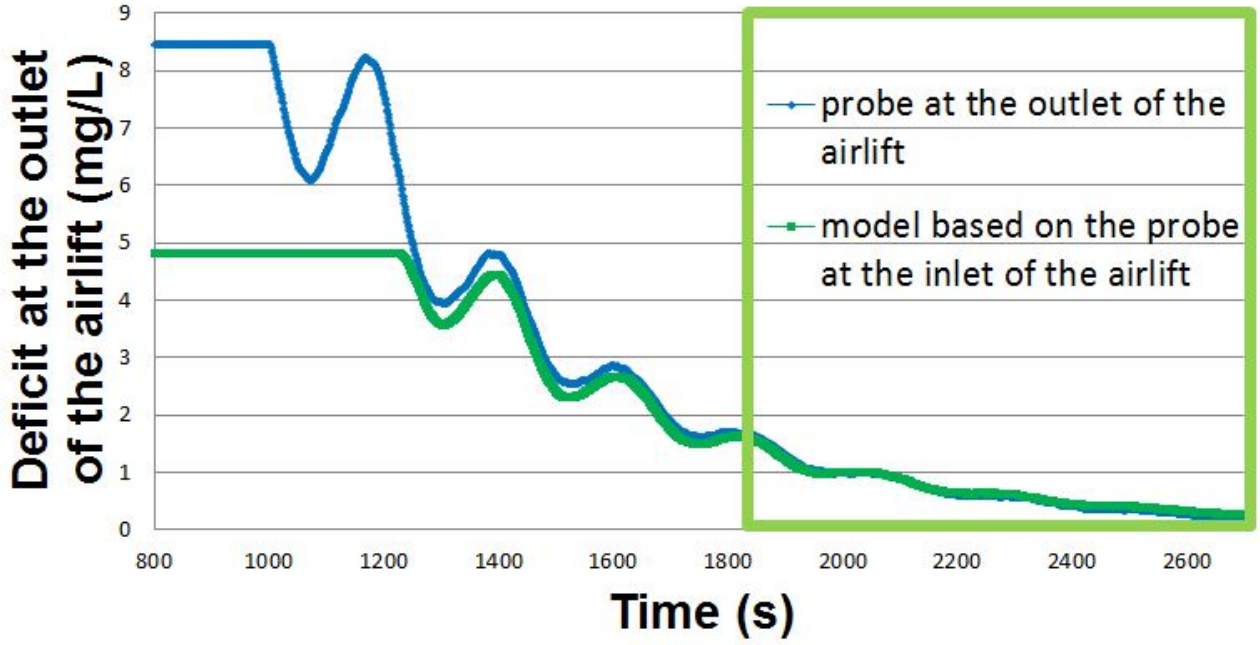

Figure 24: Evolution of the deficit at the outlet of the airlift: recorded by a probe (blue) and modelled on the basis of the data recorded at the inlet of the airlift (green) for the oxygen transfer test of September 2019; the green frame represents the zone in which the value of $(k_l a)_A$ is adjusted to model the deficit: $(k_l a)_A = 2.36 \times 10^{-2}$ s^{-1} / conditions: water temperature = 23.8°C - $V_A = 22$ L - water height = 9.8 cm - $t_A = 24$ s.

The value of $(k_l a)_{channel}$ is calculated with Equation (3.18) and the values of the three oxygen transfer coefficients of the test conducted in September 2019 are gathered in Table 2.

Table 2: Volumetric mass transfer coefficients of oxygen for the small-scale test of September 2019 in basin 1 / conditions: water temperature = 23.8°C - water height = 9.8 cm.

Part of the HRAP	Volume (L)	Circulation time (s)	$k_l a$ (s^{-1})	Uncertainty (s^{-1})
whole pond	267.1	227	2.1×10^{-3}	$\pm 2 \times 10^{-5}$
airlift	22	24	25×10^{-3}	/
channel	245.1	203	0.04×10^{-3}	/

4.3.2 Test of January 2020

During the oxygen transfer test of January 2020, 45 g of sulfite were added into basin 2 and the test was conducted during 40 minutes. The graphs related to this test are shown in Section 3.2 and in Appendix 8.3. The transfer coefficients are calculated similarly to those of the first oxygen transfer test.

The different times of this test are $t_c = 393$ s, $t_A = 130$ s and $t_{channel} = 263$ s. The values of the transfer coefficients are presented in Table 3.

Table 3: Volumetric mass transfer coefficients of oxygen for the small-scale test of January 2020 in basin 2 / conditions: water temperature = 16.2°C - water height = 7 cm.

Part of the HRAP	Volume (L)	Circulation time (s)	$k_l a$ (s^{-1})	Uncertainty (s^{-1})
whole pond	408.9	393	1.7×10^{-3}	$\pm$ 1.9×10^{-5}
airlift	70.9	130	6.4×10^{-3}	/
channel	338	263	0.8×10^{-3}	/

The problem of the too high sulfite concentration during the oxygen transfer test of September 2019 was not encountered in the test of January 2020. Moreover, this test was conducted with the experience of the previous test session. The results of the oxygen transfer test of January 2020 are thus more reliable.

4.4 CO_2 transfer tests

During each test session, two CO_2 transfer tests have been conducted in similar conditions. Each time, around nine samples have been collected per test and titrated to draw the curve of the evolution of the dissolved CO_2 concentration over time.

Among these samples, one was taken before the beginning of the test and is thus not present in the curves of the concentrations over time. This sample was taken before the sulfite addition, for two reasons.

First it gives a value of the concentration in dissolved CO_2 at saturation, which is required for the calculation of the transfer coefficient as explained previously.

The second interest of this sample is that it allows to assess the validity of the calculations leading to the concentration in CO_3 coordinates in the basin. Indeed, the difference between the concentration in CO_3 coordinates before and after the bicarbonate injection should correspond to the amount of sodium bicarbonate added into the pond: the theoretical concentration based on the amount of $NaHCO_3$ injected should be close to the concentration difference measured with the methodology. This concentration difference is calculated with the sample collected before the sodium bicarbonate injection and the sample collected at the beginning of the test, just before the acid injection.

For each test session, the first test performed is called test **A** and the second one is test **B**. As explained in the test presentation, only the transfer coefficients of the whole HRAP are evaluated for the CO_2 transfer tests.

4.4.1 Tests of September 2019

Similarly to the oxygen transfer tests, the CO_2 transfer tests carried out in September 2019 are less reliable than those of January 2020. Indeed, this type of test had never been performed before so the experimental procedures did not rely on any experience and had to be upgraded. The results of the CO_2 transfer tests of September 2019 are therefore only presented in Appendix 8.4 and more details are provided for the tests of January 2020.

As for the other tests conducted in September 2019 in basin 1, the height of water was set at 9.8 cm. For the first test, 502 g of sodium bicarbonate and 700 mL of liquid HCl 23% in mass were used while the amounts of reactant for the second test were 505 g of sulfite and 1 200 mL of acid. The amount of acid added was adapted from test **A** to test **B** seen the results of the first test and its too high water pH that made the results unusable, as explained below. A more important amount of acid was used for test **B**, which gave better results.

The first test was conducted during 30 minutes and the second one during 45 minutes.

The calculation method for the evaluation of the CO_2 concentration in the HRAP was followed and the values of all the variables for each sample are gathered in Tables 9 for test **A** and 10 for test **B**, in Appendix 8.4.

Some comments can be made concerning these results. First, the data collected during test **A** cannot be used to evaluate the transfer coefficient because the amount of acid added into the pond was not sufficient. The samples had a too high pH so the CO_3 coordinates were not in the form of $H_2CO_3^*$, which prevented the quantification of the CO_2 transfer. This fact can be observed in Figure 46 where it is shown that the pH of the samples is between 6 and 7. The evolution of the CO_2 concentration is presented in Figure 47 and it is clear that the concentration stays nearly null during the whole test, preventing the calculation of the corresponding $k_l a$.

The second test gave better results as a larger amount of acid was added into the pond so the CO_3 coordinates were in the form of $H_2CO_3^*$. However, an increase of the concentration in dissolved CO_2 occurred between 1 125 and 1 350 s after the beginning of the test, so the linear regression was only evaluated in the time interval before 1 125 s. More details are provided for the choice of this time interval in the calculation of the coefficient of test **B** of January 2020 in the following section. The volumetric mass transfer coefficient of CO_2 for test **B** of September 2019 equals $(k_l a)_{\mathrm{R}} = 1.3 \times 10^{-3}$ s^{-1} ($\pm$ 2.1×10^{-4} s^{-1}).

4.4.2 Tests of January 2020

The two CO_2 transfer tests conducted in January 2020 gave more reliable results because the samples were collected at low pH, so the CO_3 coordinates were mostly in the form of $H_2CO_3^*$.

The results and graphs of test **A** are detailed in this section. The graphs of test **B** are presented in Section 3.3 and the calculation table is in Appendix 8.4. In the calculation tables, the sample called "-1" are the samples taken before the bicarbonate injection. The other samples are named chronologically, starting with the sample "0" collected at the beginning of the test, just before the acid injection.

As all the tests conducted in January 2020, the water height in basin 2 was of 7 cm and the circulation time of 393 s. The amounts of reactants used were 808 g of sodium bicarbonate and 2 400 ml of HCl 23% in mass for test **A** and 802 g of sulfite and 1 850 ml of HCl 23% in mass for test **B**.

Both tests were conducted during 40 minutes.

The calculation method described in this report was followed for both tests and the values of all the variables calculated to measure the CO_2 concentration in the basin are presented in Table 4 for test **A** and in Table 11 in Appendix 8.4 for test **B**.

Table 4: Values of the different variables used for the determination of the CO_2 concentration in the HRAP for the small-scale test **A** of January 2020.

sample	**A-1**	**A0**	**A1**	**A2**	**A3**
sampling time (s)	/	0	390	780	1 170
t_{test} (°C)	17.1	17.1	17.3	17.3	17.3
$t_{\text{titration}}$ (°C)	25	25	25	25	25
V_{sample} (mL)	24	23.35	23.28	23.72	23.46
titrant used	HCl	HCl	NaOH	NaOH	NaOH
n_{H^+}/n_{OH^-} added (mmol)	0.17	0.66	0.17	0.11	0.08
$V_{\text{container}}$ (mL)	25.78	88.48	53.01	32.02	48.09
$[H^+_{\text{added}}]/[OH^-_{\text{added}}]$ (mmol/L)	6.55	7.47	3.25	3.45	1.75
conductivity (25°C) (μs/cm)	3 000	4 290	8 360	8 250	8 740
pH (before the titration)	8.26	7.98	2.08	2.13	2.08
Titration conditions					
$g(t_{\text{titration}})$	0.9989	0.9989	0.9989	0.9989	0.9989
$[OH_{\text{tot}}(t_{\text{titration}})]$ (mol/L)	55.35	55.35	55.35	55.35	55.35
$\epsilon(t_{\text{titration}})$	78.54	78.54	78.54	78.54	78.54
$A(t_{\text{titration}})$	0.51	0.51	0.51	0.51	0.51
ρ(20°C) (ohm.cm)	333.7	233.4	119.8	121.4	114.5
J(20°C) (mmol/L)	50.07	73.7	151.87	149.7	159.38
$J(t_{\text{titration}})$ (mmol/L)	50.01	73.61	151.69	149.53	159.19
$\gamma_1(t_{\text{titration}})$	0.819	0.794	0.745	0.746	0.741
$\gamma_2(t_{\text{titration}})$	0.45	0.398	0.308	0.309	0.302
$K_0(t_{\text{titration}})$ ($\times 10^{16}$)	1.829	1.829	1.829	1.829	1.829
$K_1(t_{\text{titration}})$ ($\times 10^{7}$)	4.452	4.452	4.452	4.452	4.452
$K_2(t_{\text{titration}})$ ($\times 10^{11}$)	4.68	4.68	4.68	4.68	4.68
pH $_{\text{initial}}$	8.3	8.1	4.5	4.5	4.5
$f_{11\ \text{initial}}$	1	1	1	1	1
$f_{12\ \text{initial}}$	0.992	1.002	1.981	1.981	1.981
pH $_{\text{final}}$	4.5	4.5	8.3	8.3	8.3
$f_{11\ \text{final}}$	1	1	1	1	1
$f_{12\ \text{final}}$	1.983	1.983	0.986	0.986	0.986
$[CO_{3_{\text{tot}}}]_{\text{container}}$ (mmol/L)	6.57	7.58	3.22	3.42	1.71
$[CO_{3_{\text{tot}}}]_{\text{sample}}$ (mmol/L)	7.06	28.74	7.33	4.62	3.51
Test conditions					
$g(t_{\text{test}})$	1.0006	1.0006	1.0005	1.0005	1.0005
$[CO_{3_{\text{tot}}}(t_{\text{test}})]$ (mmol/L)	7.07	28.79	7.34	4.63	3.52
$\epsilon(t_{\text{test}})$	81.44	81.44	81.36	81.36	81.36
$A(t_{\text{test}})$	0.5	0.5	0.5	0.5	0.5
$J(t_{\text{test}})$ (mmol/L)	50.1	73.74	151.95	149.78	159.46
$\gamma_1(t_{\text{test}})$	0.821	0.797	0.748	0.749	0.744
$\gamma_2(t_{\text{test}})$	0.455	0.403	0.312	0.314	0.307
$K_1(t_{\text{test}})$ ($\times 10^{7}$)	3.954	3.954	3.967	3.967	3.967
$K_2(t_{\text{test}})$ ($\times 10^{11}$)	3.919	3.919	3.938	3.938	3.938
pH (during the test)	8.26	8.64	1.87	1.97	1.9
d_{32}	0.01115	0.00446	0.99996	0.99995	0.99996
$[CO_2(t_{\text{test}})]$ (mmol/L)	0.08	0.13	7.34	4.63	3.52

sample	**A4**	**A5**	**A6**
sampling time (s)	1 560	1 950	2 340
t_{test} (°C)	17.4	17.4	17.5
$t_{\text{titration}}$ (°C)	25	25	25
V_{sample} (mL)	23.77	24.03	24.2
titrant used	NaOH	NaOH	NaOH
n_{H^+}/n_{OH^-} added (mmol)	0.05	0.05	0.03
$V_{\text{container}}$ (mL)	32.07	48.95	32.5
$[H^+_{\text{added}}]/[OH^-_{\text{added}}]$ (mmol/L)	1.64	0.95	0.81
conductivity (25°C) (μs/cm)	9 590	9 480	9 140
pH (before the titration)	2.05	2.08	2.1
Titration conditions			
$g(t_{\text{titration}})$	0.9989	0.9989	0.9989
$[OH_{\text{tot}}(t_{\text{titration}})]$ (mol/L)	55.35	55.35	55.35
$\epsilon(t_{\text{titration}})$	78.54	78.54	78.54
$A(t_{\text{titration}})$	0.51	0.51	0.51
ρ(20°C) (ohm.cm)	104.4	105.6	109.5
J(20°C) (mmol/L)	176.28	174.09	167.32
$J(t_{\text{titration}})$ (mmol/L)	176.08	173.89	167.12
$\gamma_1(t_{\text{titration}})$	0.734	0.735	0.738
$\gamma_2(t_{\text{titration}})$	0.291	0.292	0.296
$K_0(t_{\text{titration}})$ ($\times$ 10^{16})	1.829	1.829	1.829
$K_1(t_{\text{titration}})$ ($\times$ 10^{7})	4.452	4.452	4.452
$K_2(t_{\text{titration}})$ ($\times$ 10^{11})	4.68	4.68	4.68
pH $_{\text{initial}}$	4.5	4.5	4.5
$f_{11\ \text{initial}}$	1	1	1
$f_{12\ \text{initial}}$	1.981	1.981	1.981
pH $_{\text{final}}$	8.3	8.3	8.3
$f_{11\ \text{final}}$	1	1	1
$f_{12\ \text{final}}$	0.985	0.985	0.986
$[CO_{3_{\text{tot}}}]_{\text{container}}$ (mmol/L)	1.61	0.91	0.77
$[CO_{3_{\text{tot}}}]_{\text{sample}}$ (mmol/L)	2.17	1.85	1.03
Test conditions			
$g(t_{\text{test}})$	1.0005	1.0005	1.0005
$[CO_{3_{\text{tot}}}(t_{\text{test}})]$ (mmol/L)	2.17	1.85	1.03
$\epsilon(t_{\text{test}})$	81.33	81.33	81.29
$A(t_{\text{test}})$	0.5	0.5	0.5
$J(t_{\text{test}})$ (mmol/L)	176.38	174.18	167.4
$\gamma_1(t_{\text{test}})$	0.737	0.738	0.741
$\gamma_2(t_{\text{test}})$	0.295	0.297	0.301
$K_1(t_{\text{test}})$ ($\times$ 10^{7})	3.974	3.974	3.981
$K_2(t_{\text{test}})$ ($\times$ 10^{11})	3.948	3.948	3.957
pH (during the test)	1.79	1.82	1.82
d_{32}	0.99997	0.99996	0.99996
$[CO_2(t_{\text{test}})]$ (mmol/L)	2.17	1.85	1.03

The evolution of the pH of the water during test **A** is shown in Figure 25. The acid injection was a bit too long and nearly covered a whole loop. There was thus no pH peak and all the samples collected after the acid injection were at low pH and titrated with a base.

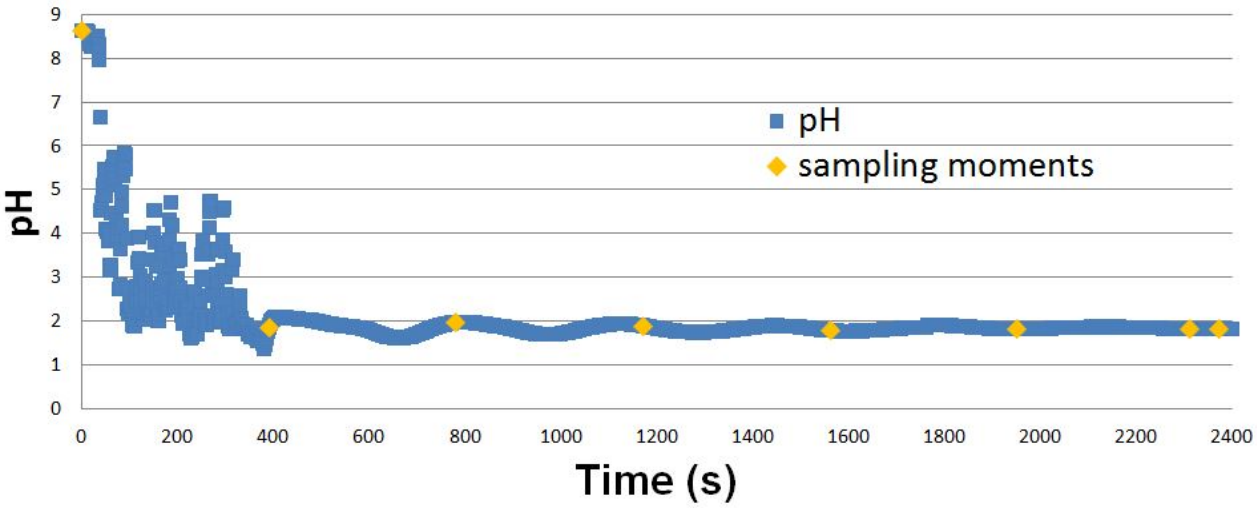

Figure 25: Evolution of the pH at the outlet of the airlift and sampling moments during the small-scale CO_2 transfer test **A** of January 2020.

The graph of the concentrations in $CO_{3_{tot}}$ and in CO_2 in the basin over time is presented in Figure 26. It can be seen in this graph that the concentration in CO_2 is very close to that in $CO_{3_{tot}}$ for all the samples after the acid injection. This is due to the fact that the pH of the water at the sampling moments was low, as shown in Figure 25, so the distribution function of $H_2CO_3^*$ was close to 1 for every sample.

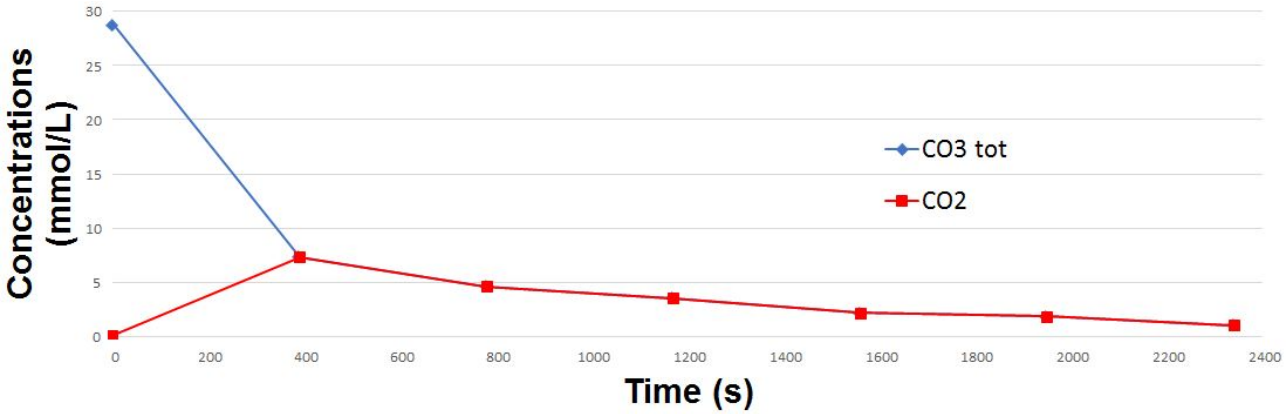

Figure 26: Evolution of $[CO_{3_{tot}}]$ and $[CO_2]$ at the outlet of the airlift during the small-scale CO_2 transfer test **A** of January 2020 / conditions: water temperature = 17.1°C - V_R = 408.9 L - water height = 7 cm - t_c = 393 s.

Between the beginning of the test and the first sampling moment, an important decrease of the concentration in $CO_{3_{tot}}$ is observed. This drop is not observed on the CO_2 curve because of the time lapse between the first and second sampling moment. The fact that this important drop of concentration is not observed on the CO_2 curve will skew the value of the transfer coefficient because the most important part of the transfer will not be taken into account in its calculation. It is therefore expected that the coefficient obtained for this test may be underestimated: the time interval in which the calculations are performed, starting at the beginning of the decrease of the CO_2 concentration so after 390 s, only considers the smooth decrease of the CO_2 concentration.

The volumetric mass transfer coefficient of CO_2 corresponding to basin 2 is calculated as explained previously. The graph of $\ln(D(t)/D_0)$ is drawn and the slope of its linear regression gives $-(k_l a)_R$. The corresponding graph is presented in Figure 27 and the value of the transfer coefficient is $(k_l a)_R = 1 \times 10^{-3}$ s^{-1} ($\pm$ 1.2×10^{-4} s^{-1}).

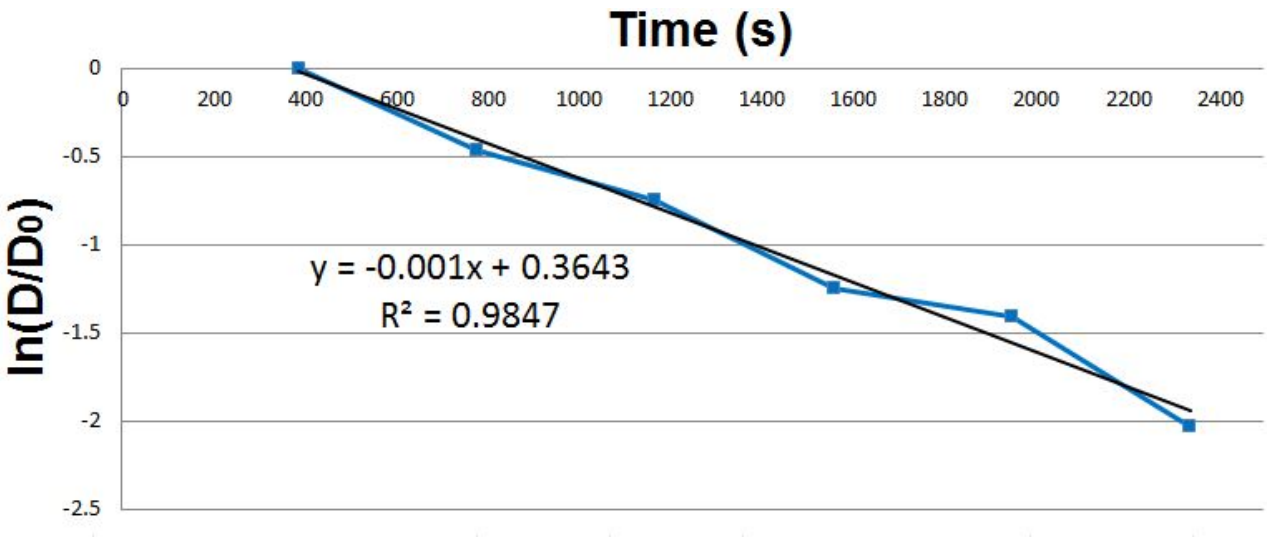

Figure 27: Curve of $\ln(D(t)/D_0)$ at the outlet of the airlift and linear regression for the small-scale CO_2 transfer test **A** of January 2020: $(k_l a)_R = 1 \times 10^{-3}$ s^{-1} ($\pm$ 1.2×10^{-4} s^{-1}) / conditions: water temperature = 17.1°C - V_R = 408.9 L - water height = 7 cm - t_c = 393 s - C_S = 0.8 mmol/L.

The results of test **B** are analysed in Section 3.3 and the obtained value of $(k_l a)_R$ is 1.2×10^{-3} s^{-1} ($\pm$ 4.6×10^{-4} s^{-1}).

A comment can be made about the curve $\ln(D(t)/D_0)$ used for the calculation of $(k_l a)_R$ of test **B** and shown in Figure 17. The linear regression is only evaluated starting from 780 s, which corresponds to the second sample taken after the acid injection. This was not the case for test **A** for which the linear regression started after 390 s.

To understand why the linear regression is only defined from 780 s onwards in test **B**, the graph in Figure 16 in Section 3.3 needs to be regarded. It can be seen in this graph that between the beginning of the test and the second sample, the CO_2 concentration increased. This is due to the fact that the pH of the sample collected at 390 s was higher than that at 780 s, such that the concentration in CO_2 was smaller at 390 s even if the concentration in $CO_{3_{tot}}$ was higher. The increase of the CO_2 concentration prevents the use of the mass balance Equation (3.3) from which Equation (3.6) is derived. Indeed, in regard to CO_2, this increase appears as a production of CO_2 and thus the mass balance written in Equation (3.3) cannot be used.

4.5 Summary of the small-scale tests

The results of all the tests are gathered in Table 5 and compared to those given in [1].

Several comments can be done concerning these results. First it can be seen that the conditions in which the test sessions have been conducted are not quite the same. Indeed, the height of the water, the fluid velocities and the proportionality between the airlift and channel volumes are different between the tests conducted in basin 1 and basin 2.

A second comment is that the same trend is observed in all the oxygen transfer tests: the transfer in the airlift is more important than that in the channel, while the transfer of the whole reactor is obviously in between. However, the difference between the transfer coefficients of the airlift and the channel was much more pronounced in the tests of [1] than in those of

Table 5: Summary of the conditions and results of the small-scale tests.

	September 2019 (basin 1)	January 2020 (basin 2)	Results in [1] (basin 2)
Conditions			
temperature (°C)	23.6 - 23.8	16.2 - 17.1	22
water height (cm)	9.8	7	7
V_R (L)	267.1	408.9	417
V_A (L)	22	70.9	no data in [1]
$V_{channel}$ (L)	245.1	338	no data in [1]
Tracer test			
t_c (s)	227	393	273
O_2 transfer			
t_A (s)	24	130	no data in [1]
$t_{channel}$ (s)	203	263	no data in [1]
$(k_la)_R$ (s^{-1})	2.1×10^{-3} $\pm$ 2×10^{-5}	1.7×10^{-3} $\pm$ 1.9×10^{-5}	3.2×10^{-3}
$(k_la)_A$ (s^{-1})	25×10^{-3}	6.4×10^{-3}	175.5×10^{-3}
$(k_la)_{channel}$ (s^{-1})	0.04×10^{-3}	0.8×10^{-3}	0.5×10^{-3}
CO_2 transfer			
$(k_la)_R$ (s^{-1}) test **A**	/	1×10^{-3} $\pm$ 1.2×10^{-4}	/
$(k_la)_R$ (s^{-1}) test **B**	1.3×10^{-3} $\pm$ 2.1×10^{-4}	1.2×10^{-3} $\pm$ 4.6×10^{-4}	/

this work. This is certainly due to the reduction in the performance of the diffusers caused by their ageing, as explained previously.

The oxygen transfer tests conducted in basin 2, so the test of January 2020 and those presented in [1], give transfer coefficients of the same order of magnitude for the whole pond. The transfer coefficient was higher in [1], but again, this is surely due to the diffusers ageing between the two test sessions.

More oxygen transfer tests are performed in [1], with varying operating parameters such as the water height or the air injection flow rate. The results obtained could serve as a basis for further studies and for up-scaling calculations, as explained in Section 7.

The last observation about Table 5, concerning the CO_2 transfer coefficients of the whole reactor, is that the three tests give rather similar results and that the transfer coefficients are close to those of the oxygen transfer. The method developed in this work seems thus to be coherent, knowing that the transfer coefficients of oxygen and carbon dioxide in water are supposed to be close to each other. A more detailed analysis of the relation between the transfer coefficients of O_2 and CO_2 is presented in Section 6.

5 Tests conducted on a large scale

The large-scale test session took place between 15 and 22 June 2020. The large-scale tests were supposed to be conducted in a HRAP in the Ninh Thuan province in Vietnam, as in [1]. This pond was built in the scope of the *Renewable* project and serves as a pilot for the design of HRAPs dedicated to the wastewater treatment of shrimp culture in Vietnam.

However, due to the international situation in the first half of the year 2020 by the Covid-19 pandemic, the test session planned in Vietnam could not take place and the tests were conducted in a basin located in Arlon, Belgium. The conditions in which the tests have been conducted were thus not optimal as the basin used was not supposed to be a HRAP and was rather different from the models in which the small-scale tests had been carried out.

The large-scale test session conducted in Arlon needs thus to be seen as a replacement option that allows to see if it is feasible to use the developed method on a large scale and to have results that can be compared to those obtained on a small scale to see if the trends are similar.

5.1 Airlift with external circulation reactor characteristics

The basin used will be defined as a "HRAP" in this master thesis as it contains an airlift and a channel, but it is important to bear in mind that it was not built for this application. This basin was built in the 1990's and has been used to develop a pattern on the airlift system for oxygenation in water systems.

There are thus several differences between this basin and the HRAP built in Vietnam: the channel length is very smaller in Arlon, the airlift size is higher in Arlon and, more importantly, the depth of the water in the channel is of around 1.5 m in Arlon, versus 30 cm in Vietnam. The depth is higher in Arlon because the basin was not dedicated to algae culture but to aerated lagoon, so there was no constraints due to the light intensity as there are in HRAPs. It is thus expected that the transfer between the atmosphere and the water in the channel will be less important as the surface of contact is proportionally smaller compared to the volume.

The conditions of the large-scale tests are thus very different from usual HRAPs. These differences are therefore also present between the basins used to perform the small-scale and large-scale test sessions as the former are models of the HRAP situated in Vietnam. The comparison of the results of the small and large-scale test sessions needs thus to be done while remembering these differences.

Moreover, the airlift system creates recirculation zones at both its inlet and outlet and the probes only measure local variables. There might thus be differences between the data recorded by the probe and the global concentration of a section of the basin as the concentration gradients are unknown along the water depth.

Pictures of the basin used for the large scale tests are presented in Figure 28.

The dimensions of the basin are presented in Figure 42 in Appendix 8.2.2. The depth of water was of around 1.5 m and was kept constant for all the tests. The volumes of the different parts of the basin are gathered in Table 6.

(a) Outlet of the airlift and beginning of the channel.

(b) Inlet of the airlift and end of the channel.

Figure 28: Large-scale pond used to perform the tests of June 2020.

Table 6: Height and volumes of water in the large-scale basin used for the test session of June 2020.

Height and volume	June 2020
water height (cm)	150
V_{R} (L)	78 400
V_{A} (L)	24 400
V_{channel} (L)	54 000

5.2 Tracer test

As in every test session, the first test conducted is a tracer test. This test took place on 15 June 2020.

Around 25 kg of salt were dissolved in water and added at the outlet of the airlift as quickly as possible. However, the tracer injection was not ideal as the saline solution had been distributed in about twenty buckets that were poured in the basin five by five during around ten seconds.

A probe was placed at the inlet of the airlift and another at its outlet, just after the injection point. Both probes were immersed approximately 10 cm below the water surface. The graphs obtained are presented in Figures 29 and 30. It should be noted that the beginning of the time axes does not represent the actual start of the test, but this fact does not disturb the interpretation as it is the time lapses between two consecutive peaks that is measured to find the circulation time.

The evolution of the conductivity recorded on these two graphs is different from those of the small-scale tests. The peaks are steeper and closer to each other. Moreover, as explained previously, the probes measure local properties so it is difficult to describe the global motion of the saline solution. Potential recirculation zones cannot be seen while looking at these two curves for instance. The interpretation of these graphs is thus complex and a precise value of the circulation time cannot be deduced.

However, the tracer test gives an idea of the circulation time as the mean time gap between the peaks of both Figures 29 and 30 is of around 20 s.

This value seems to be small regarding the geometry of the basin, is based on data recorded close to the surface of the water only and is not very precise. However, as explained previously, this test session had not for objective to provide perfectly accurate results and was mainly

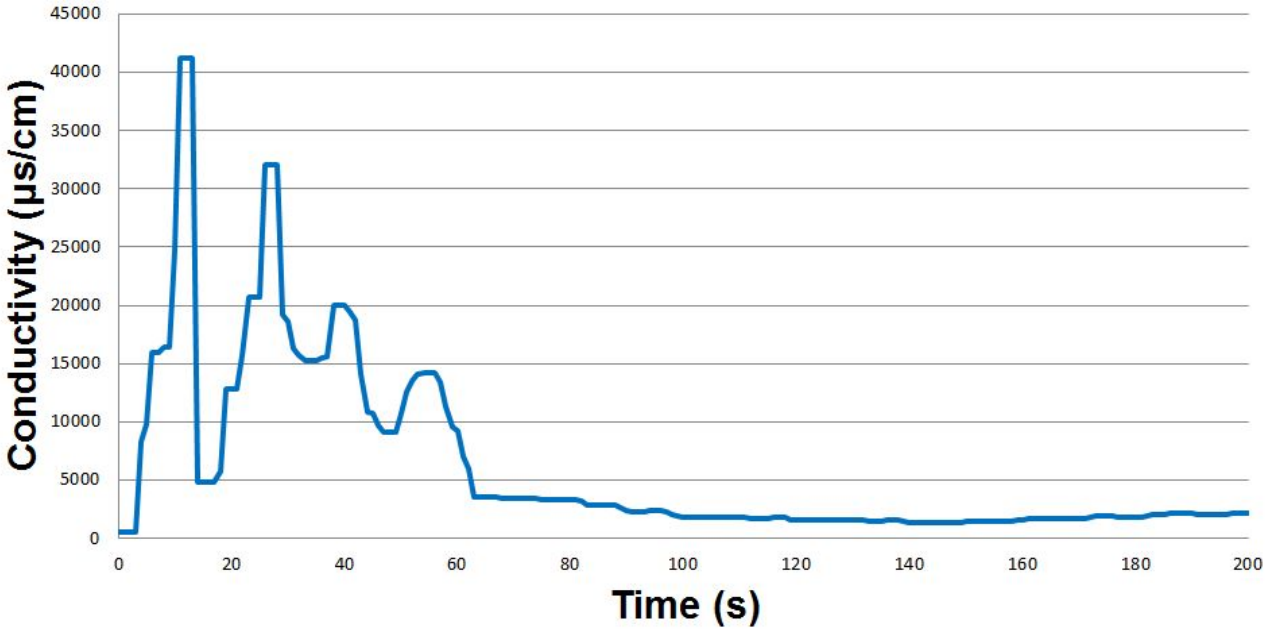

Figure 29: Evolution of the conductivity at 25°C at the outlet of the airlift during the large-scale tracer test of June 2020: $t_c \simeq 20$ s.

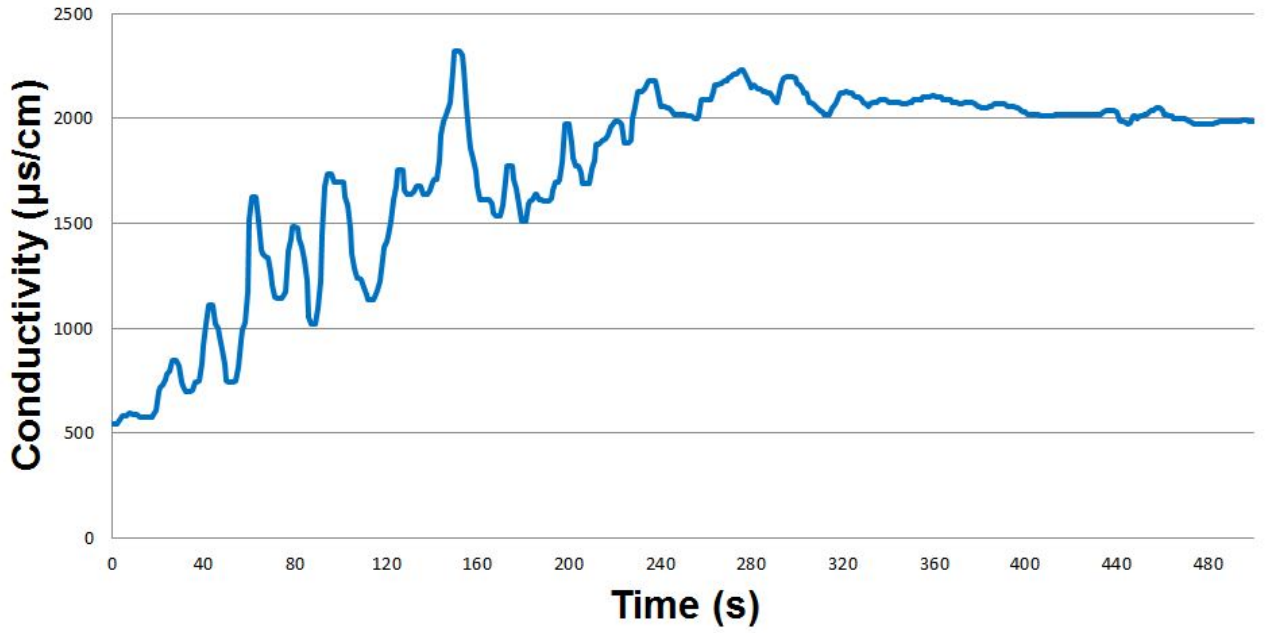

Figure 30: Evolution of the conductivity at 25°C at the inlet of the airlift during the large-scale tracer test of June 2020: $t_c \simeq 20$ s.

conducted to see if the method developed in this work is feasible on a large scale. The results of the tracer test were thus sufficient for this application as they gave an idea of the time required for one lap. The injections and sampling moments of the transfer tests were therefore based on a circulation time of 20 s.

5.3 O_2 transfer test

The oxygen transfer test took place on 19 June 2020. 12.5 kg of solid sodium sulfite in powder form were added at the outlet of the airlift in 20 s. The temperature of the water was of 15.4°C and the evolution of the concentration in dissolved oxygen was recorded with two probes immersed around 50 cm below the surface at each side of the airlift.

Unlike in the small-scale tests, only the volumetric mass transfer coefficient along the whole pond was measured in this test. Indeed, the curves recorded during the tracer test showed that it was difficult to measure precisely the circulation time, so the time lapses required to cross the channel and the airlift could not be precisely known, preventing the calculation of the corresponding transfer coefficients. Moreover, the potential concentration gradient along on the depth and the recirculation zones present in the pond increase the difference between the local measurements of the probes and the global phenomena occurring in the whole basin.

The evolution of the DO concentration over time recorded with the two probes is presented in Figure 31.

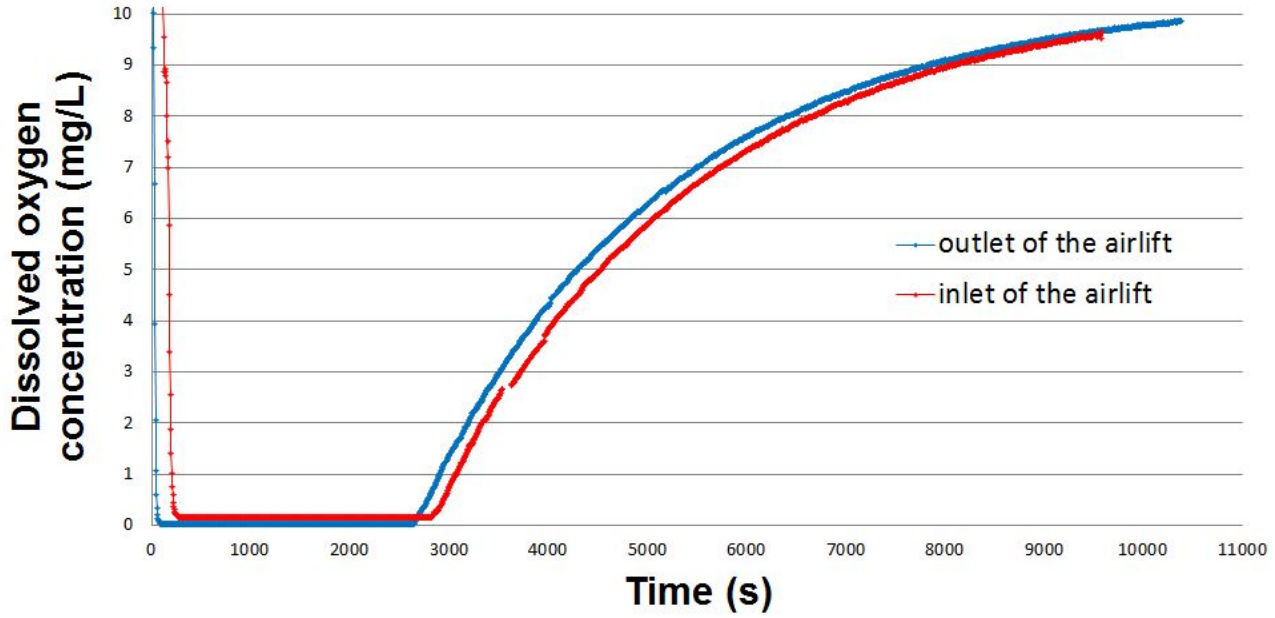

Figure 31: Evolution of the DO concentration at the inlet (red) and outlet (blue) of the airlift during the large-scale oxygen transfer test of June 2020.

This graph shows that the evolution of the DO concentration was smooth and that no peak was observed. The plug-flow with recirculation aspect of the basin is strongly attenuated and the basin can be seen as a globally perfectly mixed tank.

It may be mentioned that the small lack of continuity at around 4 000 s in the curve recorded at the inlet of the airlift is due to the fact that the test lasted longer than expected so the probe had to be reset.

The transfer coefficient of the whole pond is calculated with the method detailed in Section 3.2.2, based on the data recorded with the two probes used during the test. The linear regressions of the curves of $\ln\left(D\left(t\right)/D_0\right)$ that give the transfer coefficient are given in Figure 32 for the data recorded at the inlet of the airlift and in Figure 45 in Appendix 8.3 for the data recorded at the outlet of the airlift.

The time intervals in which the regressions are built start when the DO concentration begins to increase, depending on the probe. It is assumed that no more oxygen consumption occurred after these moments, even if it is possible that some remaining sulfite consumed dissolved oxygen afterwards but that the curves kept increasing due to the transfer from the atmosphere.

However, the shapes of the curves are those of perfectly mixed tanks and cobalt catalyst was present in the pond, so this assumption does not seem unrealistic.

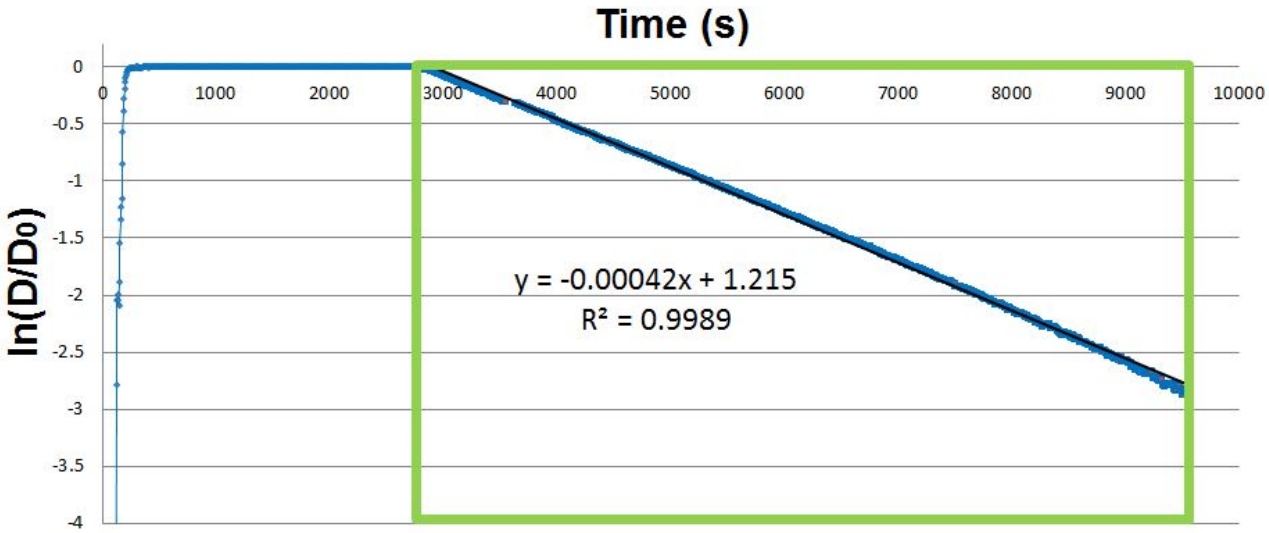

Figure 32: Curve of $\ln\left(D\left(t\right)/D_0\right)$ at the inlet of the airlift and linear regression in the relevant interval for the large-scale O_2 transfer test of June 2020: $\left(k_l a\right)_R = 4.2 \times 10^{-4}$ s^{-1} ($\pm$ 2.8×10^{-6} s^{-1}) / conditions: 15.4°C - V_R = 78 400 L - water height = 150 cm - C_S = 10.2 mg/L.

The values obtained with the two probes are close to each other and their mean gives the actual value of the volumetric mass transfer coefficient of oxygen for this test: $\left(k_l a\right)_R = 4.3 \times 10^{-4}$ s^{-1} ($\pm$ 3×10^{-6} s^{-1}).

This value is very close to that measured during other tests conducted in this basin in similar conditions: 3.4×10^{-4} s^{-1} [10]. It proves that the results of the oxygen transfer test carried out in June 2020 seem reliable.

5.4 CO_2 transfer tests

Two CO_2 transfer tests were conducted, both on 22 June 2020. The methodology followed for these two tests was slightly different from the one presented before and used on a small scale. Indeed, seen the large amounts of acid required for the tests, the order of the components injections was reversed. On a small scale, the sodium bicarbonate was added into the pond, then the acid was injected during a time nearly equal to the circulation time. This order choice was based on previous experiments conducted in the small-scale basins [10] during which the fast acid injection was possible seen the small volumes handled.

Such an injection was unfeasible in the conditions of the large-scale tests. Indeed around 250 L of liquid HCl 30% in mass should have been added in less than 20 seconds. For obvious safety reasons, it has been decided that the acid would first be carefully and slowly added into the pond and that, once it is well homogenised, the sodium bicarbonate would be added in a short amount of time.

It should be mentioned that the change of the order of injection induces that the sample collected at $t = 0$ gives the value of C_S in the calculation of the curve $\ln\left(D\left(t\right)/D_0\right)$. This sample being collected before the bicarbonate injection, it represents the concentration in dissolved CO_2 at equilibrium. It is for this reason that there is no sample "B-1" in Tables 12 and 13 in Appendix 8.5.

5.4.1 Large-scale CO_2 transfer test A

The first CO_2 transfer test was conducted with water at 16.1°C. The first step of this test consisted in the acid injection. 220 L of liquid HCl 30% in mass were added into the pond and a pH of less than 1.5 was reached.

Once the acid was well homogenised in the water, a solution of dissolved sodium bicarbonate was injected in 20 s, *i.e.* the circulation time measured with the tracer test. 125 kg of solid sodium bicarbonate were supposed to be injected in the basin to reach a concentration close to 13 mmol/L. The powder was first dissolved in a tank with water but an important part of it remained solid. The saturated water was thus split into several buckets and acid was added into the tank in order to dissolve a maximum of the residual solid. The tap of the tank was opened during the injection period while the buckets were poured into the water, but unfortunately, an important part of the sodium bicarbonate remained in the tank at the end of the injection period. Only a part of the initial 125 kg of sodium bicarbonate was thus actually added into the pond and the concentrations in CO_3 coordinates were smaller than planned.

The pH was recorded during the whole test and its evolution is presented in Figure 51 in Appendix 8.5. It can be seen in this graph that, except at the injection moment, the pH remained nearly constant at around 2.1 during the whole test due to an excess of acid as the expected amount of bicarbonate had not been added into the pond.

Samples were collected every 20 s after the beginning of the injection, which corresponds to $t = 0$, during 5 minutes, then one sample was taken every 5 minutes for one hour. Most of these samples were titrated and the methodology developed in this work was applied to calculate the corresponding CO_2 concentrations in order to compute the CO_2 transfer coefficient of the pond. The calculation of these concentrations is presented in Table 12 in Appendix 8.5. Some of the samples collected during the first CO_2 transfer test were not titrated due to a lack of time and in order to focus on those taken during the second test that seemed to be more promising, as explained afterwards.

The curves of the evolution of the concentrations in CO_3 coordinates and in CO_2 during this test are presented in Figure 33.

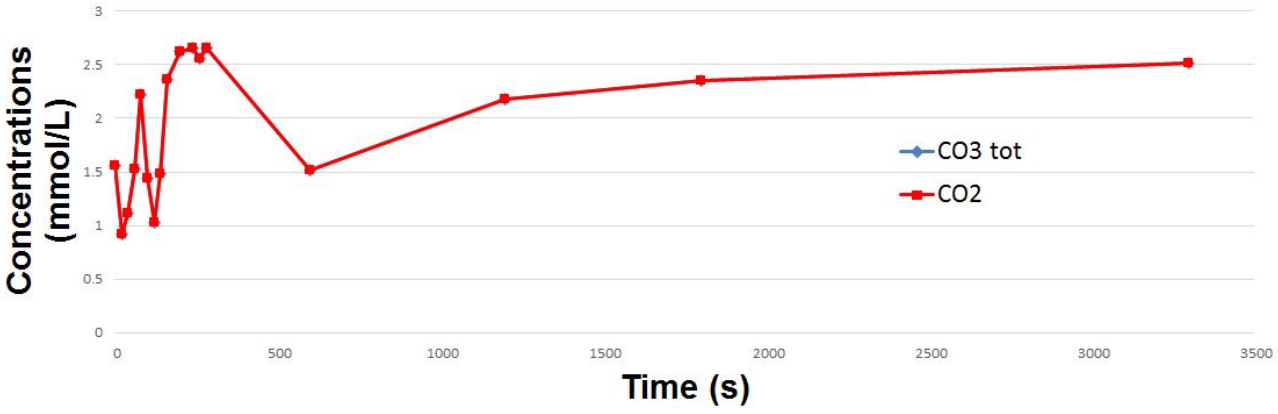

Figure 33: Evolution of $[CO_{3_{tot}}]$ and $[CO_2]$ at the outlet of the airlift during the large-scale CO_2 transfer test **A** of June 2020 / conditions: water temperature = 16.1°C - V_R = 78 400 L - water height = 150 cm - $t_c \simeq 20$ s.

Some comments can be done about these curves. First, as expected, the concentrations in CO_3 coordinates and in CO_2 were equal during the whole test due to the very low pH. Then it can be seen that these concentrations were only of around 2.5 mmol/L, which shows that the amount of sodium bicarbonate non-injected was indeed important as concentrations of more than 10 mmol/L were expected.

These curves show that the test did not give conclusive results. Indeed, the concentration in CO_2 increased over time, which prevents the calculation of the transfer coefficient from the water to the atmosphere. This CO_2 transfer test is thus considered as unsuccessful and its results will not be used in the further analysis.

5.4.2 Large-scale CO_2 transfer test B

The main difference between the first and the second CO_2 transfer tests conducted on a large scale was the sodium bicarbonate injection method. Due to the complications encountered during the injection of the first test, it had been decided that the bicarbonate would be added directly in its powder form in order to make sure that the whole amount was injected. A liquid injection is usually preferred because it is essential that all the sodium bicarbonate dissolves instantaneously in the basin. Otherwise, the remaining solid would dissolve later and transform into CO_2, so the curve of the evolution of the CO_2 concentration would reflect both its transfer to the atmosphere and its production due to the dissolution of bicarbonate. The interpretation of the curve would thus be impossible as the two phenomena could not be differentiated.

The water temperature during the test was of 16.5°C. 200 L of acid were first poured into the pond to make sure that the stoichiometric amount was present to obtain only CO_3 coordinates in the form of $H_2CO_3^*$. The pH of the water dropped to around 1.8 and remained nearly constant during the whole test, as shown in Figure 52 in Appendix 8.5.

Once the acid was homogenised, the sodium bicarbonate was added. Five bags of 25 kg were added simultaneously at the outlet of the airlift during 40 s. The injection time was higher than in test **A** to enhance the dissolution of the powder in the water and avoid the presence of residual solid bicarbonate.

While no visual phenomenon had occurred during the first CO_2 transfer test, the propagation of the sodium bicarbonate along the channel was observed during its injection. An effervescent white streak spread along the basin while the sodium bicarbonate dissolved in the water. The water then regained its initial clear appearance rather quickly, which seemed to indicate that the bicarbonate had dissolved quantitatively.

As in test **A**, samples were collected since the beginning, every 20 s during 5 minutes, then every 5 minutes until one hour. All the samples were titrated and Table 13 in Appendix 8.5 describes the calculation of the concentrations in $CO_{3_{tot}}$ and in CO_2 for each of them. The evolution over time of these concentrations is presented in Figure 34.

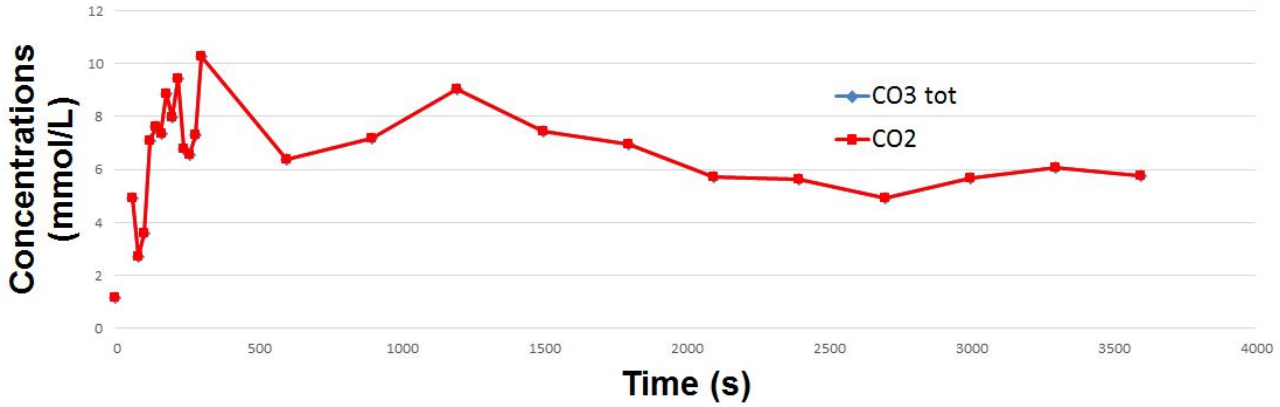

Figure 34: Evolution of $[CO_{3_{tot}}]$ and $[CO_2]$ at the outlet of the airlift during the large-scale CO_2 transfer test **B** of June 2020 / conditions: water temperature = 16.5°C - V_R = 78 400 L - water height = 150 cm - $t_c \simeq 20$ s.

As during test **A**, the low pH induced that the concentration in CO_2 was equal to that in $CO_{3_{tot}}$. The concentrations measured during test **B** were larger than in test **A** and closer to the expected amounts. Moreover, after the first five minutes during which the concentration in CO_2 mostly increased, probably due to the dissolution of residual solid bicarbonate, the CO_2 concentration globally decreased during the rest of the test. The results seem thus to be usable as this decrease allows to calculate a transfer coefficient for the transfer from the water to the atmosphere.

This transfer coefficient is calculated with the method described previously. However, looking at the curve of the concentration in CO_2, various possibilities exist for the definition of the time interval in which the linear regression is built.

Indeed, the regression is supposed to be in the time interval where CO_2 is transferred from water to atmosphere, so when the concentration in dissolved CO_2 decreases. Figure 34 shows that the concentration in CO_2 still rises twice after the first five minutes. These peaks in the curve might be due to local phenomena in the basin such as recirculation or dead zones, or some sodium bicarbonate might have stayed in a solid form and dissolved afterward, which would prevent the interpretation of the test, as explained previously. This possibility needs to be considered, but the clear appearance that the water resumed a few minutes after the injection seems to indicate otherwise.

Be that as it may, the method to measure the transfer coefficient can be applied: the graph of $\ln\left(D\left(t\right)/D_0\right)$ is drawn and its slope gives the value of $-\left(k_l a\right)_{\mathrm{R}}$. However, the increases in concentration, although relatively small, will impact the calculation of $\left(k_l a\right)_{\mathrm{R}}$. The difference compared to the small-scale tests is that three time intervals can be defined here, leading to three values for the transfer coefficient. Considering the whole interval between 300 and 3 600 s is the first option, reducing this interval to 1 200 to 3 600 s is the second one and considering only the decrease between 1 200 and 2 700 s is the third.

For each time interval considered, the curve of $\ln\left(D\left(t\right)/D_0\right)$ is drawn and the linear regression is built. These curves are presented in Figure 35.

The obtained values are gathered in Table 7.

Table 7: Values of the CO_2 transfer coefficient of the large-scale test **B** of June 2020 for the different time intervals used for its calculation / conditions: water temperature = 16.5°C - V_{R} = 78 400 L - water height = 150 cm - $t_{\mathrm{c}} \simeq 20$ s.

Time interval (s)	$\left(k_l a\right)_{\mathrm{R}}$ (s^{-1})	Uncertainty (s^{-1})
1: 300 - 3 600	1.8×10^{-4}	$\pm\ 1 \times 10^{-4}$
2: 1 200 - 3 600	2×10^{-4}	$\pm\ 1.4 \times 10^{-4}$
3: 1 200 - 2 700	4.7×10^{-4}	$\pm\ 8.8 \times 10^{-5}$

It can be seen in Table 7 that the two first time intervals give values rather close to each other but that the third time interval gives a value more than twice as high as the other two. This is logical as the third time interval only considers the decrease of the CO_2 concentration while the others contain the concentration rises such that the transfer is globally smaller.

The uncertainties on the slopes are also higher for the two first time intervals as the curves in Figures 35 do not really evolve linearly. The values of the corresponding transfer coefficients need thus to be regarded along with their uncertainties. The third time interval gives a value that seems more reliable than the other two but its uncertainty remains high.

The impact of the choice of the time interval is studied in the following section, along with the results of the tests conducted on a small-scale.

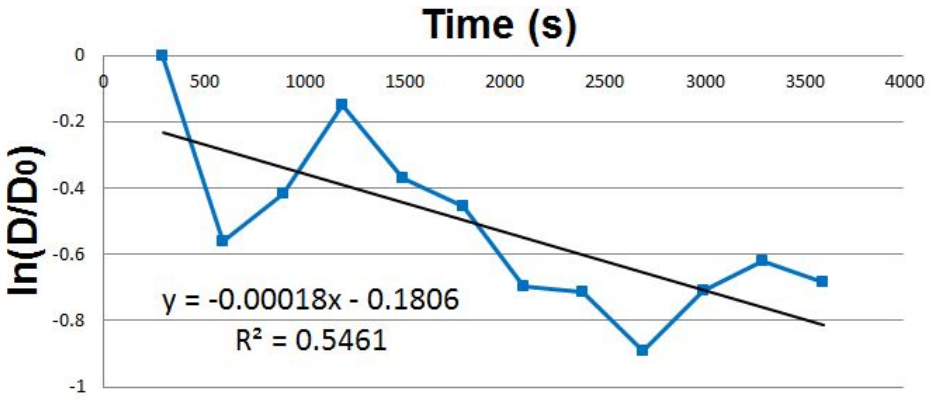

(a) First time interval: 300 s - 3 600 s

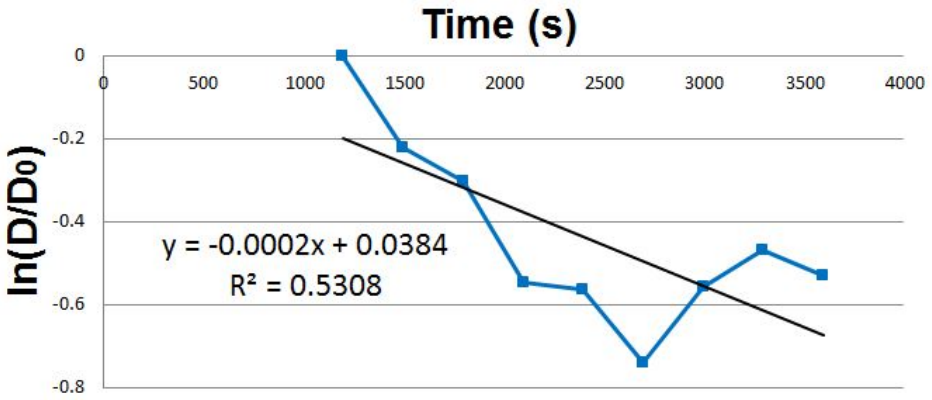

(b) First time interval: 1 200 s - 3 600 s

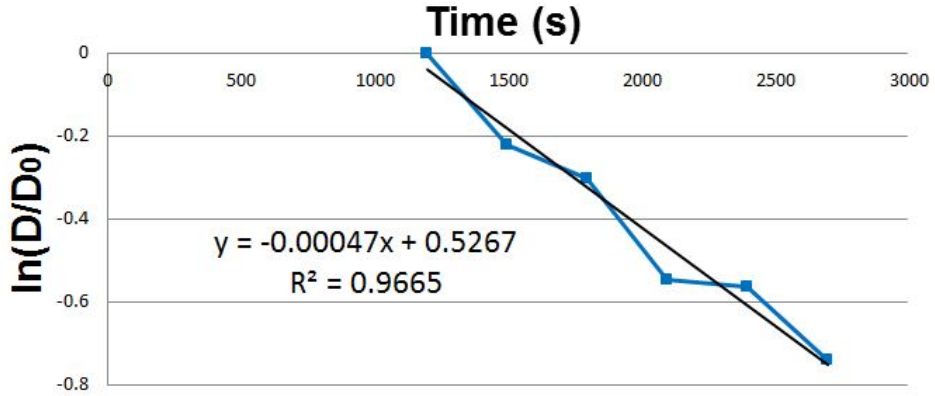

(c) First time interval: 1 200 s - 2 700 s

Figure 35: Curves of $\ln\left(D\left(t\right)/D_0\right)$ at the outlet of the airlift and linear regressions for the large-scale CO_2 transfer test **B** of June 2020 for the three time intervals considered / conditions: water temperature = 16.5°C - V_R = 78 400 L - water height = 150 cm - $t_c \simeq 20$ s - C_S = 1.16 mmol/L.

As explained before, several challenges due to practical considerations have been met while conducting the large-scale tests. The conditions were less ideal than for the tests performed on a small scale and the proposed methodology has sometimes had to be adapted to make the manipulations feasible and safe. If more means were available and if more precise results were required, these challenges could be overcome and the methodology could be followed accurately.

However, as mentioned earlier, the purpose of the large-scale tests session conducted in June 2020 was mainly to see if the methodology was feasible on a large scale and if the obtained results were coherent, bearing in mind the less than ideal conditions under which the tests have been carried out. The former objective was reached and the required adjustments are detailed above; the later is discussed in Section 6.

5.4.3 Comment about the titrations

Before analysing the results of all the tests conducted during this master thesis, a comment should be made concerning the pH-curves obtained with the samples of the large-scale CO_2 transfer tests. Indeed, these curves were different from those obtained for the small-scale tests as the second equivalent point was not at 8.3 but around 7.

All the samples were titrated with NaOH solutions seen the low pH recorded during the tests. A typical example of the pH-curves obtained during the titrations is presented in Figure 36.

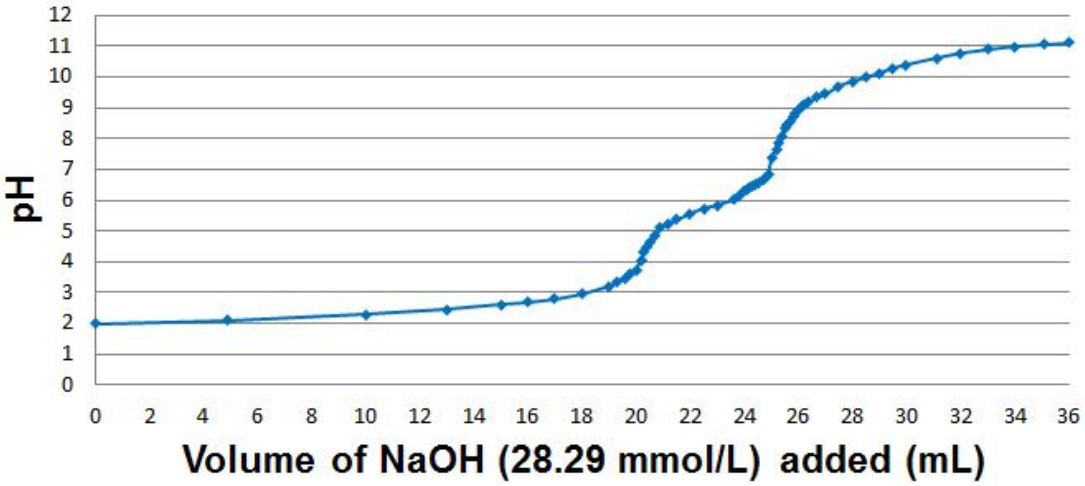

Figure 36: pH-curve of sample "B24" of 24.46 mL (conductivity of 14 850 μs/cm at 25°C) collected during the large-scale CO_2 transfer test **B** of June 2020, titrated at 25°C with a NaOH solution of 28.29 mmol/L.

In Figure 36, it can be seen that the first equivalent point of the carbonate pH-curve is reached at around 4.5, which proves the presence of CO_3 coordinates in the samples, but the second equivalent point is around 7. This second equivalent point is certainly the equivalent point of the titration of HCl with NaOH.

The replacement of the second equivalent point of the carbonate pH-curve by this equivalent point at pH = 7 comes from the large excess of acid in the water during the test compared to the amount of CO_3 coordinates. Indeed, as detailed in the test description, the amount of acid added into the basin was largely superior to the amount of bicarbonate injected during test **A**.

The acid excess might have been smaller during test **B** as all the sodium bicarbonate was injected, but the amount of acid added before this second test has been calculated as if no acid was in the water in the first place, while the remaining acid from test **A** was in fact still present in the pond after the end of this test. This excessive acid injection was however made on purpose to make sure that all the solid sodium bicarbonate would dissolve quickly in order to have analysable results, as explained previously.

This excess of acid resulted in the presence of a higher HCl concentration, which prevailed in the titration curve over the other acid-base couples whose equivalent points are close to 7. For this reason, the second equivalent point of the carbonate pH-curve was not detected in Figure 36, as well as in the pH-curves of all the samples collected during the two large-scale tests.

In the calculation of the concentrations in CO_3 coordinates and in CO_2, the initial pH is taken close to the first equivalent point, so at a pH of around 4.5, and the final point is taken at around 8.3, as for the small-scale tests.

In Figure 36, the volume of the titrant added between these two points is equal to $25.5 - 20.4 = 5.1$ mL.

6 Results analysis

To compare the results of the different tests, the method used to compute the CO_2 transfer coefficients based on the evolution of the concentration is applied in reverse. The fitted values of the transfer coefficients are used to determine the CO_2 concentration over time: Equation (3.6) becomes

$$D(t) = D_0 \exp\left(-\left(k_l a\right)_{\mathrm{R}}\ t\right) \tag{6.1}$$

so the concentration at time t is given by

$$C(t) = C_{\mathrm{S}} - D_0 \exp\left(-\left(k_l a\right)_{\mathrm{R}}\ t\right) \tag{6.2}$$

The theoretical curve of the evolution of the concentration for the given transfer coefficient can thus be drawn and compared to the actual evolution measured during the test.

Before comparing all the CO_2 transfer tests conducted in this master thesis, this method is applied to the three values of $(k_l a)_{\mathrm{R}}$ obtained for the large-scale test **B** of June 2020. Each coefficient from Table 7 gives a curve and the three curves are compared with the actual concentration in Figure 37.

The time interval in which the curves are drawn starts at 300 s as the evolution of the concentration before this moment is too irregular to be used for the calculation of the transfer coefficient.

In Equation (6.2), C_{S} is the CO_2 concentration measured before the bicarbonate injection and $D_0 = C_{\mathrm{S}} - C_0$, where C_0 is the concentration measured at 300 s. In the conditions of test **B** of June 2020, $C_{\mathrm{S}} = 1.16$ mmol/L and $C_0 = 10.3$ mmol/L.

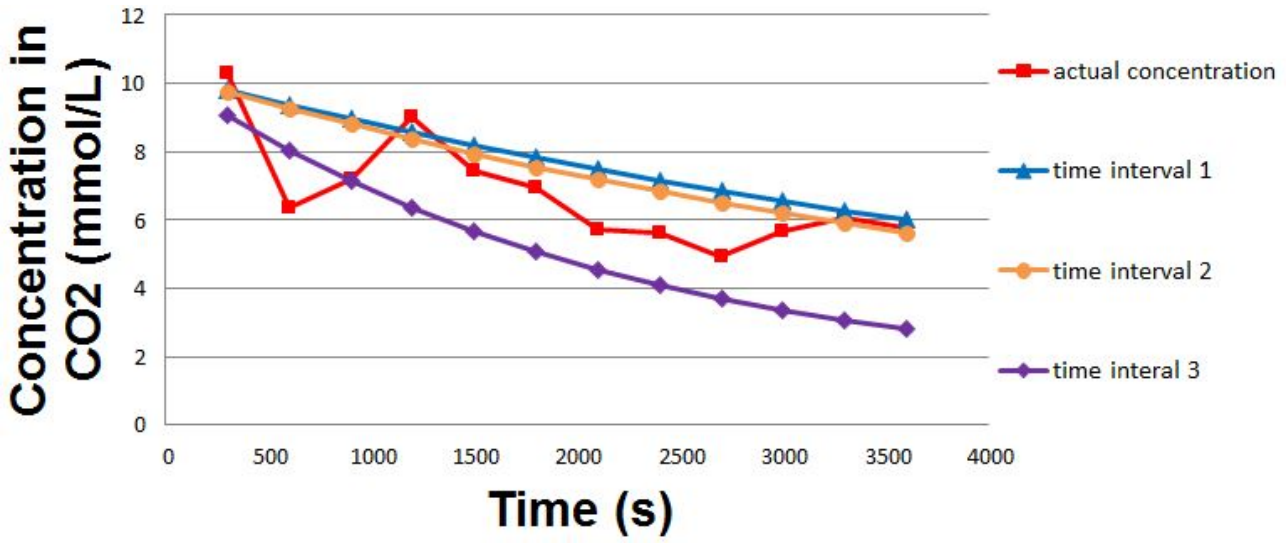

Figure 37: Actual and theoretical curves of the CO_2 concentration for test **B** of June 2020, for the three CO_2 transfer coefficients obtained with the different time intervals.

The first observation is that the actual evolution of the concentration is globally between the "theoretical" curves. Indeed, logically, considering the whole interval underestimates the transfer coefficient while focusing only on the interval in which the concentration decreases overestimates it. This graph shows thus what has already been stated: the CO_2 transfer coefficients obtained with the large-scale test **B** of June 2020 are not extremely reliable.

Regarding the uncertainties on the slopes corresponding to these coefficients, it can be seen that the values of the transfer coefficients might be rather different from those used to draw the curves of Figure 37. A value between 1.8×10^{-4} s^{-1} and 4.7×10^{-4} s^{-1} could be considered

to better model the evolution of the concentration over time. The sum of the square of the differences between the actual and theoretical curves is minimised to this end, varying the value of the transfer coefficient.

The obtained value of $(k_l a)_{\mathrm{R}}$ is 2.6×10^{-4} s^{-1}. The method used to obtain this value being different from the linear regression method, the confidence interval cannot be calculated with the same equations as before. The purpose here being to obtain a single value for the transfer coefficient, the assessment of its 95% confidence interval is not of the highest importance. This confidence interval is thus arbitrarily set at $\pm$ 1.4×10^{-4} s^{-1}, which is the largest confidence interval of Table 7, in order to consider the worst-case scenario. The main point here is that this value is not very reliable, seen the conditions of the test and the calculations made to obtain it, but that it will be used in the further analysis to only have one value to refer to.

The corresponding curve is compared to the others in Figure 38 and it can be seen that the theoretical evolution is closer to the actual evolution with this coefficient.

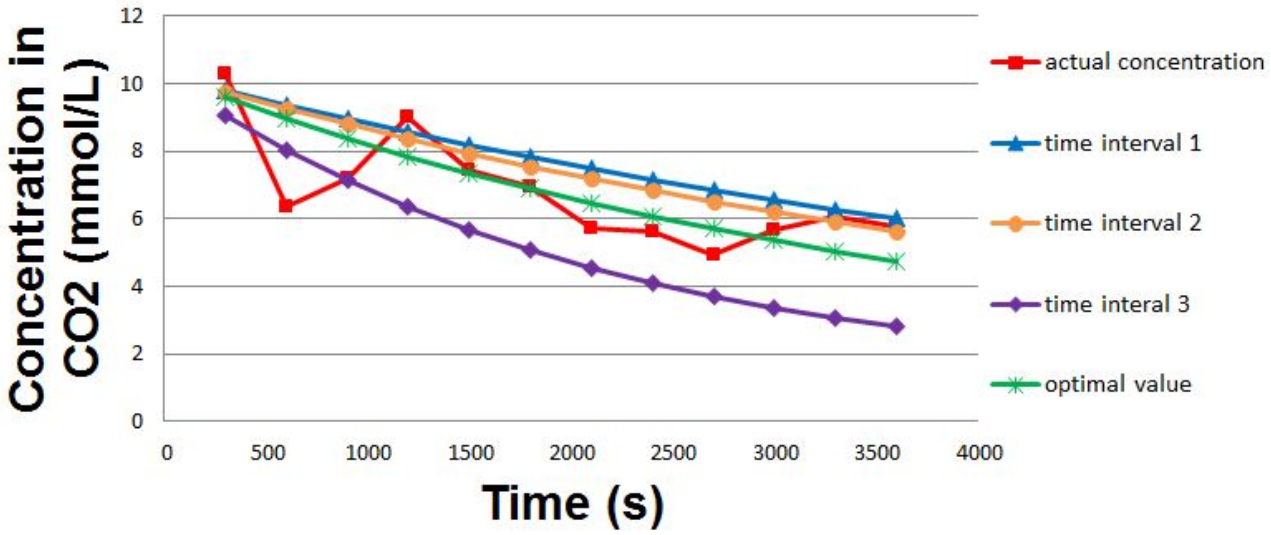

Figure 38: Actual and theoretical curves of the CO_2 concentration for test **B** of June 2020, for the three CO_2 transfer coefficients obtained with the different time intervals and for the optimum of these coefficients.

In the following, this value will be taken as the transfer coefficient of the large-scale CO_2 transfer test **B** in order to have a unique value for the comparisons. Nevertheless, it must be kept in mind that this value is not very reliable, taking into account the initial rises in the curve of the CO_2 concentration and the conditions in which the test has been conducted.

The results of all the tests can then be compared with each other. However, comparing directly volumetric mass transfer coefficients from tests conducted in different basins with different water volumes and at different temperatures is not appropriate. Indeed, mass transfer is characterised by the product of the transfer coefficient with the water volume and the concentration gradient between the two phases. Seen the differences between the conditions of each test, another way is used to compare the results, as explained below.

One of the objectives of this master thesis is to see if a relationship between the volumetric mass transfer coefficients of oxygen and carbon dioxide exists, based on the results of the tests, and if this potential relation verifies Equation (2.2) found in several scientific papers [8, 34, 44, 45]. Verifying such a relation would allow future studies to perform only oxygen transfer tests, which are easier and faster to conduct, and to deduce the value of the CO_2 transfer coefficients from the results of these tests. The CO_2 transfer coefficients are already often calculated based on the oxygen transfer coefficients with Equation (2.2), but very few studies have verified it in the case of HRAPs [8, 10].

Equation (2.2) can be written as

$$\frac{(k_l a)_{CO_2}}{(k_l a)_{O_2}} = \sqrt{\frac{D_{CO_2}}{D_{O_2}}} \tag{6.3}$$

It is thus the ratio of the CO_2 and O_2 transfer coefficients that is regarded, along with the diffusion coefficients at the temperature of the tests. Only the oxygen transfer coefficients of the whole HRAP are used here as they are compared to the transfer coefficients of CO_2 that have only been calculated for the whole basin. A similar approach could be followed in future studies for the transfer coefficients of both airlift and channel if these were measured during the CO_2 transfer tests.

The diffusion coefficients used in the present work come from [85]. Linear interpolations between the two nearest values are used to calculate the coefficients at the desired temperature.

The results of the different tests and the corresponding ratios of volumetric mass transfer and diffusion coefficients are gathered in Table 8. As explained in the description of the tests conducted in Arlon, two CO_2 transfer tests did not give conclusive results: test **A** of the small-scale test session of September 2019 and test **A** of the large-scale test session of June 2020. They are thus not included in Table 8.

Table 8: Summary of the O_2 and CO_2 transfer coefficients of the whole HRAP for all the transfer tests conducted and ratios of the transfer and diffusion coefficients.

	September 2019 **B**	January 2020 **A**	January 2020 **B**	June 2020 **B**
Conditions of the tests				
mean temperature (°C)	23.7	16.6	16.3	16
water height (cm)	9.8	7	7	150
water volume (L)	267.1	408.9	408.9	78 400
t_c (s)	227	393	393	~ 20
Transfer coefficients				
$(k_l a)_{O_2}$ (s^{-1})	2.1×10^{-3} $\pm 2 \times 10^{-5}$	1.7×10^{-3} $\pm 1.9 \times 10^{-5}$	1.7×10^{-3} $\pm 1.9 \times 10^{-5}$	4.3×10^{-4} $\pm 3 \times 10^{-6}$
$(k_l a)_{CO_2}$ (s^{-1})	1.3×10^{-3} $\pm 2.1 \times 10^{-4}$	1×10^{-3} $\pm 1.2 \times 10^{-4}$	1.2×10^{-3} $\pm 4.6 \times 10^{-4}$	2.6×10^{-4} $\pm 1.4 \times 10^{-4}$
Diffusion coefficients				
D_{O_2} (m^2/s)	2.3×10^{-9}	1.9×10^{-9}	1.9×10^{-9}	1.9×10^{-9}
D_{CO_2} (m^2/s)	1.9×10^{-9}	1.6×10^{-9}	1.6×10^{-9}	1.5×10^{-9}
Terms of Equation (6.3)				
$(k_l a)_{CO_2} / (k_l a)_{O_2}$	0.64 $\pm$ 0.11	0.58 $\pm$ 0.08	0.7 $\pm$ 0.28	0.6 $\pm$ 0.33
$\sqrt{D_{CO_2}/D_{O_2}}$	0.89	0.89	0.89	0.89

The results gathered in Table 8 show that a trend seems to emerge.

First, it can be noted that the square root of the ratio of diffusion coefficients in water remains nearly constant in the range of temperature of the tests. According to Equation (6.3), this means that the ratio of mass transfer coefficients should remain constant too.

This trend is indeed observed: the ratios of mass transfer coefficients of all the tests are between 0.58 and 0.7. This range may even be reduced as the value of the CO_2 mass transfer coefficient of test **A** of January 2020 may have been underestimated, as explained in Section 4.4.2. The CO_2 transfer coefficient of this test will thus not be taken into account in further analysis.

The ratios of transfer coefficients obtained for the three test sessions are thus close to each other, even on different scales. This seems to indicate that there is a relationship between the transfer coefficients of oxygen and carbon dioxide and that this relationship is verified on both small and large scales.

However, seen the conditions in which the large-scale tests have been conducted, the value of the ratio of transfer coefficients corresponding to the large-scale tests might not reflect perfectly the behaviour of large-scale HRAPs and it must be kept in mind that many approximations were necessary to obtain it.

The values of the transfer coefficients ratios are nevertheless smaller than what Equation (6.3) suggests. Indeed, to verify this equation, the exponent applied on the ratio of the diffusion coefficients should be of around 3/2 instead of 1/2.

The impact of this difference can be visualised by drawing the theoretical curves of the concentration in CO_2 over time, similarly to those in Figures 37 and 38. The large-scale test **B** is taken as a basis to draw the curves such that D_0 and C_S are the same as above.

Four curves are drawn in addition to that of the actual evolution of the concentration measured during the test. These curves are presented in Figure 39 and represent the theoretical evolution of the concentration for different CO_2 transfer coefficients.

The first three CO_2 transfer coefficients are calculated with the ratios $(k_l a)_{CO_2} / (k_l a)_{O_2}$ obtained for the tests **B** of the different test sessions. Each ratio is multiplied by the O_2 transfer coefficient of June 2020 as it is this test session that serves as a basis for the comparison. The obtained CO_2 transfer coefficients are then used to build the curve of the concentrations similarly to Figure 37 and 38.

The fourth curve presented in Figure 39 corresponds to the CO_2 transfer coefficient expected by Equation (6.3). The ratio of the diffusion coefficients in the conditions of the test session of June 2020 is multiplied by the O_2 transfer coefficient of June 2020.

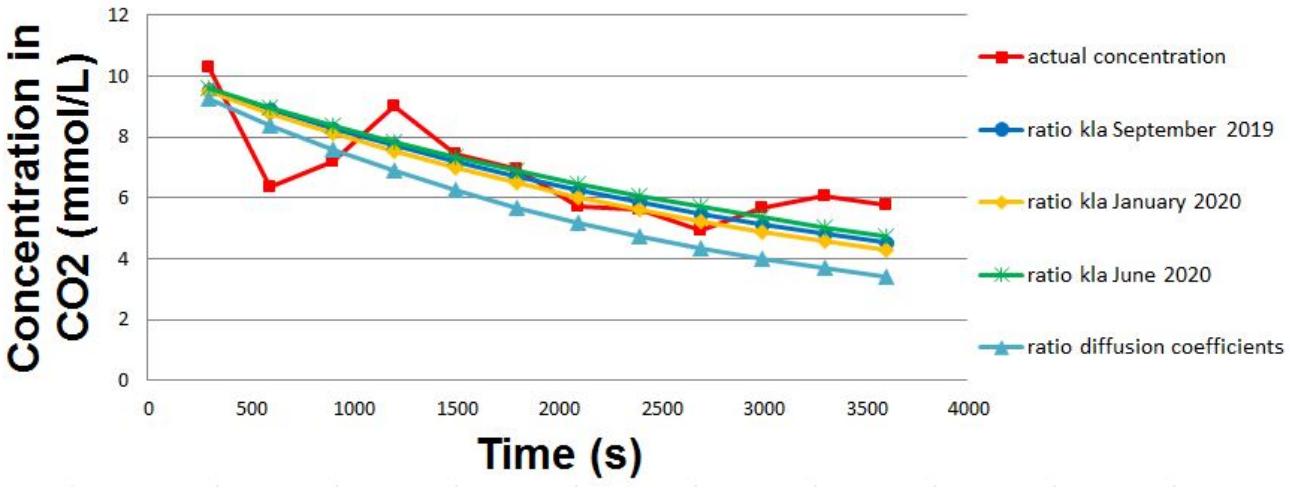

Figure 39: Actual and theoretical curves of the CO_2 concentration for test **B** of June 2020, for four CO_2 transfer coefficients obtained with different ratios $(k_l a)_{CO_2} / (k_l a)_{O_2}$ and with the O_2 transfer coefficient of June 2020.

Several comments can be done regarding Figure 39. First it can be seen that, logically, the best ratio for the modelling of the actual evolution of the CO_2 concentration of June 2020 is the ratio corresponding to the test of June 2020. Indeed, this ratio has been determined to fit as much as possible this particular curve. The ratios based on the other tests slightly overestimate the transfer because they are based on curves where no concentration increase occurred, which was not the case in June 2020. These curves are yet really close to that based on the ratio of June 2020.

The fact that the three curves obtained with the different test sessions are close to each other is encouraging as this ratio is supposed to remain constant seen Equation (6.3). The results show thus that the ratio of mass transfer coefficients is almost constant for tests conducted in different conditions, with different hydrodynamics and on different scales.

The final comment concerning Figure 39 is that Equation (6.3) seems to overestimate the CO_2 transfer coefficient. Even if the difference between the ratio suggested in the literature and the ratios obtained for the different test sessions is relatively small, Equation (6.3) is not verified by the data obtained with the tests conducted in the course of this work. As mentioned previously, the ratio of the diffusion coefficient should be raised to a power of around 3/2 instead of 1/2 to verify the equation.

The results of the tests indicate thus that Equation (6.3) does not seem to be suitable for the case of HRAPs. However, this conclusion is only drawn based on the results of two small-scale tests that seemed successful and one large-scale test for which many complications have been encountered and that gave less trustworthy results.

Moreover, the uncertainty on the actual values of the ratios of mass transfer coefficients is rather important. Stating that Equation (6.3) is wrong for HRAPs seems thus a bit irrelevant seen the small amount of reliable results available.

However, if the absolute numbers are regarded, it can be seen that the values obtained with the relation provided in the literature stay close to those calculated with the presented method. Indeed, for test **B** of January 2020, Equation (6.3) gives a CO_2 transfer coefficient of 1.5×10^{-3} s^{-1} while the value obtained with the methodology is of 1.2×10^{-3} s^{-1}. The two transfer coefficients are thus really close to each other. This is also the case for the tests **B** of September 2019 and June 2020: the orders of magnitude are similar.

The results of the tests seem thus to indicate that, if the precision required for the value of the CO_2 volumetric mass transfer coefficient is not too high, Equation (6.3) can be used to calculate it.

More tests should be conducted to decrease the uncertainty of the results and be able to draw a conclusion about the reliability of Equation (6.3) for HRAPs. These tests should be conducted on both small and large scales and in conditions closer to those of functionning HRAPs for the large-scale tests. More samples should also be collected to decrease the standard deviations of the slopes of the linear regressions.

Seen the data available from the different tests conducted in the course of this master thesis, no more relevant conclusion can be drawn without making too much assumptions. The results of the tests have been compared to the correlation found in the literature, which was one of the objectives of this work.

As already mentioned several times, it must be kept in mind while reading the analyses that the CO_2 transfer tests had never been conducted before in this types of reactor, so that they relied on very few experience. The method seems to give reliable results on a small scale, but the results of the large-scale CO_2 transfer tests are less trustworthy due to the difficult conditions in which the test session has been conducted and the different geometry of the pond compared to common HRAPs.

However, the main objective of this master thesis was to develop a methodology for the evaluation of the CO_2 volumetric mass transfer coefficient in HRAPs and to see if this method was feasible on both small and large scales, with some modifications that have been detailed when necessary. These purposes have been fulfilled and the proposed methodology seems to offer an interesting possibility for the quantification of the CO_2 transfer in HRAPs.

7 Conclusion and perspectives

Some general statements can be drawn about the methodology developed in this master thesis.

First it has been shown that the method is feasible for small-scale tests. The experiments are quite easy to carry out and the results seem reliable. For large-scale tests, the method had to be slightly modified for safety reasons as the acid injection could not be performed in such a short time. However, if more resources were available, the methodology followed on a small scale could be strictly followed on a large scale too: a pump could be used to make the acid injection safer for instance, or larger containers could serve for the dissolution of the sodium bicarbonate before it is added to the pond.

The other important comment concerning the methodology is that it is applied to the specific case of clear tap water. These conditions were chosen to perform the tests, but some modifications would be necessary in other cases. For instance, if salt water was used, which would be the case for the wastewater treatment of shrimp cultures in the HRAP built for the *Renewable* project, the amounts of salt added during the tracer tests would have to be increased to make sure that peaks are detected on the conductivity curve.

Another modification would be related to the presence of other acid-base couples. If phosphorus or silica were present in the water for instance, the corresponding acid-base couples would have to be considered in the equation defining the total potential acidity. The amounts of phosphorus and silica would also have to be titrated in this case, and equations giving their concentration would be required, similarly to those used for the quantification of the CO_2 concentration. Such equations already exist and many are presented in [9].

It is thus essential to know the elemental composition of the water before performing the tests.

The methodology as it is presented in this master thesis is therefore limited to certain conditions, but it can serve as a useful basis for further developments in other specific situations. Based on our knowledge, it is the first time that such a method is used for the quantification of CO_2 transfer between water and atmosphere, so the method can surely be refined in the future.

As the *Renewable* project comes to an end next year, it is interesting to summarise the contributions of the master thesis of D. Royaux, [1], and the work presented here. In [1], the hydrodynamics of the HRAP built in the Ninh Thuan province has been studied and the pilot has been successfully launched to perform oxygen transfer tests. Two years later, a methodology for the quantification of the CO_2 transfer in HRAPs has been developed and would have been tested on the same pilot in the absence of the Covid-19 pandemic of 2020.

The results presented in this master thesis show that the CO_2 transfer coefficient of the HRAP pilot built in the Ninh Thuan province may be calculated based on the oxygen transfer coefficients measured in [1]. Equation (2.2) can be used to obtain a good estimation of the coefficient, or the methodology detailed in this master thesis may be followed to obtain a more accurate value.

By combining the work of D. Royaux, [1], with the current master thesis results, a basis for scaling-up the quantification of O_2 and CO_2 mass transfer coefficients in HRAPs is provided.

On the one hand, the results presented in [1] allow the oxygen mass transfer coefficient to be estimated as a function of operating conditions such as the water level and the injected air flow rate. With the description of the pond used for the tests in [1], it is thus possible to develop equations to calculate the O_2 transfer coefficient in the up-scaling process of the HRAP.

On the other hand, the current work has shown that there seems to be a relationship between the O_2 and CO_2 mass transfer coefficients in HRAPs. Even if Equation (2.2) from the literature could not be validated seen the small number of tests conducted during this master

thesis, the nearly constant ratios $(k_l a)_{CO_2} / (k_l a)_{O_2}$ obtained for the two small-scale tests, and the relatively close ratio obtained on a large scale as well, suggest that the transfer coefficients of oxygen and carbon dioxide are indeed linked to each other.

If equations for the up-scaling of the quantification of the O_2 mass transfer coefficient are developed and if an accurate relationship between the O_2 and CO_2 transfer coefficients is found, this could lead to the calculation of both oxygen and carbon dioxide mass transfer coefficients as a function of the operating conditions. Further work would obviously be necessary to obtain these equations and experimental sessions based on the methodology detailed in this master thesis would certainly be required to achieve this objective, but the results might be worthwhile for future studies.

To help in this process, Table 14 is presented in Appendix 8.6. This table contains the conditions of all the tests and the value of each mass transfer coefficient obtained in the scope of this master thesis.

Moreover, the knowledge of the O_2 and CO_2 transfer coefficients is an important step in the *Renewable* project as they play a part in the calculation of the HRAP surface necessary for the treatment of the wastewater from the shrimp cultures in Vietnam.

Indeed, these coefficients appear in the balance equations of oxygen and carbon dioxide in the water. These mass balances have the form of Equation (7.1):

$$V \frac{dC}{dt} = Q_{\text{inlet}} C_{\text{inlet}} - Q_{\text{outlet}} C_{\text{outlet}} + k_l a \, V \, (C_S - C(t)) + P + R \tag{7.1}$$

where Q_{inlet} and Q_{outlet} are respectively the water flow rates entering and leaving the HRAP and the terms P and R represent the photosynthesis and respiration terms.

The knowledge of the mass transfer coefficients allows to study the algae activity since all the terms of Equation (7.1) are known except P and R. The respiration can be measured by night and, assuming that it stays constant over 24 h, the photosynthetic performances of the algae can be deduced during the day. A more complicated calculation would obviously be required, but following this principle would allow to quantify the algae activity.

The surface of HRAPs necessary for the wastewater treatment could then be calculated, as well as the optimal conditions for the oxygen and carbon dioxide gas injections, to end the design phase of the project. The high rate algal ponds could eventually be built and treat the wastewater before its discharge to the sea, which would help protecting the environment and ecosystems there.

The injection of carbon dioxide from industrial waste gases would also be another benefit of the system and the harvesting of the produced algae would allow to obtain a valuable product that could be sold and increase the plant's profitability.

The work conducted in the course of this master thesis thus intends to play a role, however modest, in the global efforts against water pollution and climate change. The developed methodology is designed for HRAPs, but it could be adapted to other water systems. As it represents a possibility to quantify the CO_2 transfer between water and atmosphere in this type of pond, which is currently a scarcely studied field, this method may lead some industrialists to consider HRAPs as a sustainable solution for their wastewater treatment, or help others in the optimisation of their already functional plants.

References

[1] D. Royaux. Installation and hydrodynamic characterization of a high rate algal pond pilot for the aquaculture wastewater treatment in vietnam. Master's thesis, Université de Liège, Liège, Belgique, 2018.

[2] Stanislav V. Vassilev and Christina G. Vassileva. Composition, properties and challenges of algae biomass for biofuel application: An overview. *Fuel*, 181:1 – 33, 2016.

[3] Zane N. Norvill, Andy Shilton, and Benoit Guieysse. Emerging contaminant degradation and removal in algal wastewater treatment ponds: Identifying the research gaps. *Journal of Hazardous Materials*, 313:291 – 309, 2016.

[4] Armin Hallmann. Algae biotechnology - green cell-factories on the rise. *Current Biotechnology*, 05:1–1, 11 2015.

[5] John J Milledge. Commercial application of microalgae other than as biofuels: a brief review. *Reviews in Environmental Science and Bio/Technology*, 10(1):31–41, 2011.

[6] Anne Flesch, Tom Beer, Peter K Campbell, David Batten, and Tim Grant. Greenhouse gas balance and algae-based biodiesel. In *Algae for Biofuels and Energy*, pages 233–254. Springer, 2013.

[7] Malti Goel, M Sudhakar, and RV Shahi. *Carbon capture, storage and utilization: a possible climate change solution for energy industry*. CRC Press, 2019.

[8] Mbalo Ndiaye, Emilie Gadoin, and Caroline Gentric. Co2 gas–liquid mass transfer and kla estimation: Numerical investigation in the context of airlift photobioreactor scale-up. *Chemical Engineering Research and Design*, 133:90 – 102, 2018.

[9] J. Hissel. *La chimie des eaux - la pratique du calcul des équilibres*. Centre belge d'étude et de documentation des eaux (Cebedeau), 2, rue A Stevart, 4000 Liège, 1975.

[10] Jean-Luc Vasel. personal communication.

[11] Ijaz Rasul, Farrukh Azeem, Muhammad Hussnain Siddique, Saima Muzammil, Azhar Rasul, Anam Munawar, Muhammad Afzal, Muhammad Amjad Ali, and Habib Nadeem. *Algae Biotechnology*, pages 301–334. 12 2017.

[12] Ayhan Demirbas. Use of algae as biofuel sources. *Energy Conversion and Management*, 51(12):2738 – 2749, 2010.

[13] Emily M Trentacoste, Alice M Martinez, and Tim Zenk. The place of algae in agriculture: policies for algal biomass production. *Photosynthesis research*, 123(3):305–315, 2015.

[14] V. Venn. Cyanobacteria: Definition, characteristics and species, November 2014. `https://www.youtube.com/watch?v=VBluODfrP9w`, accessed on March 27, 2020.

[15] Chemisty Libre texts. Formation of carbohydrates by photosynthesis, June 2019. `https://chem.libretexts.org/Bookshelves/Organic_Chemistry/Book%3A_Basic_Principles_of_Organic_Chemistry_(Roberts_and_Caserio)/20%3A_Carbohydrates/20.10%3A_Formation_of_Carbohydrates_by_Photosynthesis`, accessed on April 20, 2020.

[16] Scott J. Edmundson and Michael H. Huesemann. The dark side of algae cultivation: Characterizing night biomass loss in three photosynthetic algae, chlorella sorokiniana, nannochloropsis salina and picochlorum sp. *Algal Research*, 12:470 – 476, 2015.

[17] Quang Hu, N Kurano, M Kawachi, I Iwasaki, and S Miyachi. Ultrahigh-cell-density culture of a marine green alga chlorococcum littorale in a flat-plate photobioreactor. *Applied Microbiology and Biotechnology*, 49(6):655–662, 1998.

[18] G Torzillo, A Sacchi, R Materassi, and A Richmond. Effect of temperature on yield and night biomass loss in spirulina platensis grown outdoors in tubular photobioreactors. *Journal of Applied Phycology*, 3(2):103–109, 1991.

[19] Shaikh A. Razzak, Mohammad M. Hossain, Rahima A. Lucky, Amarjeet S. Bassi, and Hugo de Lasa. Integrated co2 capture, wastewater treatment and biofuel production by microalgae culturing—a review. *Renewable and Sustainable Energy Reviews*, 27:622 – 653, 2013.

[20] Yordanka Reyes Cruz, Donato AG Aranda, Peter R Seidl, Gisel C Diaz, Rene G Carliz, Mariana M Fortes, DAMP da Ponte, Rosa CV de Paula, et al. Cultivation systems of microalgae for the production of biofuels. *Biofuels-State of Development*, 2018.

[21] A. Richel D. Toye, F. Delvigne. *Questions avancées en Génie Chimique : Biotechnologie*. University of Liège, 2019.

[22] Donghee Hoh, Stuart Watson, and Eunsung Kan. Algal biofilm reactors for integrated wastewater treatment and biofuel production: A review. *Chemical Engineering Journal*, 287:466 – 473, 2016.

[23] T Van Harmelen and H Oonk. Microalgae biofixation processes: applications and potential contributions to greenhouse gas mitigation options. *TNO Built Environment and Geosciences, Apeldoorn, The Netherlands*, 56, 2006.

[24] Lisa Jackson. Pond-cultivated algae: Slimy superhero for aquafeeds? - using photosynthesis instead of industrial fermentation, qualitas health turns desert land into fatty acid farms, May 2019. `https://www.aquaculturealliance.org/advocate/pond-cultivated-algae-slimy-superhero-aquafeeds/`, accessed on April 19, 2020.

[25] Zouhayr Arbib, Jesús Ruiz, Pablo Álvarez Díaz, Carmen Garrido-Pérez, Jesus Barragan, and José A. Perales. Long term outdoor operation of a tubular airlift pilot photobioreactor and a high rate algal pond as tertiary treatment of urban wastewater. *Ecological Engineering*, 52:143 – 153, 2013.

[26] R.N. Singh and Shaishav Sharma. Development of suitable photobioreactor for algae production – a review. *Renewable and Sustainable Energy Reviews*, 16(4):2347 – 2353, 2012.

[27] C.U. Ugwu, H. Aoyagi, and H. Uchiyama. Photobioreactors for mass cultivation of algae. *Bioresource Technology*, 99(10):4021 – 4028, 2008.

[28] A. Alaswad, Michele Dassisti, T. Prescott, and Abdul Ghani Olabi. Technologies and developments of third generation biofuel production. *Renewable and Sustainable Energy Reviews*, 51:1446–1460, 08 2015.

[29] Donna L Sutherland, Matthew H Turnbull, and Rupert J Craggs. Increased pond depth improves algal productivity and nutrient removal in wastewater treatment high rate algal ponds. *Water Research*, 53:271–281, 2014.

[30] Larissa Terumi Arashiro, Neus Montero, Ivet Ferrer, Francisco Gabriel Acién, Cintia Gómez, and Marianna Garfí. Life cycle assessment of high rate algal ponds for wastewater treatment and resource recovery. *Science of The Total Environment*, 622-623:1118 – 1130, 2018.

[31] R Craggs, J Park, S Heubeck, and D Sutherland. High rate algal pond systems for low-energy wastewater treatment, nutrient recovery and energy production. *New Zealand Journal of Botany*, 52(1):60–73, 2014.

[32] Teresa M Mata, Antonio A Martins, and Nidia S Caetano. Microalgae for biodiesel production and other applications: a review. *Renewable and sustainable energy reviews*, 14(1):217–232, 2010.

[33] Rupert Craggs, Donna Sutherland, and Helena Campbell. Hectare-scale demonstration of high rate algal ponds for enhanced wastewater treatment and biofuel production. *Journal of Applied Phycology*, 24(3):329–337, 2012.

[34] R. Puskeiler, M. Edler, K. Didzus, R. Müller, and J. Gabelsberger. Mass transfer considerations for scale-up and scale-down of animal cell bioprocesses. In Nigel Jenkins, Niall Barron, and Paula Alves, editors, *Proceedings of the 21st Annual Meeting of the European Society for Animal Cell Technology (ESACT), Dublin, Ireland, June 7-10, 2009*, pages 451–454, Dordrecht, 2012. Springer Netherlands.

[35] Abbas Mehrabadi, Rupert Craggs, and Mohammed M. Farid. Wastewater treatment high rate algal ponds (wwt hrap) for low-cost biofuel production. *Bioresource Technology*, 184:202 – 214, 2015. Advances in biofuels and chemicals from algae.

[36] JBK Park, RJ Craggs, and AN Shilton. Wastewater treatment high rate algal ponds for biofuel production. *Bioresource technology*, 102(1):35–42, 2011.

[37] I Rawat, R Ranjith Kumar, T Mutanda, and F Bux. Dual role of microalgae: phycoremediation of domestic wastewater and biomass production for sustainable biofuels production. *Applied energy*, 88(10):3411–3424, 2011.

[38] Stephen L Pahl, Andrew K Lee, Theo Kalaitzidis, Peter J Ashman, Suraj Sathe, and David M Lewis. Harvesting, thickening and dewatering microalgae biomass. In *Algae for biofuels and energy*, pages 165–185. Springer, 2013.

[39] John R Benemann. Bio-fixation of co2 and greenhouse gas abatement with microalgae-technology roadmap. *Final Report to the US Department of Energy. National Energy Technology Laboratory*, 2003.

[40] J. B. K. Park and R. J. Craggs. Algal production in wastewater treatment high rate algal ponds for potential biofuel use. *Water Science and Technology*, 63(10):2403–2410, 05 2011.

[41] H. El Ouarghi, B. E. Boumansour, O. Dufayt, B. El Hamouri, and J. L. Vasel. Hydrodynamics and oxygen balance in a high-rate algal pond. *Water Science and Technology*, 42(10-11):349–356, 11 2000.

[42] Aidong Yang. Modeling and evaluation of co2 supply and utilization in algal ponds. *Industrial & engineering chemistry research*, 50(19):11181–11192, 2011.

[43] Gordon A. Hill. Measurement of overall volumetric mass transfer coefficients for carbon dioxide in a well-mixed reactor using a ph probe. *Industrial & Engineering Chemistry Research*, 45(16):5796–5800, 2006.

[44] J. de la Noüe P. Talbot, R. W. Lencki. Carbon dioxide absorption characterization of a bioreactor for biomass production of phormidium bohneri: comparative study of three types of diffuser. *Journal of Applied Phycology*, 2:341–350, 1990.

[45] P. Talbot, M. P. Gortares, R. W. Lencki, and J. de la Noüe. Absorption of co2 in algal mass culture systems: A different characterization approach. *Biotechnology and Bioengineering*, 37(9):834–842, 1991.

[46] Garima Goswami, Vinal Bang, and Shubham Agarwal. Diverse applications of algae. *International Journal of Advance Research In Science And Engineering*, 4(1):1102–1109, 2015.

[47] Rupert J Craggs, Tryg J Lundquist, and John R Benemann. Wastewater treatment and algal biofuel production. In *Algae for biofuels and energy*, pages 153–163. Springer, 2013.

[48] Richard Sayre. Microalgae: The Potential for Carbon Capture. *BioScience*, 60(9):722–727, 10 2010.

[49] Diana Moreira and José C.M. Pires. Atmospheric co2 capture by algae: Negative carbon dioxide emission path. *Bioresource Technology*, 215:371 – 379, 2016. Waste Biorefinery - Advocating Circular Economy.

[50] Nicholas Sazdanoff. *Modeling and simulation of the algae to biodiesel fuel cycle*. PhD thesis, The Ohio State University, 2006.

[51] Gerhard Knothe. Production and properties of biodiesel from algal oils. In *Algae for biofuels and energy*, pages 207–221. Springer, 2013.

[52] Nathan Whitely, Riko Ozao, Ramon Artiaga, Yan Cao, and Wei-Ping Pan. Multi-utilization of chicken litter as biomass source. part i. combustion. *Energy & Fuels*, 20(6):2660–2665, 2006.

[53] Altas Pro. Eutrophication explained, October 2018. `https://www.youtube.com/watch?v=mLbDbmmV6Qc`, accessed on April 6, 2020.

[54] Pavlo Bohutskyi, Kexin Liu, Ben A Kessler, Thomas Kula, Yongseok Hong, Edward J Bouwer, Michael J Betenbaugh, and FC Thomas Allnutt. Mineral and non-carbon nutrient utilization and recovery during sequential phototrophic-heterotrophic growth of lipid-rich algae. *Applied microbiology and biotechnology*, 98(11):5261–5273, 2014.

[55] Dajana J Kovač, Jelica B Simeunović, Olivera B Babić, Aleksandra Č Mišan, and Ivan Lj Milovanović. Algae in food and feed. *Food and Feed Research*, 40(1):21–32, 2013.

[56] Indira Priyadarshani and Biswajit Rath. Commercial and industrial applications of micro algae–a review. *Journal of Algal Biomass Utilization*, 3(4):89–100, 2012.

[57] Sharma Poonam and Sharma Nivedita. Industrial and biotechnological applications of algae: A review. *Journal of Advances in Plant Biology*, 1(1):01 – 25, 2017.

[58] Global algae products market is expected to reach usd 5.60 billion by 2025, April 2019. `https://stocknewsmagazine.com/global-algae-products-market-expected-reach-usd-5-60-billion-2025-key-analysis`, accessed on April 23, 2020.

[59] Christos Chatzissavvidis and Ioannis Therios. *Role of algae in agriculture*, pages 1–37. 01 2014.

[60] Neveen Abdel-Raouf, Ali Al-Homaidan, and Ibraheem Ibraheem. Agricultural importance of algae. *African journal of biotechnology*, 11:11648–11658, 07 2012.

[61] VK Dhargalkar and Neelam Pereira. Seaweed: promising plant of the millennium. *Science and culture*, 71:60–66, 04 2005.

[62] Irum Sarfaraz. The effects of chemical fertilizers on soil, July 2017. `https://www.hunker.com/13427782/the-effects-of-chemical-fertilizers-on-soil`, accessed on April 23, 2020.

[63] Danny Lipford. The debate over organic vs. chemical fertilizers. `https://todayshomeowner.com/debate-over-organic-chemical-fertilizers/`, accessed on March 30, 2020.

[64] A.B. Ross, J.M. Jones, M.L. Kubacki, and T. Bridgeman. Classification of macroalgae as fuel and its thermochemical behaviour. *Bioresource Technology*, 99(14):6494 – 6504, 2008.

[65] Liang Wang, Johan Hustad, Øyvind Skreiberg, Geir Skjevrak, and Morten Grønli. A critical review on additives to reduce ash related operation problems in biomass combustion applications. *Energy Procedia*, 20:20–29, 12 2012.

[66] Simon Jegan Porphy Jegathese and Mohammed Farid. Microalgae as a renewable source of energy: A niche opportunity. *Journal of Renewable Energy*, 2014, 2014.

[67] F.B. Green, T.J. Lundquist, and W.J. Oswald. Energetics of advanced integrated wastewater pond systems. *Water Science and Technology*, 31(12):9 – 20, 1995. Waste Stabilisation Ponds and the Reuse of Pond Effluents.

[68] Dionissios Mantzavinos and Nicolas Kalogerakis. Treatment of olive mill effluents: Part i. organic matter degradation by chemical and biological processes—an overview. *Environment international*, 31(2):289–295, 2005.

[69] Raul Muñoz and Benoit Guieysse. Algal–bacterial processes for the treatment of hazardous contaminants: A review. *Water Research*, 40(15):2799 – 2815, 2006.

[70] John R Benemann. Bio-fixation of co2 and greenhouse gas abatement with microalgae-technology roadmap. *Final Report to the US Department of Energy. National Energy Technology Laboratory*, 2003.

[71] Abdul Raheem, W.A.K.G. [Wan Azlina], Y.H. [Taufiq Yap], Michael K. Danquah, and Razif Harun. Thermochemical conversion of microalgal biomass for biofuel production. *Renewable and Sustainable Energy Reviews*, 49:990 – 999, 2015.

[72] John S Burlew et al. Algal culture from laboratory to pilot plant. *Algal culture from laboratory to pilot plant.*, 1953.

[73] S. Gerbinet A. Leonard. *Life cycle assessment - Ecodesign.* University of Liège, 2019.

[74] Roy Haggerty, Sean A. McKenna, and Lucy C. Meigs. On the late-time behavior of tracer test breakthrough curves. *Water Resources Research*, 36(12):3467–3479, 2000.

[75] H Scott Fogler. *Essentials of Chemical Reaction Engineering: Essenti Chemica Reactio Engi.* Pearson Education, 2010.

[76] Said Nacir, Fouad Zouhir, Naila Ouazzani, Hugues Jupsin, Jean-Luc Vasel, and Laila Mandi. Comparaison des systèmes d'agitation par diffuseur d'air et roue à aube dans un chenal algal à haut rendement. *Revue des sciences de l'eau/Journal of Water Science*, 25(3):287–299, 2012.

[77] Maine Volunteer Lake Monitoring Programme. Maximum dissolved oxygen concentration saturation table, June 2014. `http://www.mainevlmp.org/wp-content/uploads/2014/01/Maximum-Dissolved-Oxygen-Concentration-Saturation-Table.pdf`, accessed on February 26, 2020.

[78] Faith A Morrison. Obtaining uncertainty measures on slope and intercept of a least squares fit with excel's linest. *Houghton, MI: Department of Chemical Engineering, Michigan Technological University. Retrieved August*, 6:2015, 2014.

[79] Harvard University. A summary of error propagation, 2007. `http://ipl.physics.harvard.edu/wp-uploads/2013/03/PS3_Error_Propagation_sp13.pdf`.

[80] Ole Pedersen, Timothy Colmer, and Kaj Sand-Jensen. Underwater photosynthesis of submerged plants – recent advances and methods. *Frontiers in plant science*, 4:140, 05 2013.

[81] Henri Roques. *Fondements théoriques du traitement chimique des eaux*. Technique et documentation-Lavoisier, 1990.

[82] Utah State University. Carbon dioxide and carbonic acid, December 2006. `http://ion.chem.usu.edu/~sbialkow/Classes/3650/Carbonate/Carbonic%20Acid.html`, accessed on May 1, 2020.

[83] Sylvie Gillot, Fairouz Kies, Christophe Amiel, Michel Roustan, and Alain Héduit. Application of the off-gas method to the measurement of oxygen transfer in biofilters. *Chemical Engineering Science*, 60(22):6336 – 6345, 2005. 7th International Conference on Gas-Liquid and Gas-Liquid-Solid Reactor Engineering.

[84] David Redmon, William C Boyle, and Lloyd Ewing. Oxygen transfer efficiency measurements in mixed liquor using off-gas techniques. *Journal (Water Pollution Control Federation)*, pages 1338–1347, 1983.

[85] Michel Roustan. Transferts gaz-liquide dans les procédés de traitement des eaux et des effluents gazeux. 2003.

8 Appendices

8.1 Glossary

- A: function of the water temperature
- C: concentration (mol/L)
- C_{S}: concentration at saturation (mol/L)
- $\mathrm{CO}_{3_{\mathrm{tot}}}$: total amount of CO_3 coordinates in the water (mol)
- CCS: carbon capture and storage
- CFD: computational fluid dynamics
- γ_i: activity coefficient of the CO_3 coordinate form i
- D: deficit (mol/L)
- D_i: diffusion coefficient of component i (m^2/s)
- d_{32}: distribution function of the $\mathrm{H_2CO_3^*}$ form among the CO_3 coordinates
- DO: dissolved oxygen (mol)
- Δ: difference between the initial and final points of the range of pH of interest
- ϵ: dielectric constant of water
- f_{11} and f_{12}: distribution functions of real solutions
- FAME: fatty acid methyl ester
- g: relative volume of water
- HRAP: high rate algal pond
- J: ionic force of water (mol/L)
- K_0: equilibrium constant of water dissociation
- K_i: equilibrium constant of the CO_3 coordinate form i
- $k_l a$: volumetric mass transfer coefficient (s^{-1})
- $(k_l a)_{\mathrm{A}}$: volumetric mass transfer coefficient in the airlift (s^{-1})
- $(k_l a)_{\mathrm{channel}}$: volumetric mass transfer coefficient along the channel (s^{-1})
- $(k_l a)_{\mathrm{R}}$: volumetric mass transfer coefficient along the whole reactor (s^{-1})
- $\widehat{m}$: mean of a slope
- m_i: concentration of component i (mol/L)
- $n(i)$: amount of component i (mol)
- n_{H^+}: amount of H^+ ions (mol)

- n_{OH^-}: amount of OH^- ions (mol)
- NET: negative emission technology
- $[OH_{tot}]$: concentration of water in water
- P: photosynthesis term in the mass balance (7.1)
- PUFA: polyunsaturated fatty acid
- ρ: resistivity of water (ohm.cm)
- Q: water flow rate (m^3/s)
- R: respiration term in the mass balance (7.1)
- s_m: standard deviation of a slope
- t: time (s) or temperature (°C)
- T: temperature (K)
- t_A: time required by the water to cross the airlift (s)
- t_c: circulation time (s)
- $t_{channel}$: time required by the water to cross the channel (s)
- t_{probe}: temperature at which a probe records the measured variable (°C)
- t_{test}: water temperature during the test (°C)
- $t_{titration}$: water temperature during the titration (°C)
- TPA, or $[H^+_{tot}]$: total potential acidity (mol/L)
- V: volume of a water packet of interest (L)
- V_A: volume of water in the airlift (L)
- $V_{channel}$: volume of water in the channel (L)
- $V_{container}$: volume of liquid in the container at the end of the titration (L)
- V_R: volume of water in the whole reactor (L)
- V_{sample}: initial volume of water in the sample before the titration (L)
- WWT: wastewater treatment
- z_i: valence of component i

8.2 Dimensions of the HRAPs

8.2.1 Small-scale ponds

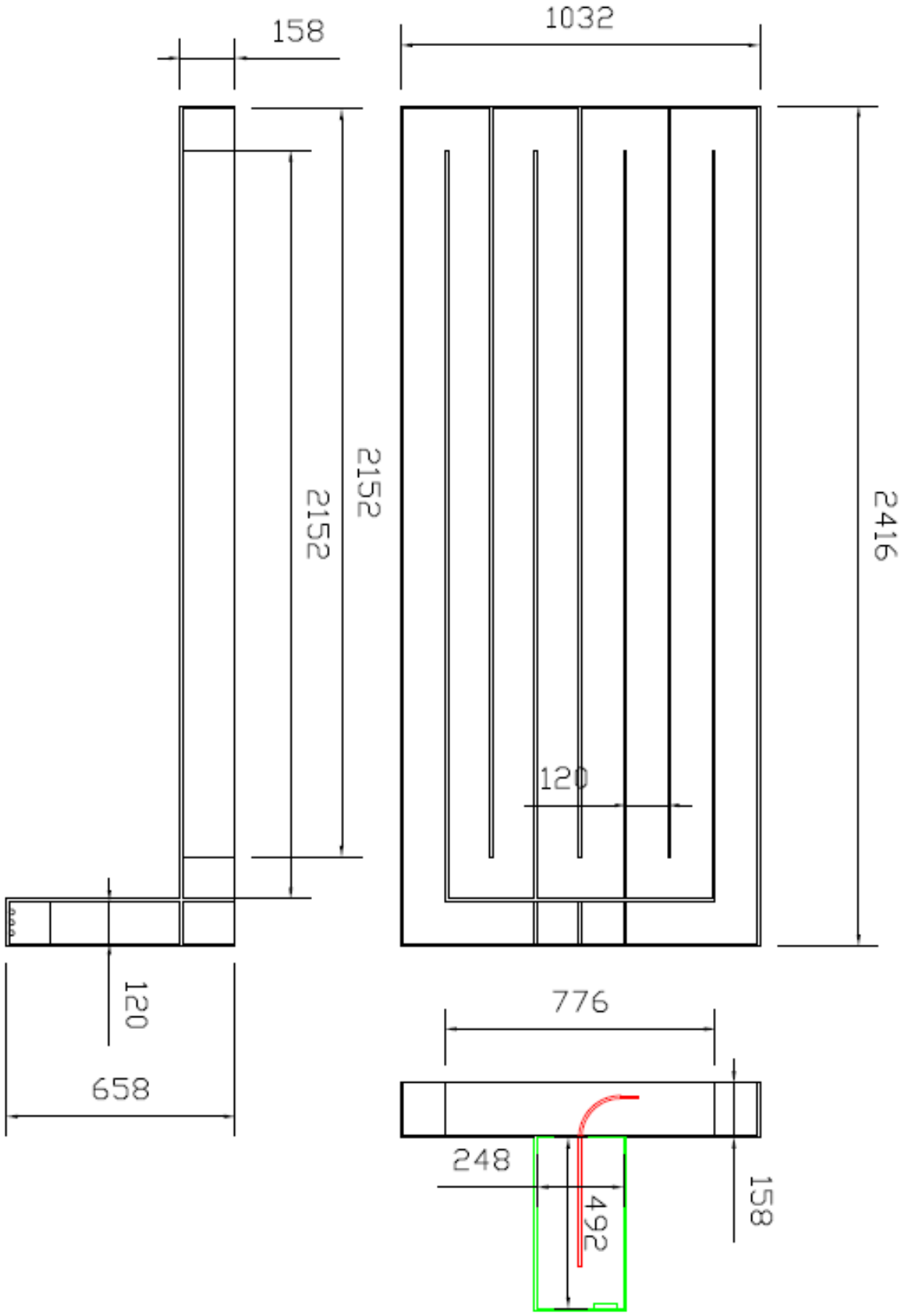

Figure 40: Dimensions of the small-scale basin 1 used for the test session of September 2019.

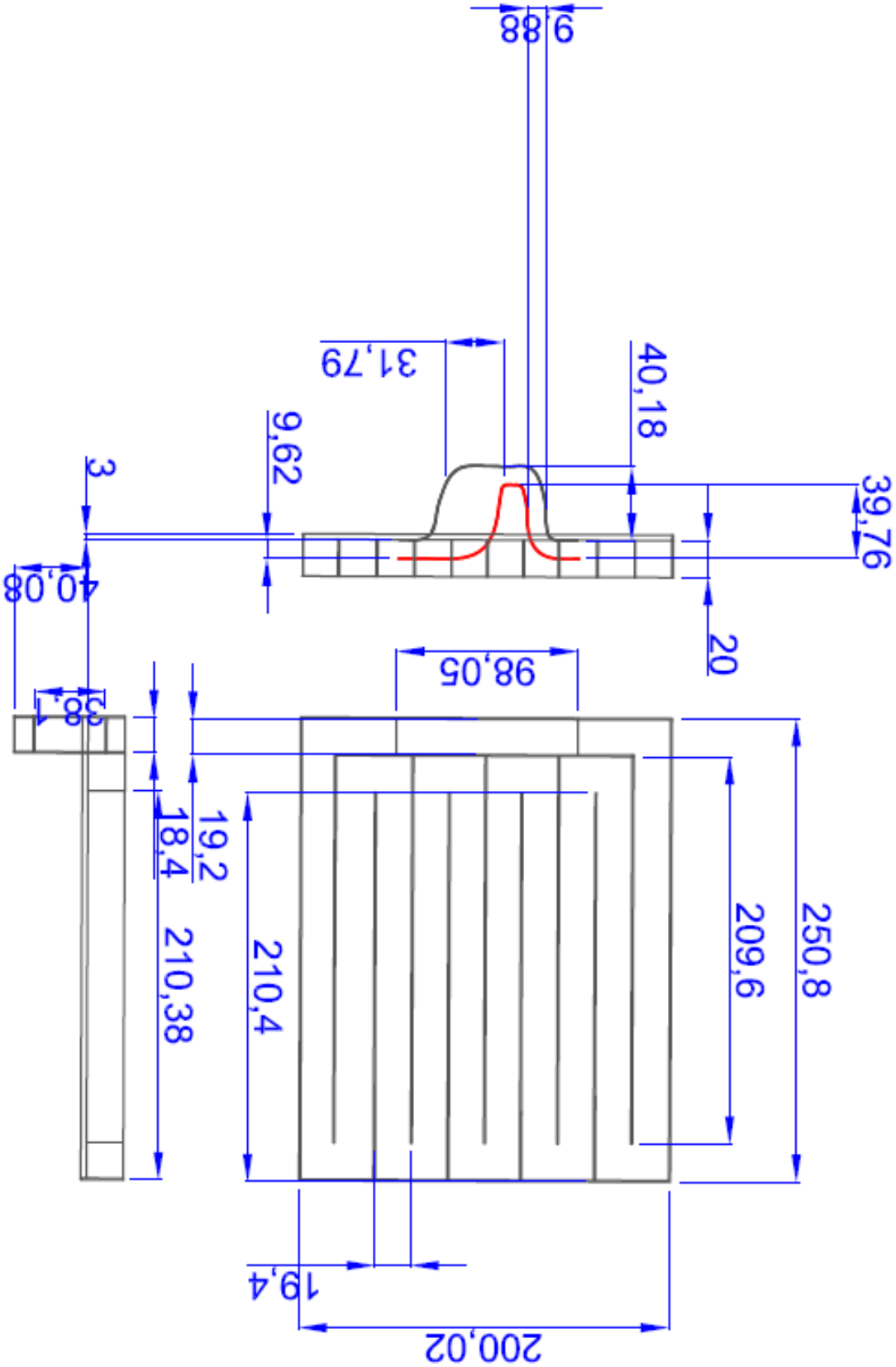

Figure 41: Dimensions of the small-scale basin 2 used for the test session of January 2020.

8.2.2 Large-scale pond

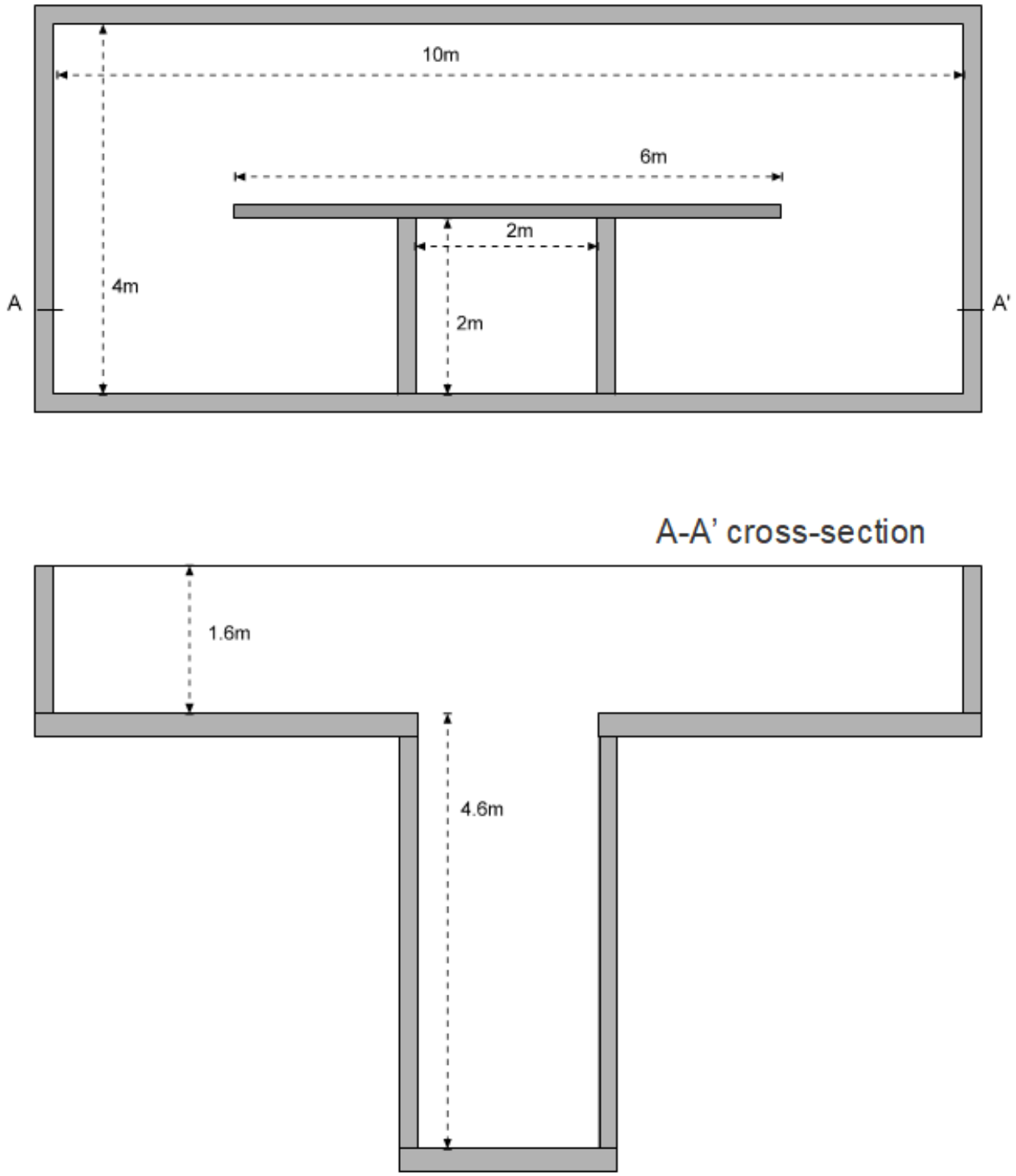

Figure 42: Dimensions of the large-scale basin used for the test session of June 2020.

8.3 Oxygen transfer tests

8.3.1 September 2019

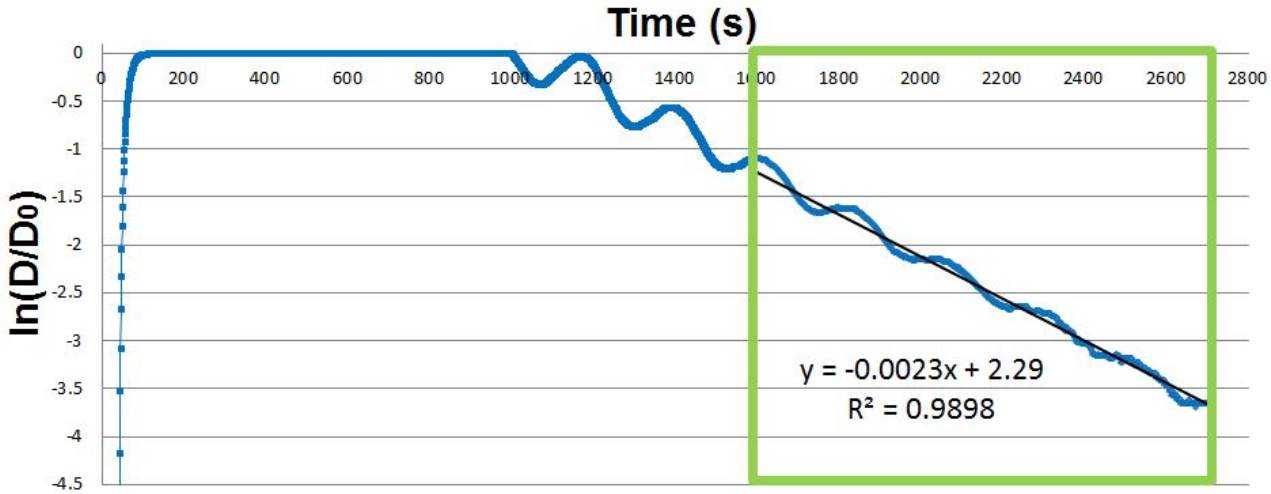

Figure 43: Curve of $\ln\left(D\left(t\right)/D_0\right)$ at the outlet of the airlift and linear regression in the relevant interval for the small-scale O_2 transfer test of September 2019: $\left(k_l a\right)_{\mathrm{R}} = 2.3 \times 10^{-3}$ s^{-1} ($\pm$ 1.3×10^{-5} s^{-1}) / conditions: water temperature = 23.8°C - $V_{\mathrm{R}} = 267.1$ L - water height = 9.8 cm - $t_{\mathrm{c}} = 227$ s - $C_{\mathrm{S}} = 8.5$ mg/L.

8.3.2 January 2020

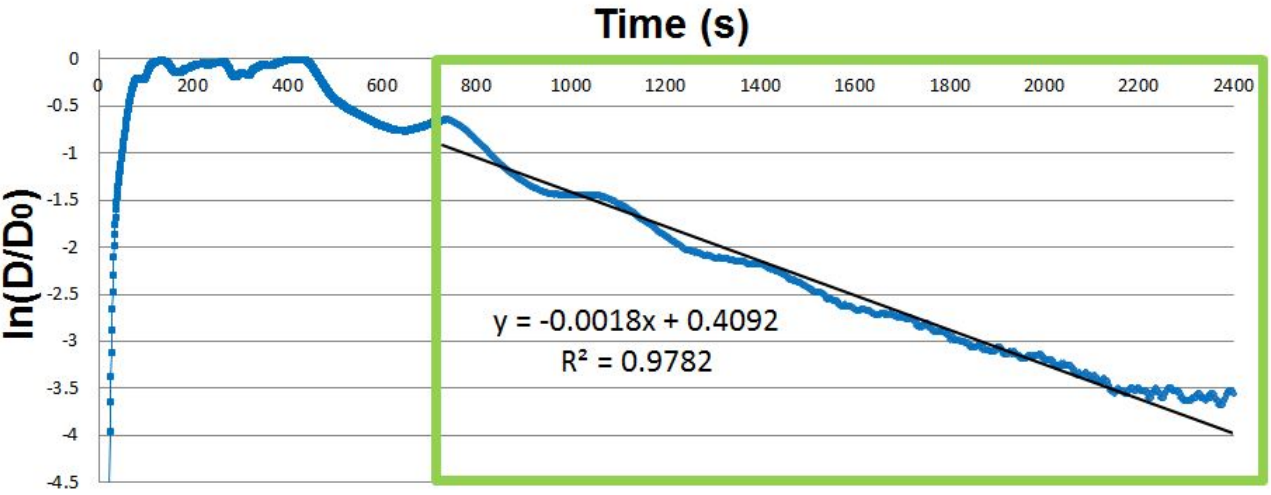

Figure 44: Curve of $\ln\left(D\left(t\right)/D_0\right)$ at the outlet of the airlift and linear regression in the relevant interval for the small-scale O_2 transfer test of January 2020: $\left(k_l a\right)_{\mathrm{R}} = 1.8 \times 10^{-3}$ s^{-1} ($\pm$ 1.2×10^{-5} s^{-1}) / conditions: water temperature = 16.2°C - $V_{\mathrm{R}} = 408.9$ L - water height = 7 cm - $t_{\mathrm{c}} = 393$ s - $C_{\mathrm{S}} = 9.97$ mg/L.

8.3.3 June 2020

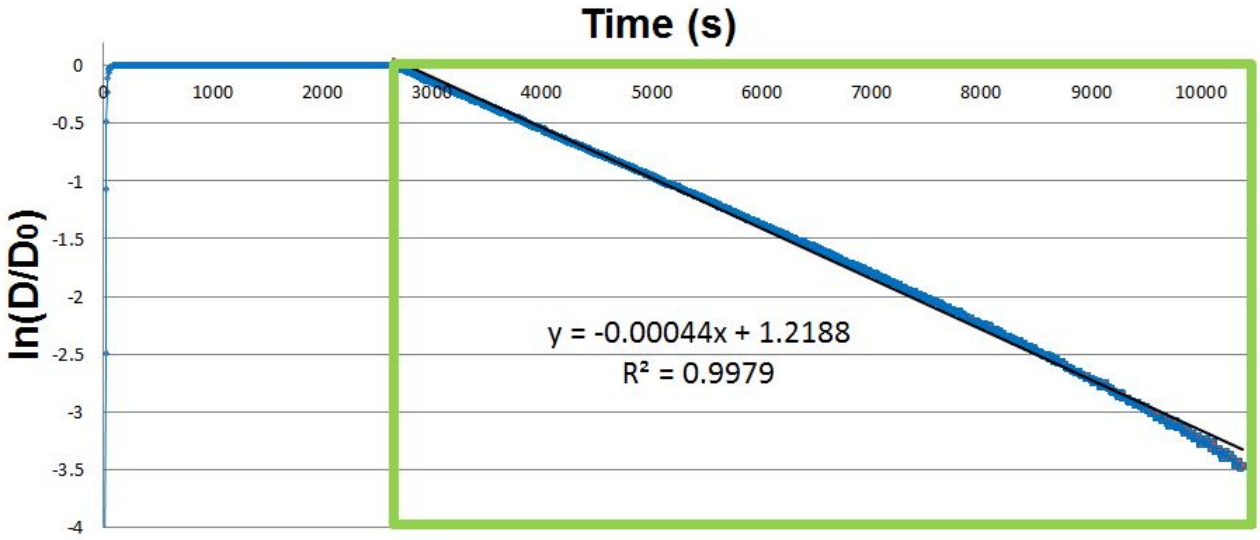

Figure 45: Curve of $\ln\left(D\left(t\right)/D_0\right)$ at the outlet of the airlift and linear regression in the relevant interval for the large-scale O_2 transfer test of June 2020: $\left(k_l a\right)_{\mathrm{R}} = 4.4 \times 10^{-4}$ s^{-1} ($\pm$ 1×10^{-6} s^{-1}) / conditions: water temperature = 15.4°C - V_{R} = 78 400 L - water height = 150 cm - $t_{\mathrm{c}} \simeq 20$ s - $C_{\mathrm{S}} = 10.2$ mg/L.

8.4 Small-scale CO_2 transfer tests

8.4.1 September 2019 - test A

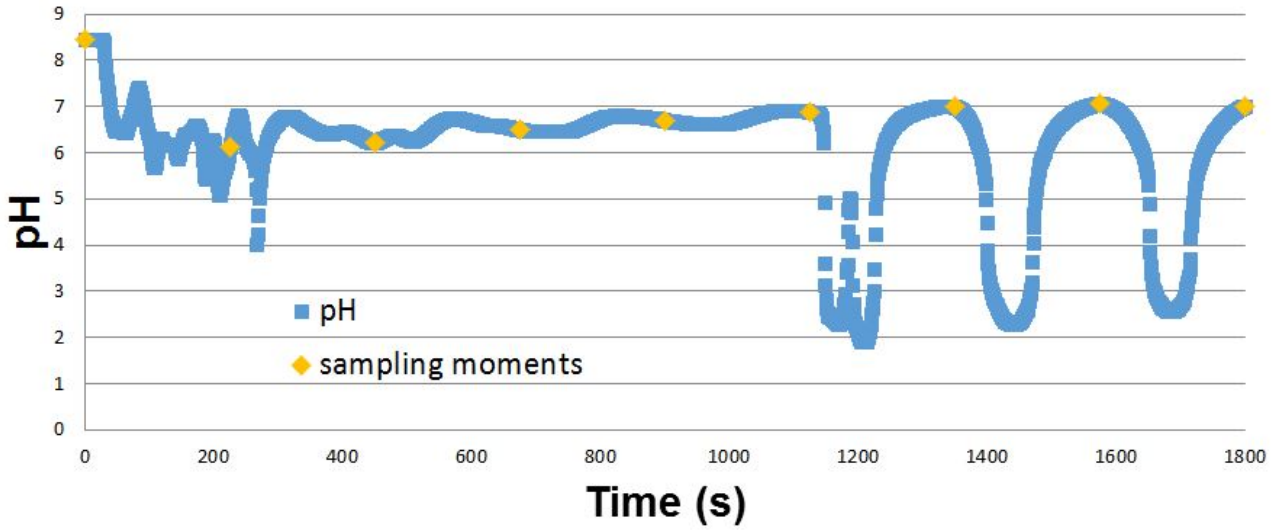

Figure 46: Evolution of the pH at the outlet of the airlift and sampling moments during the small-scale CO_2 transfer test **A** of September 2019.

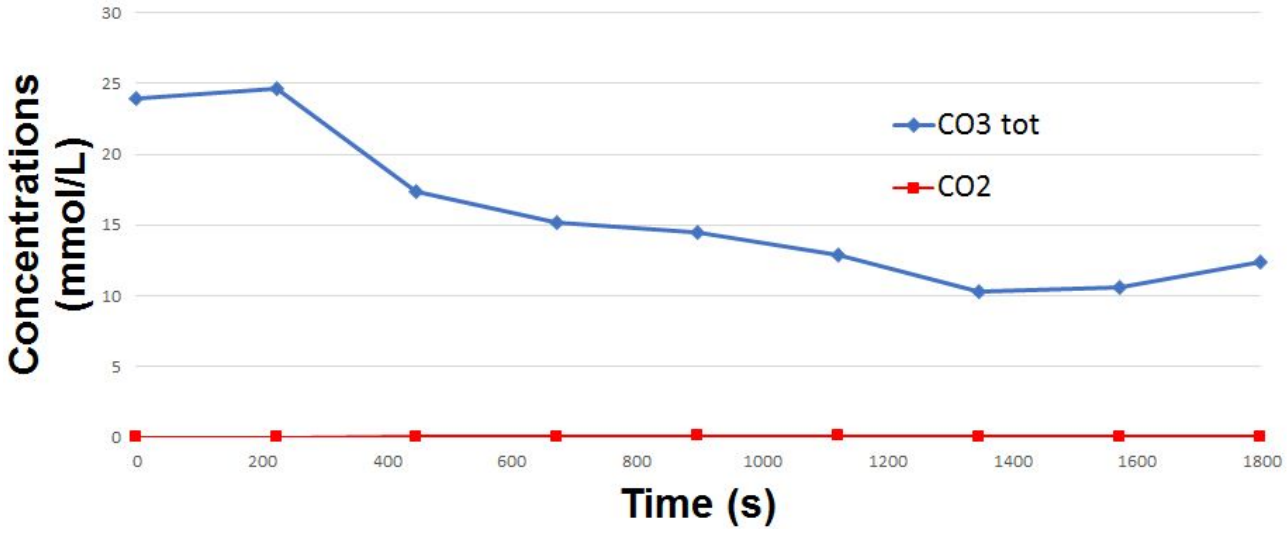

Figure 47: Evolution of $[CO_{3_{tot}}]$ and $[CO_2]$ at the outlet of the airlift during the small-scale CO_2 transfer test **A** of September 2019 / conditions: water temperature = 23.6°C - V_R = 267.1 L - water height = 9.8 cm - t_c = 227 s.

Table 9: Values of the different variables used for the determination of the CO_2 concentration in the HRAP for the small-scale test **A** of September 2019.

sample	**A-1**	**A0**	**A1**	**A2**	**A3**
sampling time (s)	/	0	225	450	675
t_{test} (°C)	23.6	23.6	23.6	23.6	23.6
$t_{\text{titration}}$ (°C)	22.5	22.5	22.5	20.8	21.5
V_{sample} (mL)	23.42	22.94	23.33	22.96	23.46
titrant used	HCl	HCl	HCl	HCl	HCl
n_{H^+}/n_{OH^-} added (mmol)	0.08	0.53	0.54	0.22	0.19
$V_{\text{container}}$ (mL)	24.22	28.34	28.83	44.96	41.96
$[H^+_{\text{added}}]/[OH^-_{\text{added}}]$ (mmol/L)	3.27	18.85	18.88	4.91	4.43
conductivity (25°C) (μs/cm)	7 600	7 600	7 680	7 900	8 290
pH (before the titration)	7.58	8.16	7.6	6.37	6.32
Titration conditions					
$g(t_{\text{titration}})$	0.9994	0.9994	0.9994	0.9998	0.9997
$[OH_{\text{tot}}(t_{\text{titration}})]$ (mol/L)	55.38	55.38	55.38	55.4	55.39
$\epsilon(t_{\text{titration}})$	79.45	79.45	79.45	80.07	79.81
$A(t_{\text{titration}})$	0.51	0.51	0.51	0.51	0.51
ρ(20°C) (ohm.cm)	131.7	131.7	130.4	126.7	120.8
J(20°C) (mmol/L)	136.94	136.94	138.51	142.82	150.49
$J(t_{\text{titration}})$ (mmol/L)	136.87	136.87	138.43	142.79	150.44
$\gamma_1(t_{\text{titration}})$	0.753	0.753	0.752	0.751	0.747
$\gamma_2(t_{\text{titration}})$	0.322	0.322	0.32	0.318	0.311
$K_0(t_{\text{titration}})$ ($\times 10^{16}$)	1.506	1.506	1.506	1.316	1.392
$K_1(t_{\text{titration}})$ ($\times 10^{7}$)	4.306	4.306	4.306	4.2	4.244
$K_2(t_{\text{titration}})$ ($\times 10^{11}$)	4.441	4.441	4.441	4.277	4.344
pH $_{\text{initial}}$	7.58	8.16	7.6	6.37	6.32
$f_{11\ \text{initial}}$	1	1	1	1	1
$f_{12\ \text{initial}}$	1.04	0.997	1.038	1.432	1.457
pH $_{\text{final}}$	4.85	4.73	4.48	4.51	4.66
$f_{11\ \text{final}}$	1	1	1	1	1
$f_{12\ \text{final}}$	1.961	1.97	1.983	1.982	1.975
$[CO_{3_{\text{tot}}}]_{\text{container}}$ (mmol/L)	3.53	19.35	19.93	8.86	8.5
$[CO_{3_{\text{tot}}}]_{\text{sample}}$ (mmol/L)	3.65	23.91	24.63	17.35	15.19
Test conditions					
$g(t_{\text{test}})$	0.9992	0.9992	0.9992	0.9992	0.9992
$[CO_{3_{\text{tot}}}(t_{\text{test}})]$ (mmol/L)	3.65	23.9	24.62	17.34	15.19
$\epsilon(t_{\text{test}})$	79.05	79.05	79.05	79.05	79.05
$A(t_{\text{test}})$	0.51	0.51	0.51	0.51	0.51
$J(t_{\text{test}})$ (mmol/L)	136.83	136.83	138.39	142.7	150.37
$\gamma_1(t_{\text{test}})$	0.753	0.753	0.752	0.75	0.746
$\gamma_2(t_{\text{test}})$	0.321	0.321	0.319	0.316	0.31
$K_1(t_{\text{test}})$ ($\times 10^{7}$)	4.371	4.371	4.371	4.371	4.371
$K_2(t_{\text{test}})$ ($\times 10^{11}$)	4.546	4.546	4.546	4.546	4.546
pH (during the test)	7.58	10.98	10.87	8.6	8.52
d_{32}	0.04316	0	0	0.00411	0.00495
$[CO_2(t_{\text{test}})]$ (mmol/L)	0.16	0	0	0.07	0.08

sample	**A4**	**A5**	**A6**	**A7**	**A8**
sampling time (s)	900	1 125	1 350	1 575	1 800
t_{test} (°C)	23.6	23.7	23.7	23.7	23.7
$t_{\text{titration}}$ (°C)	21.3	21.2	20	21	22
V_{sample} (mL)	22.94	22.77	23.6	22.79	24.06
titrant used	HCl	HCl	HCl	HCl	HCl
n_{H^+}/n_{OH^-} added (mmol)	0.2	0.21	0.09	0.14	0.21
$V_{\text{container}}$ (mL)	42.44	43.77	32.6	36.79	45.06
$[H^+_{\text{added}}]/[OH^-_{\text{added}}]$ (mmol/L)	4.61	4.82	2.77	3.82	4.68
conductivity (25°C) (μs/cm)	8 730	8 690	3 060	3 600	3 510
pH (before the titration)	6.42	6.66	6.11	6.43	6.7
Titration conditions					
$g(t_{\text{titration}})$	0.9997	0.9997	1	0.9998	0.9996
$[OH_{\text{tot}}(t_{\text{titration}})]$ (mol/L)	55.4	55.4	55.41	55.4	55.39
$\epsilon(t_{\text{titration}})$	79.89	79.92	80.36	80	79.63
$A(t_{\text{titration}})$	0.51	0.51	0.5	0.51	0.51
ρ(20°C) (ohm.cm)	114.7	115.2	327.2	278.1	285.2
J(20°C) (mmol/L)	159.18	158.39	51.15	60.97	59.32
$J(t_{\text{titration}})$ (mmol/L)	159.14	158.35	51.15	60.96	59.3
$\gamma_1(t_{\text{titration}})$	0.743	0.743	0.819	0.808	0.809
$\gamma_2(t_{\text{titration}})$	0.305	0.305	0.451	0.426	0.429
$K_0(t_{\text{titration}})$ ($\times 10^{16}$)	1.37	1.359	1.234	1.338	1.448
$K_1(t_{\text{titration}})$ ($\times 10^{7}$)	4.231	4.225	4.148	4.212	4.275
$K_2(t_{\text{titration}})$ ($\times 10^{11}$)	4.325	4.315	4.199	4.296	4.393
pH $_{\text{initial}}$	6.42	6.66	6.11	6.43	6.7
$f_{11\ \text{initial}}$	1	1	1	1	1
$f_{12\ \text{initial}}$	1.4	1.277	1.605	1.416	1.274
pH $_{\text{final}}$	4.47	4.36	4.71	4.34	4.64
$f_{11\ \text{final}}$	1	1	1	1	1
$f_{12\ \text{final}}$	1.983	1.987	1.975	1.989	1.977
$[CO_{3_{\text{tot}}}]_{\text{container}}$ (mmol/L)	7.83	6.7	7.44	6.57	6.61
$[CO_{3_{\text{tot}}}]_{\text{sample}}$ (mmol/L)	14.49	12.89	10.27	10.61	12.38
Test conditions					
$g(t_{\text{test}})$	0.9992	0.9992	0.9992	0.9992	0.9992
$[CO_{3_{\text{tot}}}(t_{\text{test}})]$ (mmol/L)	14.48	12.88	10.27	10.6	12.37
$\epsilon(t_{\text{test}})$	79.05	79.01	79.01	79.01	79.01
$A(t_{\text{test}})$	0.51	0.51	0.51	0.51	0.51
$J(t_{\text{test}})$ (mmol/L)	159.05	158.26	51.11	60.92	59.28
$\gamma_1(t_{\text{test}})$	0.742	0.742	0.818	0.807	0.809
$\gamma_2(t_{\text{test}})$	0.303	0.304	0.448	0.425	0.428
$K_1(t_{\text{test}})$ ($\times 10^{7}$)	4.371	4.377	4.377	4.377	4.377
$K_2(t_{\text{test}})$ ($\times 10^{11}$)	4.546	4.556	4.556	4.556	4.556
pH (during the test)	8.25	8.2	8.3	8.36	8.43
d_{32}	0.00927	0.01041	0.00913	0.00783	0.00667
$[CO_2(t_{\text{test}})]$ (mmol/L)	0.13	0.13	0.09	0.08	0.08

8.4.2 September 2019 - test B

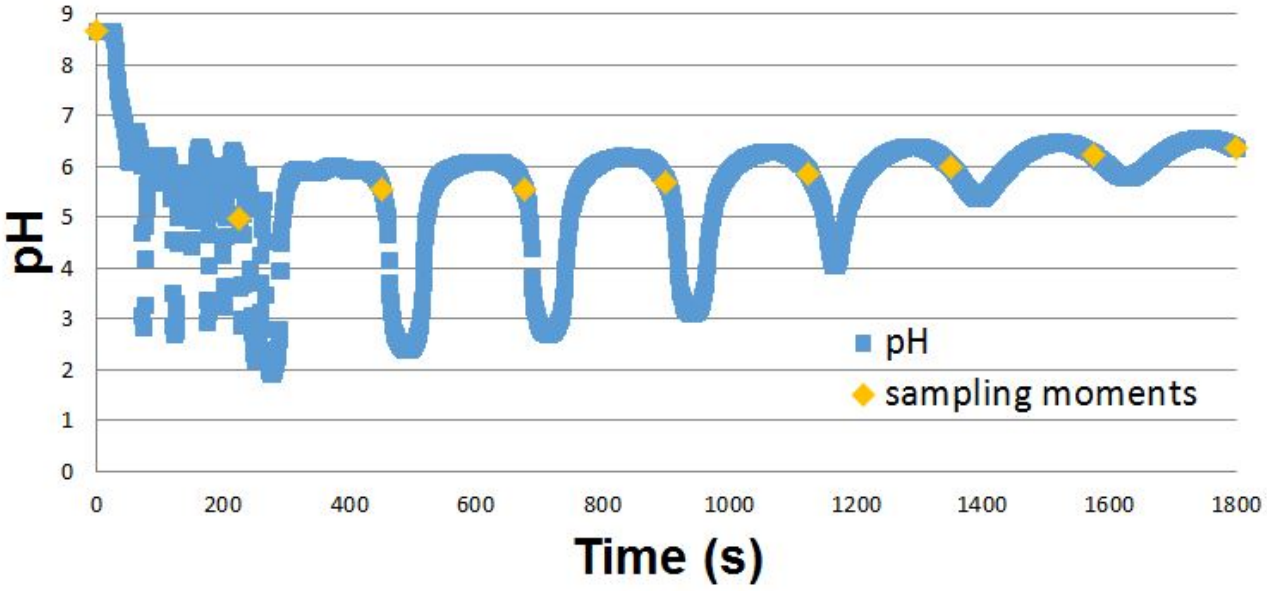

Figure 48: Evolution of the pH at the outlet of the airlift and sampling moments during the small-scale CO_2 transfer test **B** of September 2019.

Table 10: Values of the different variables used for the determination of the CO_2 concentration in the HRAP for the small-scale test **B** of September 2019.

sample	**B-1**	**B0**	**B1**	**B2**	**B3**
sampling time (s)	/	0	225	450	675
t_{test} (°C)	23.6	23.6	23.6	23.6	23.6
$t_{\text{titration}}$ (°C)	21	22.5	21	22.5	22.5
V_{sample} (mL)	22.66	24.61	23.7	23.56	23.24
titrant used	HCl	HCl	HCl	NaOH	NaOH
n_{H^+}/n_{OH^-} added (mmol)	0.7	0.64	0.27	0.16	0.12
$V_{\text{container}}$ (mL)	29.41	31.21	50.8	54.56	41.74
$[H^+_{\text{added}}]/[OH^-_{\text{added}}]$ (mmol/L)	2.3	20.61	5.36	2.99	2.8
conductivity (25°C) (μs/cm)	5 370	5 370	5 940	7 780	6 790
pH (before the titration)	6.32	8.22	6.11	2.1	2.4
Titration conditions					
$g(t_{\text{titration}})$	0.9998	0.9994	0.9998	0.9994	0.9994
$[OH_{\text{tot}}\ (t_{\text{titration}})]$ (mol/L)	55.4	55.38	55.4	55.38	55.38
$\epsilon(t_{\text{titration}})$	80	79.45	80	79.45	79.45
$A(t_{\text{titration}})$	0.51	0.51	0.51	0.51	0.51
ρ(20°C) (ohm.cm)	186.4	186.4	168.5	128.7	147.4
J(20°C) (mmol/L)	93.97	93.97	104.83	140.46	121.18
$J(t_{\text{titration}})$ (mmol/L)	93.95	93.92	104.8	140.39	121.11
$\gamma_1(t_{\text{titration}})$	0.78	0.779	0.772	0.751	0.762
$\gamma_2(t_{\text{titration}})$	0.369	0.368	0.355	0.318	0.336
$K_0(t_{\text{titration}})$ ($\times 10^{16}$)	1.338	1.506	1.338	1.506	1.506
$K_1(t_{\text{titration}})$ ($\times 10^{7}$)	4.212	4.306	4.212	4.306	4.306
$K_2(t_{\text{titration}})$ ($\times 10^{11}$)	4.296	4.441	4.296	4.441	4.441
pH $_{\text{initial}}$	6.51	8.1	6.32	4.45	4.46
$f_{11\ \text{initial}}$	1	1	1	1	1
$f_{12\ \text{initial}}$	1.364	1.002	1.467	1.984	1.984
pH $_{\text{final}}$	4.51	4.61	4.58	8.25	8.29
$f_{11\ \text{final}}$	1	1	1	1	1
$f_{12\ \text{final}}$	1.983	1.978	1.98	0.991	0.99
$[CO_{3_{\text{tot}}}]_{\text{container}}$ (mmol/L)	3.66	21.1	10.38	2.96	2.77
$[CO_{3_{\text{tot}}}]_{\text{sample}}$ (mmol/L)	4.75	26.76	22.26	6.85	4.97
Test conditions					
$g(t_{\text{test}})$	0.9992	0.9992	0.9992	0.9992	0.9992
$[CO_{3_{\text{tot}}}(t_{\text{test}})]$ (mmol/L)	4.74	26.75	22.24	6.85	4.97
$\epsilon(t_{\text{test}})$	79.05	79.05	79.05	79.05	79.05
$A(t_{\text{test}})$	0.51	0.51	0.51	0.51	0.51
$J(t_{\text{test}})$ (mmol/L)	93.9	93.9	104.74	140.35	121.08
$\gamma_1(t_{\text{test}})$	0.779	0.779	0.771	0.751	0.761
$\gamma_2(t_{\text{test}})$	0.368	0.368	0.354	0.318	0.336
$K_1(t_{\text{test}})$ ($\times 10^{7}$)	4.371	4.371	4.371	4.371	4.371
$K_2(t_{\text{test}})$ ($\times 10^{11}$)	4.546	4.546	4.546	4.546	4.546
pH (during the test)	6.32	7.92	6.47	2.35	2.75
d_{32}	0.46016	0.02076	0.37191	0.99987	0.99968
$[CO_2(t_{\text{test}})]$ (mmol/L)	2.18	0.56	8.27	6.85	4.96

sample	**B4**	**B5**	**B6**	**B7**	**B8**
sampling time (s)	900	1 125	1 350	1 575	1 800
t_{test} (°C)	23.6	23.6	23.6	23.6	23.7
$t_{\text{titration}}$ (°C)	22.5	22.5	21	21	21
V_{sample} (mL)	23.36	23.61	23.47	23.6	22.96
titrant used	NaOH	NaOH	HCl	HCl	HCl
n_{H^+}/n_{OH^-} added (mmol)	0.08	0.07	0.01	0.02	0.03
$V_{\text{container}}$ (mL)	33.46	31.01	24.37	25.35	25.76
$[H^+_{\text{added}}]/[OH^-_{\text{added}}]$ (mmol/L)	2.34	2.16	0.37	0.69	1.09
conductivity (25°C) (μs/cm)	6 500	6 350	6 310	6 290	6 260
pH (before the titration)	2.84	3.56	4.8	5.33	5.63
Titration conditions					
$g(t_{\text{titration}})$	0.9994	0.9994	0.9998	0.9998	0.9998
$[OH_{\text{tot}}\ (t_{\text{titration}})]$ (mol/L)	55.38	55.38	55.4	55.4	55.4
$\epsilon(t_{\text{titration}})$	79.45	79.45	80	80	80
$A(t_{\text{titration}})$	0.51	0.51	0.51	0.51	0.51
ρ(20°C) (ohm.cm)	154	157.7	158.7	159.2	159.9
J(20°C) (mmol/L)	115.58	112.69	111.92	111.54	110.96
$J(t_{\text{titration}})$ (mmol/L)	115.52	112.63	111.9	111.51	110.94
$\gamma_1(t_{\text{titration}})$	0.765	0.767	0.768	0.768	0.768
$\gamma_2(t_{\text{titration}})$	0.342	0.345	0.347	0.348	0.348
$K_0(t_{\text{titration}})$ ($\times 10^{16}$)	1.506	1.506	1.338	1.338	1.338
$K_1(t_{\text{titration}})$ ($\times 10^{7}$)	4.306	4.306	4.212	4.212	4.212
$K_2(t_{\text{titration}})$ ($\times 10^{11}$)	4.441	4.441	4.296	4.296	4.296
pH $_{\text{initial}}$	4.42	4.4	5.09	5.54	5.82
$f_{11\ \text{initial}}$	1	1	1	1	1
$f_{12\ \text{initial}}$	1.985	1.986	1.937	1.84	1.734
pH $_{\text{final}}$	8.3	8.15	4.38	4.67	4.54
$f_{11\ \text{final}}$	1	1	1	1	1
$f_{12\ \text{final}}$	0.989	0.999	1.987	1.975	1.981
$[CO_{3_{\text{tot}}}]_{\text{container}}$ (mmol/L)	2.29	2.13	6.51	4.96	4.27
$[CO_{3_{\text{tot}}}]_{\text{sample}}$ (mmol/L)	3.28	2.8	6.76	5.33	4.79
Test conditions					
$g(t_{\text{test}})$	0.9992	0.9992	0.9992	0.9992	0.9992
$[CO_{3_{\text{tot}}}(t_{\text{test}})]$ (mmol/L)	3.28	2.8	6.75	5.33	4.79
$\epsilon(t_{\text{test}})$	79.05	79.05	79.05	79.05	79.01
$A(t_{\text{test}})$	0.51	0.51	0.51	0.51	0.51
$J(t_{\text{test}})$ (mmol/L)	115.49	112.6	111.83	111.45	110.87
$\gamma_1(t_{\text{test}})$	0.764	0.766	0.767	0.767	0.767
$\gamma_2(t_{\text{test}})$	0.341	0.345	0.345	0.346	0.346
$K_1(t_{\text{test}})$ ($\times 10^{7}$)	4.371	4.371	4.371	4.371	4.377
$K_2(t_{\text{test}})$ ($\times 10^{11}$)	4.546	4.546	4.546	4.546	4.556
pH (during the test)	3.13	4.04	5.18	5.6	6.36
d_{32}	0.99923	0.99384	0.91988	0.81539	0.43398
$[CO_2(t_{\text{test}})]$ (mmol/L)	3.28	2.78	6.21	4.34	2.08

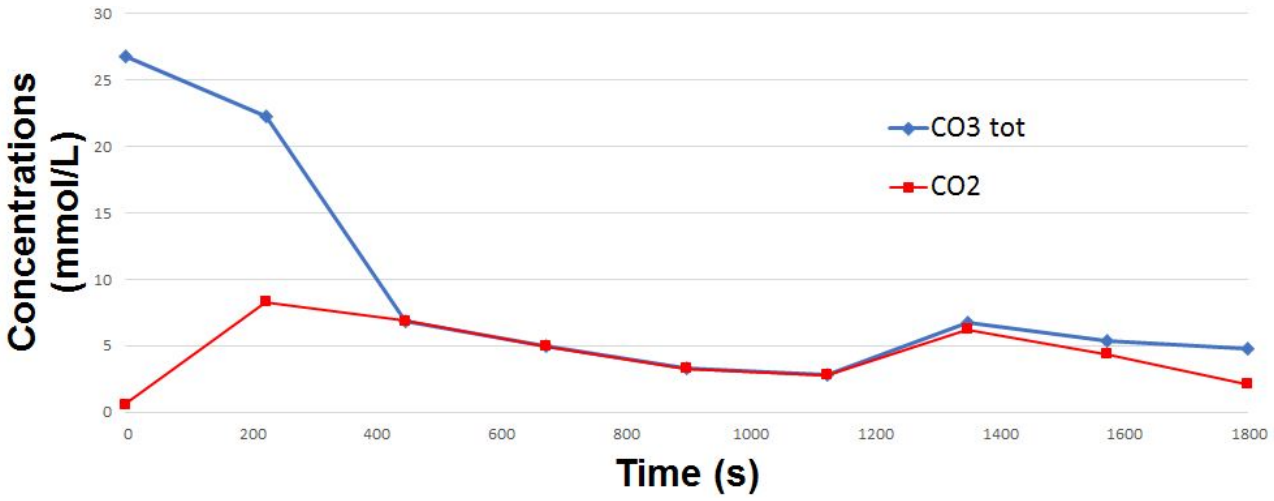

Figure 49: Evolution of $[CO_{3_{tot}}]$ and $[CO_2]$ at the outlet of the airlift during the small-scale CO_2 transfer test **B** of September 2019 / conditions: water temperature = 23.6°C - V_R = 267.1 L - water height = 9.8 cm - t_c = 227 s.

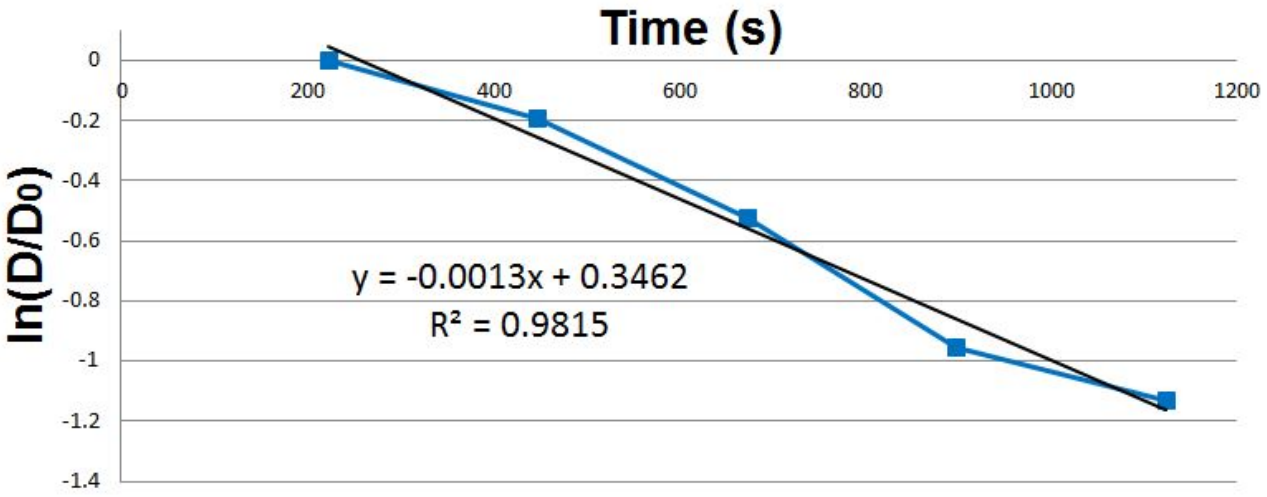

Figure 50: Curve of $\ln(D(t)/D_0)$ at the outlet of the airlift and linear regression for the small-scale CO_2 transfer test **B** of September 2019: $(k_l a)_R = 1.3 \times 10^{-3}$ s^{-1} ($\pm$ 2.1×10^{-4} s^{-1}) / conditions: water temperature = 23.6°C - V_R = 267.1 L - water height = 9.8 cm - t_c = 227 s - C_S = 0.16 mmol/L.

8.4.3 January 2020 - test B

Table 11: Values of the different variables used for the determination of the CO_2 concentration in the HRAP for the small-scale test **B** of January 2020.

sample	**B-1**	**B0**	**B1**	**B2**	**B3**
sampling time (s)	/	0	390	780	1 170
t_{test} (°C)	16.2	16.3	16.4	16.4	16.4
$t_{\text{titration}}$ (°C)	25	25	25	25	25
V_{sample} (mL)	24.63	23.9	23.85	23.47	23.24
titrant used	HCl	HCl	HCl	HCl	NaOH
n_{H^+}/n_{OH^-} added (mmol)	0.04	0.64	0.55	0.12	0.12
$V_{\text{container}}$ (mL)	28.37	30.53	80.67	35.28	43.16
$[H^+_{\text{added}}]/[OH^-_{\text{added}}]$ (mmol/L)	1.28	21.07	6.86	3.26	2.8
conductivity (25°C) (μs/cm)	3 000	4 300	4 620	7 500	9 880
pH (before the titration)	6.38	7.9	7.07	5.68	2.29
Titration conditions					
$g(t_{\text{titration}})$	0.9989	0.9989	0.9989	0.9989	0.9989
$[OH_{\text{tot}}\ (t_{\text{titration}})]$ (mol/L)	55.35	55.35	55.35	55.35	55.35
$\epsilon(t_{\text{titration}})$	78.54	78.54	78.54	78.54	78.54
$A(t_{\text{titration}})$	0.51	0.51	0.51	0.51	0.51
ρ(20°C) (ohm.cm)	333.7	232.8	216.7	133.5	101.3
J(20°C) (mmol/L)	50.07	73.88	79.85	134.99	182.09
$J(t_{\text{titration}})$ (mmol/L)	50.01	73.8	79.76	134.83	181.88
$\gamma_1(t_{\text{titration}})$	0.819	0.794	0.789	0.753	0.732
$\gamma_2(t_{\text{titration}})$	0.45	0.398	0.388	0.322	0.287
$K_0(t_{\text{titration}})$ ($\times 10^{16}$)	1.829	1.829	1.829	1.829	1.829
$K_1(t_{\text{titration}})$ ($\times 10^{7}$)	4.452	4.452	4.452	4.452	4.452
$K_2(t_{\text{titration}})$ ($\times 10^{11}$)	4.68	4.68	4.68	4.68	4.68
pH initial	6.42	8.02	7.28	6	4.5
f_{11} initial	1	1	1	1	1
f_{12} initial	1.411	1.007	1.083	1.628	1.981
pH final	4.5	4.5	4.5	4.5	8.3
f_{11} final	1	1	1	1	1
f_{12} final	1.983	1.983	1.982	1.982	0.985
$[CO_{3_{\text{tot}}}]_{\text{container}}$ (mmol/L)	2.18	21.56	7.58	9.12	2.76
$[CO_{3_{\text{tot}}}]_{\text{sample}}$ (mmol/L)	2.51	27.55	25.65	13.7	5.13
Test conditions					
$g(t_{\text{test}})$	1.0007	1.0007	1.0007	1.0007	1.0007
$[CO_{3_{\text{tot}}}(t_{\text{test}})]$ (mmol/L)	2.52	27.6	25.7	13.73	5.14
$\epsilon(t_{\text{test}})$	81.77	81.74	81.7	81.7	81.7
$A(t_{\text{test}})$	0.5	0.5	0.5	0.5	0.5
$J(t_{\text{test}})$ (mmol/L)	50.11	73.94	79.91	135.08	182.21
$\gamma_1(t_{\text{test}})$	0.822	0.797	0.792	0.756	0.735
$\gamma_2(t_{\text{test}})$	0.456	0.403	0.393	0.327	0.292
$K_1(t_{\text{test}})$ ($\times 10^{7}$)	3.891	3.898	3.905	3.905	3.905
$K_2(t_{\text{test}})$ ($\times 10^{11}$)	3.832	3.842	3.851	3.851	3.851
pH (during the test)	6.38	8.07	7.09	5.07	1.95
d_{32}	0.46816	0.01692	0.14252	0.94268	0.99995
$[CO_2(t_{\text{test}})]$ (mmol/L)	1.18	0.47	3.66	12.94	5.14

sample	**B4**	**B5**	**B6**	**B7**
sampling time (s)	1 560	1 950	2 340	2 400
t_{test} (°C)	16.4	16.4	16.4	16.4
$t_{\text{titration}}$ (°C)	25	25	25	25
V_{sample} (mL)	23.79	22.72	23.44	23.23
titrant used	NaOH	NaOH	NaOH	NaOH
n_{H^+}/n_{OH^-} added (mmol)	0.06	0.05	0.05	0.04
$V_{\text{container}}$ (mL)	46.07	47.26	47.32	43.96
$[H^+_{\text{added}}]/[OH^-_{\text{added}}]$ (mmol/L)	1.23	1.05	0.97	0.88
conductivity (25°C) (μs/cm)	11 530	10 290	9 400	8 920
pH (before the titration)	2.17	2.12	2.11	2.18
Titration conditions				
$g(t_{\text{titration}})$	0.9989	0.9989	0.9989	0.9989
$[OH_{\text{tot}}\ (t_{\text{titration}})]$ (mol/L)	55.35	55.35	55.35	55.35
$\epsilon(t_{\text{titration}})$	78.54	78.54	78.54	78.54
$A(t_{\text{titration}})$	0.51	0.51	0.51	0.51
ρ(20°C) (ohm.cm)	86.8	97.3	106.5	112.2
J(20°C) (mmol/L)	215.38	190.31	172.49	162.95
$J(t_{\text{titration}})$ (mmol/L)	215.13	190.09	172.3	162.76
$\gamma_1(t_{\text{titration}})$	0.72	0.729	0.736	0.74
$\gamma_2(t_{\text{titration}})$	0.269	0.282	0.293	0.3
$K_0(t_{\text{titration}})$ ($\times 10^{16}$)	1.829	1.829	1.829	1.829
$K_1(t_{\text{titration}})$ ($\times 10^{7}$)	4.452	4.452	4.452	4.452
$K_2(t_{\text{titration}})$ ($\times 10^{11}$)	4.68	4.68	4.68	4.68
pH $_{\text{initial}}$	4.5	4.5	4.5	4.5
$f_{11\ \text{initial}}$	1	1	1	1
$f_{12\ \text{initial}}$	1.981	1.981	1.981	1.981
pH $_{\text{final}}$	8.3	8.3	8.3	8.3
$f_{11\ \text{final}}$	1	1	1	1
$f_{12\ \text{final}}$	0.984	0.985	0.985	0.986
$[CO_{3_{\text{tot}}}]_{\text{container}}$ (mmol/L)	1.19	1.01	0.93	0.84
$[CO_{3_{\text{tot}}}]_{\text{sample}}$ (mmol/L)	2.3	2.1	1.88	1.59
Test conditions				
$g(t_{\text{test}})$	1.0007	1.0007	1.0007	1.0007
$[CO_{3_{\text{tot}}}(t_{\text{test}})]$ (mmol/L)	2.3	2.1	1.88	1.59
$\epsilon(t_{\text{test}})$	81.7	81.7	81.7	81.7
$A(t_{\text{test}})$	0.5	0.5	0.5	0.5
$J(t_{\text{test}})$ (mmol/L)	215.53	190.45	172.62	163.06
$\gamma_1(t_{\text{test}})$	0.723	0.732	0.739	0.743
$\gamma_2(t_{\text{test}})$	0.274	0.287	0.298	0.305
$K_1(t_{\text{test}})$ ($\times 10^{7}$)	3.905	3.905	3.905	3.905
$K_2(t_{\text{test}})$ ($\times 10^{11}$)	3.851	3.851	3.851	3.851
pH (during the test)	1.77	1.73	1.77	1.81
d_{32}	0.99997	0.99997	0.99997	0.99997
$[CO_2(t_{\text{test}})]$ (mmol/L)	2.3	2.1	1.88	1.59

8.5 Large-scale CO_2 transfer tests

8.5.1 June 2020 - test A

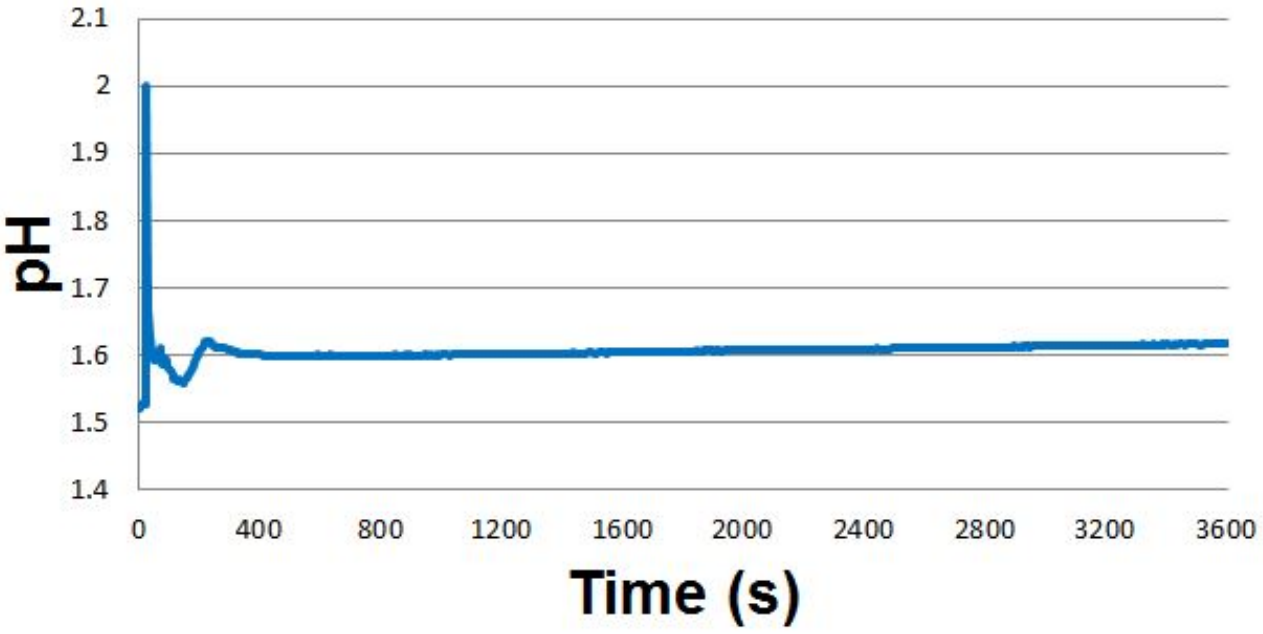

Figure 51: Evolution of the pH at the outlet of the airlift during the large-scale CO_2 transfer test **A** of June 2020.

Table 12: Values of the different variables used for the determination of the CO_2 concentration in the HRAP for the large-scale test **A** of June 2020.

sample	**A0**	**A1**	**A2**	**A3**	**A4**	**A5**
sampling time (s)	0	20	40	60	80	100
t_{test} (°C)	16	16	16	16	16	16
$t_{\text{titration}}$ (°C)	20.8	24	25	25	25	25
V_{sample} (mL)	23.02	22.09	23.39	22.87	23.42	22.8
titrant used	NaOH	NaOH	NaOH	NaOH	NaOH	NaOH
n_{H^+}/n_{OH^-} added (mmol)	37.76	23.68	27.88	36.88	54.02	35.51
$V_{\text{container}}$ (mL)	41.67	75.79	42.89	43.17	44.32	45.8
$[H^+_{\text{added}}]/[OH^-_{\text{added}}]$ (mmol/L)	0.91	0.31	0.65	0.85	1.22	0.78
conductivity (25°C) (μs/cm)	11 930	10 090	11 570	11 380	11 310	11 570
pH (before the titration)	1.87	1.88	1.88	1.96	1.92	1.97
Titration conditions						
$g(t_{\text{titration}})$	0.9998	0.9991	0.9989	0.9989	0.9989	0.9989
$[OH_{\text{tot}}\ (t_{\text{titration}})]$ (mol/L)	55.4	55.36	55.35	55.35	55.35	55.35
$\epsilon(t_{\text{titration}})$	80.07	78.9	78.54	78.54	78.54	78.54
$A(t_{\text{titration}})$	0.51	0.51	0.51	0.51	0.51	0.51
ρ(20°C) (ohm.cm)	83.9	99.2	86.5	88	88.5	86.5
J(20°C) (mmol/L)	223.52	186.3	216.19	212.33	210.91	216.19
$J(t_{\text{titration}})$ (mmol/L)	223.48	186.13	215.94	212.09	210.67	215.94
$\gamma_1(t_{\text{titration}})$	0.719	0.731	0.72	0.721	0.721	0.72
$\gamma_2(t_{\text{titration}})$	0.267	0.285	0.268	0.27	0.271	0.268
$K_0(t_{\text{titration}})$ ($\times 10^{16}$)	1.316	1.693	1.829	1.829	1.829	1.829
$K_1(t_{\text{titration}})$ ($\times 10^{7}$)	4.2	4.395	4.452	4.452	4.452	4.452
$K_2(t_{\text{titration}})$ ($\times 10^{11}$)	4.277	4.585	4.68	4.68	4.68	4.68
pH $_{\text{initial}}$	4.5	4.5	4.5	4.45	4.5	4.42
$f_{11\ \text{initial}}$	1	1	1	1	1	1
$f_{12\ \text{initial}}$	1.982	1.981	1.981	1.983	1.981	1.984
pH $_{\text{final}}$	8.3	8.29	8.29	8.25	8.31	8.33
$f_{11\ \text{final}}$	1	1	1	1	1	1
$f_{12\ \text{final}}$	0.986	0.986	0.984	0.987	0.983	0.981
$[CO_{3_{\text{tot}}}]_{\text{container}}$ (mmol/L)	0.86	0.27	0.61	0.81	1.17	0.72
$[CO_{3_{\text{tot}}}]_{\text{sample}}$ (mmol/L)	1.56	0.92	1.11	1.52	2.22	1.44
Test conditions						
$g(t_{\text{test}})$	1.0008	1.0008	1.0008	1.0008	1.0008	1.0008
$[CO_{3_{\text{tot}}}(t_{\text{test}})]$ (mmol/L)	1.57	0.92	1.11	1.52	2.23	1.44
$\epsilon(t_{\text{test}})$	81.85	81.85	81.85	81.85	81.85	81.85
$A(t_{\text{test}})$	0.5	0.5	0.5	0.5	0.5	0.5
$J(t_{\text{test}})$ (mmol/L)	223.69	186.44	216.36	212.5	211.08	216.36
$\gamma_1(t_{\text{test}})$	0.721	0.734	0.723	0.725	0.725	0.723
$\gamma_2(t_{\text{test}})$	0.27	0.29	0.274	0.276	0.276	0.274
$K_1(t_{\text{test}})$ ($\times 10^{7}$)	3.876	3.876	3.876	3.876	3.876	3.876
$K_2(t_{\text{test}})$ ($\times 10^{11}$)	3.813	3.813	3.813	3.813	3.813	3.813
pH (during the test)	2.05	2.05	2.11	2.09	2.08	2.07
d_{32}	0.99994	0.99994	0.99993	0.99993	0.99994	0.99994
$[CO_2(t_{\text{test}})]$ (mmol/L)	1.57	0.92	1.11	1.52	2.23	1.44

sample	**A6**	**A7**	**A8**	**A9**	**A10**	**A11**
sampling time (s)	120	140	160	200	240	260
t_{test} (°C)	16	16	16	16	16.1	16.1
$t_{\text{titration}}$ (°C)	25	25	25	25	25	25
V_{sample} (mL)	23.58	23	22.57	22.67	24.08	24.36
titrant used	NaOH	NaOH	NaOH	NaOH	NaOH	NaOH
n_{H^+}/n_{OH^-} added (mmol)	26.41	35.94	54.65	61.01	65.54	64.66
$V_{\text{container}}$ (mL)	47.88	43.52	39.62	43.17	40.83	48.66
$[H^+_{\text{added}}]/[OH^-_{\text{added}}]$ (mmol/L)	0.55	0.83	1.38	1.41	1.61	1.33
conductivity (25°C) (μs/cm)	11 690	11 650	11 360	10 580	10 820	10 820
pH (before the titration)	1.97	1.96	1.97	1.96	2	1.99
Titration conditions						
g($t_{\text{titration}}$)	0.9989	0.9989	0.9989	0.9989	0.9989	0.9989
$[OH_{\text{tot}}$ ($t_{\text{titration}}$)] (mol/L)	55.35	55.35	55.35	55.35	55.35	55.35
$\epsilon(t_{\text{titration}})$	78.54	78.54	78.54	78.54	78.54	78.54
$A(t_{\text{titration}})$	0.51	0.51	0.51	0.51	0.51	0.51
ρ(20°C) (ohm.cm)	85.6	85.9	88.1	94.6	92.5	92.5
J(20°C) (mmol/L)	218.63	217.82	211.93	196.15	200.99	200.99
$J(t_{\text{titration}})$ (mmol/L)	218.38	217.57	211.68	195.93	200.76	200.76
$\gamma_1(t_{\text{titration}})$	0.719	0.719	0.721	0.727	0.725	0.725
$\gamma_2(t_{\text{titration}})$	0.267	0.267	0.27	0.279	0.276	0.276
$K_0(t_{\text{titration}})$ ($\times 10^{16}$)	1.829	1.829	1.829	1.829	1.829	1.829
$K_1(t_{\text{titration}})$ ($\times 10^{7}$)	4.452	4.452	4.452	4.452	4.452	4.452
$K_2(t_{\text{titration}})$ ($\times 10^{11}$)	4.68	4.68	4.68	4.68	4.68	4.68
pH $_{\text{initial}}$	4.51	4.5	4.5	4.53	4.5	4.42
$f_{11\ \text{initial}}$	1	1	1	1	1	1
$f_{12\ \text{initial}}$	1.98	1.981	1.981	1.98	1.981	1.984
pH $_{\text{final}}$	8.29	8.3	8.22	8.33	8.3	8.27
$f_{11\ \text{final}}$	1	1	1	1	1	1
$f_{12\ \text{final}}$	0.984	0.984	0.989	0.982	0.984	0.986
$[CO_{3_{\text{tot}}}]_{\text{container}}$ (mmol/L)	0.51	0.78	1.34	1.37	1.56	1.28
$[CO_{3_{\text{tot}}}]_{\text{sample}}$ (mmol/L)	1.03	1.48	2.36	2.61	2.65	2.55
Test conditions						
g(t_{test})	1.0008	1.0008	1.0008	1.0008	1.0008	1.0008
$[CO_{3_{\text{tot}}}(t_{\text{test}})]$ (mmol/L)	1.03	1.48	2.37	2.62	2.66	2.56
$\epsilon(t_{\text{test}})$	81.85	81.85	81.85	81.85	81.81	81.81
$A(t_{\text{test}})$	0.5	0.5	0.5	0.5	0.5	0.5
$J(t_{\text{test}})$ (mmol/L)	218.8	217.99	212.09	196.3	201.15	201.15
$\gamma_1(t_{\text{test}})$	0.722	0.723	0.725	0.73	0.728	0.728
$\gamma_2(t_{\text{test}})$	0.272	0.273	0.276	0.284	0.281	0.281
$K_1(t_{\text{test}})$ ($\times 10^{7}$)	3.876	3.876	3.876	3.876	3.884	3.884
$K_2(t_{\text{test}})$ ($\times 10^{11}$)	3.813	3.813	3.813	3.813	3.822	3.822
pH (during the test)	2.07	2.06	2.07	2.11	2.12	2.12
d_{32}	0.99994	0.99994	0.99994	0.99993	0.99993	0.99993
$[CO_2(t_{\text{test}})]$ (mmol/L)	1.03	1.48	2.36	2.62	2.66	2.55

sample	**A12**	**A13**	**A14**	**A15**	**A16**
sampling time (s)	280	600	1 200	1 800	3 300
t_{test} (°C)	16.1	16.1	16.1	16.1	16.2
$t_{\text{titration}}$ (°C)	25	25	25	25	26
V_{sample} (mL)	24.12	24.09	24.36	24.94	23.36
titrant used	NaOH	NaOH	NaOH	NaOH	NaOH
n_{H^+}/n_{OH^-} added (mmol)	66.6	39.16	54.81	60.81	60.84
$V_{\text{container}}$ (mL)	40.99	46.89	43.44	43.99	41.36
$[H^+_{\text{added}}]/[OH^-_{\text{added}}]$ (mmol/L)	1.62	0.84	1.26	1.38	1.47
conductivity (25°C) (μs/cm)	10 860	10 850	10 270	10 920	10 710
pH (before the titration)	2	1.96	1.99	2.06	1.99
Titration conditions					
g($t_{\text{titration}}$)	0.9989	0.9989	0.9989	0.9989	0.9986
$[OH_{\text{tot}}\ (t_{\text{titration}})]$ (mol/L)	55.35	55.35	55.35	55.35	55.33
$\epsilon(t_{\text{titration}})$	78.54	78.54	78.54	78.54	78.18
$A(t_{\text{titration}})$	0.51	0.51	0.51	0.51	0.51
ρ(20°C) (ohm.cm)	92.2	92.3	97.5	91.7	93.5
J(20°C) (mmol/L)	201.8	201.6	189.91	203.01	198.77
$J(t_{\text{titration}})$ (mmol/L)	201.57	201.37	189.69	202.78	198.49
$\gamma_1(t_{\text{titration}})$	0.725	0.725	0.729	0.724	0.725
$\gamma_2(t_{\text{titration}})$	0.276	0.276	0.282	0.275	0.277
$K_0(t_{\text{titration}})$ ($\times 10^{16}$)	1.829	1.829	1.829	1.829	1.974
$K_1(t_{\text{titration}})$ ($\times 10^{7}$)	4.452	4.452	4.452	4.452	4.507
$K_2(t_{\text{titration}})$ ($\times 10^{11}$)	4.68	4.68	4.68	4.68	4.776
pH $_{\text{initial}}$	4.38	4.41	4.5	4.5	4.5
$f_{11\ \text{initial}}$	1	1	1	1	1
$f_{12\ \text{initial}}$	1.985	1.984	1.981	1.981	1.981
pH $_{\text{final}}$	8.3	8.34	8.3	8.37	8.4
$f_{11\ \text{final}}$	1	1	1	1	1
$f_{12\ \text{final}}$	0.984	0.981	0.985	0.979	0.976
$[CO_{3_{\text{tot}}}]_{\text{container}}$ (mmol/L)	1.56	0.78	1.22	1.33	1.42
$[CO_{3_{\text{tot}}}]_{\text{sample}}$ (mmol/L)	2.65	1.51	2.17	2.35	2.51
Test conditions					
g(t_{test})	1.0008	1.0008	1.0008	1.0008	1.0007
$[CO_{3_{\text{tot}}}(t_{\text{test}})]$ (mmol/L)	2.66	1.51	2.18	2.36	2.51
$\epsilon(t_{\text{test}})$	81.81	81.81	81.81	81.81	81.77
$A(t_{\text{test}})$	0.5	0.5	0.5	0.5	0.5
$J(t_{\text{test}})$ (mmol/L)	201.96	201.75	190.06	203.17	198.92
$\gamma_1(t_{\text{test}})$	0.728	0.728	0.732	0.728	0.729
$\gamma_2(t_{\text{test}})$	0.281	0.281	0.288	0.28	0.283
$K_1(t_{\text{test}})$ ($\times 10^{7}$)	3.884	3.884	3.884	3.884	3.891
$K_2(t_{\text{test}})$ ($\times 10^{11}$)	3.822	3.822	3.822	3.822	3.832
pH (during the test)	2.11	2.11	2.1	2.1	2.08
d_{32}	0.99993	0.99993	0.99993	0.99993	0.99994
$[CO_2(t_{\text{test}})]$ (mmol/L)	2.66	1.51	2.18	2.36	2.51

8.5.2 June 2020 - test B

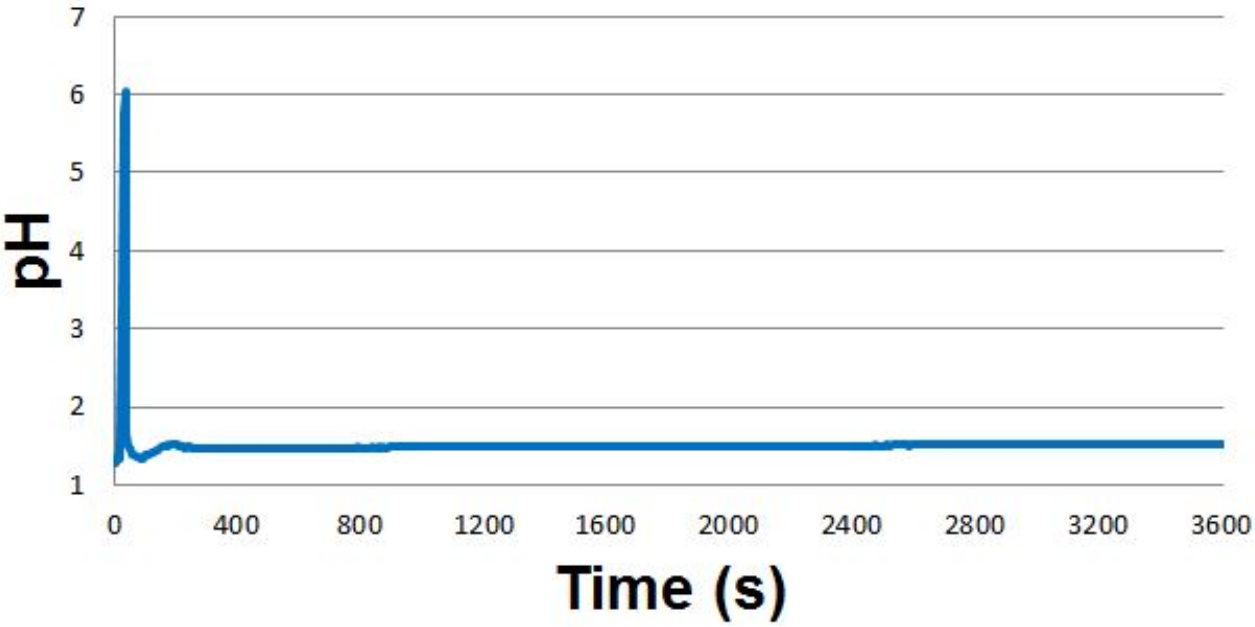

Figure 52: Evolution of the pH at the outlet of the airlift during the large-scale CO_2 transfer test **B** of June 2020.

Table 13: Values of the different variables used for the determination of the CO_2 concentration in the HRAP for the large-scale test **B** of June 2020.

sample	**B0**	**B1**	**B2**	**B3**	**B4**
sampling time (s)	0	60	80	100	120
t_{test} (°C)	16.5	16.4	16.4	16.5	16.5
$t_{\text{titration}}$ (°C)	24.6	24.2	24.5	25.8	25
V_{sample} (mL)	23.99	23.02	23.31	23.27	24.11
titrant used	NaOH	NaOH	NaOH	NaOH	NaOH
n_{H^+}/n_{OH^-} added (mmol)	30.96	115.55	66.94	88.33	172.12
$V_{\text{container}}$ (mL)	63.29	50.45	54.51	67.27	53.71
$[H^+_{\text{added}}]/[OH^-_{\text{added}}]$ (mmol/L)	0.49	2.29	1.23	1.31	3.2
conductivity (25°C) (μs/cm)	21 700	17 420	19 410	18 750	17 160
pH (before the titration)	1.62	1.77	1.69	1.78	1.82
Titration conditions					
$g(t_{\text{titration}})$	0.999	0.999	0.999	0.9986	0.9989
$[OH_{\text{tot}}\ (t_{\text{titration}})]$ (mol/L)	55.35	55.36	55.35	55.34	55.35
$\epsilon(t_{\text{titration}})$	78.68	78.83	78.72	78.25	78.54
$A(t_{\text{titration}})$	0.51	0.51	0.51	0.51	0.51
ρ(20°C) (ohm.cm)	46.1	57.5	51.6	53.4	58.3
J(20°C) (mmol/L)	429	337.57	379.84	365.77	332.08
$J(t_{\text{titration}})$ (mmol/L)	428.55	337.25	379.45	265.28	331.7
$\gamma_1(t_{\text{titration}})$	0.671	0.688	0.68	0.682	0.689
$\gamma_2(t_{\text{titration}})$	0.203	0.224	0.214	0.216	0.225
$K_0(t_{\text{titration}})$ ($\times 10^{16}$)	1.774	1.72	1.76	1.944	1.829
$K_1(t_{\text{titration}})$ ($\times 10^{7}$)	4.429	4.406	4.423	4.496	4.452
$K_2(t_{\text{titration}})$ ($\times 10^{11}$)	4.642	4.604	4.633	4.757	4.68
pH $_{\text{initial}}$	4.5	4.5	4.37	4.44	4.45
$f_{11\ \text{initial}}$	1	1	1	1	1
$f_{12\ \text{initial}}$	1.98	1.98	1.985	1.982	1.982
pH $_{\text{final}}$	8.29	8.3	8.32	8.38	8.2
$f_{11\ \text{final}}$	1	1	1	1	1
$f_{12\ \text{final}}$	0.979	0.98	0.977	0.972	0.987
$[CO_{3_{\text{tot}}}]_{\text{container}}$ (mmol/L)	0.44	2.24	1.15	1.24	3.17
$[CO_{3_{\text{tot}}}]_{\text{sample}}$ (mmol/L)	1.16	4.91	2.7	3.59	7.06
Test conditions					
$g(t_{\text{test}})$	1.0007	1.0007	1.0007	1.0007	1.0007
$[CO_{3_{\text{tot}}}(t_{\text{test}})]$ (mmol/L)	1.16	4.92	2.7	3.6	7.07
$\epsilon(t_{\text{test}})$	81.66	81.7	81.7	81.66	81.66
$A(t_{\text{test}})$	0.5	0.5	0.5	0.5	0.5
$J(t_{\text{test}})$ (mmol/L)	429.29	337.81	380.11	366.03	332.31
$\gamma_1(t_{\text{test}})$	0.675	0.692	0.683	0.686	0.693
$\gamma_2(t_{\text{test}})$	0.208	0.229	0.218	0.221	0.23
$K_1(t_{\text{test}})$ ($\times 10^{7}$)	3.912	3.905	3.905	3.912	3.912
$K_2(t_{\text{test}})$ ($\times 10^{11}$)	3.861	3.851	3.851	3.861	3.861
pH (during the test)	1.66	1.92	1.8	1.77	1.8
d_{32}	0.99997	0.99995	0.99996	0.99997	0.99996
$[CO_2(t_{\text{test}})]$ (mmol/L)	1.16	4.92	2.7	3.6	7.07

sample	**B5**	**B6**	**B7**	**B8**	**B9**
sampling time (s)	140	160	180	200	220
t_{test} (°C)	16.5	16.5	16.5	16.5	16.5
$t_{\text{titration}}$ (°C)	25	25	25	25	25
V_{sample} (mL)	22.94	23.34	23.74	24.05	24.13
titrant used	NaOH	NaOH	NaOH	NaOH	NaOH
n_{H^+}/n_{OH^-} added (mmol)	178.27	175.2	211.61	194	230.52
$V_{\text{container}}$ (mL)	48.84	46.44	48.99	47.16	49.93
$[H^+_{\text{added}}]/[OH^-_{\text{added}}]$ (mmol/L)	3.65	3.77	4.32	4.11	4.62
conductivity (25°C) (μs/cm)	14 940	14 680	14 070	14 420	14 820
pH (before the titration)	1.86	1.92	1.95	1.91	1.9
Titration conditions					
$g(t_{\text{titration}})$	0.9989	0.9989	0.9989	0.9989	0.9989
$[OH_{\text{tot}}\ (t_{\text{titration}})]$ (mol/L)	55.35	55.35	55.35	55.35	55.35
$\epsilon(t_{\text{titration}})$	78.54	78.54	78.54	78.54	78.54
$A(t_{\text{titration}})$	0.51	0.51	0.51	0.51	0.51
ρ(20°C) (ohm.cm)	67	68.2	71.2	69.4	67.6
J(20°C) (mmol/L)	285.55	280.14	267.49	274.74	283.05
$J(t_{\text{titration}})$ (mmol/L)	285.22	279.82	267.18	274.43	282.73
$\gamma_1(t_{\text{titration}})$	0.7	0.701	0.704	0.703	0.7
$\gamma_2(t_{\text{titration}})$	0.24	0.242	0.246	0.244	0.241
$K_0(t_{\text{titration}})$ ($\times 10^{16}$)	1.829	1.829	1.829	1.829	1.829
$K_1(t_{\text{titration}})$ ($\times 10^{7}$)	4.452	4.452	4.452	4.452	4.452
$K_2(t_{\text{titration}})$ ($\times 10^{11}$)	4.68	4.68	4.68	4.68	4.68
pH $_{\text{initial}}$	4.4	4.49	4.5	4.5	4.42
$f_{11\ \text{initial}}$	1	1	1	1	1
$f_{12\ \text{initial}}$	1.984	1.981	1.98	1.98	1.984
pH $_{\text{final}}$	8.32	8.39	8.3	8.3	8.28
$f_{11\ \text{final}}$	1	1	1	1	1
$f_{12\ \text{final}}$	0.98	0.974	0.982	0.982	0.983
$[CO_{3_{\text{tot}}}]_{\text{container}}$ (mmol/L)	3.57	3.7	4.28	4.07	4.56
$[CO_{3_{\text{tot}}}]_{\text{sample}}$ (mmol/L)	7.61	7.36	8.83	7.98	9.43
Test conditions					
$g(t_{\text{test}})$	1.0007	1.0007	1.0007	1.0007	1.0007
$[CO_{3_{\text{tot}}}(t_{\text{test}})]$ (mmol/L)	7.62	7.37	8.85	8	9.45
$\epsilon(t_{\text{test}})$	81.66	81.66	81.66	81.66	81.66
$A(t_{\text{test}})$	0.5	0.5	0.5	0.5	0.5
$J(t_{\text{test}})$ (mmol/L)	285.75	280.34	267.67	274.93	283.25
$\gamma_1(t_{\text{test}})$	0.703	0.705	0.708	0.706	0.704
$\gamma_2(t_{\text{test}})$	0.245	0.247	0.251	0.249	0.246
$K_1(t_{\text{test}})$ ($\times 10^{7}$)	3.912	3.912	3.912	3.912	3.912
$K_2(t_{\text{test}})$ ($\times 10^{11}$)	3.861	3.861	3.861	3.861	3.861
pH (during the test)	1.83	1.89	1.92	1.92	1.91
d_{32}	0.99996	0.99996	0.99995	0.99995	0.99996
$[CO_2(t_{\text{test}})]$ (mmol/L)	7.62	7.37	8.84	8	9.45

sample	**B10**	**B11**	**B12**	**B13**	**B14**
sampling time (s)	240	260	280	300	600
t_{test} (°C)	16.5	16.5	16.5	16.5	16.5
$t_{\text{titration}}$ (°C)	25	25	25	25	25
V_{sample} (mL)	24.07	24.42	24.03	23.95	24.84
titrant used	NaOH	NaOH	NaOH	NaOH	NaOH
n_{H^+}/n_{OH^-} added (mmol)	164.06	162.09	181.34	249.15	159.28
$V_{\text{container}}$ (mL)	51.47	48.14	50.83	52.45	44.64
$[H^+_{\text{added}}]/[OH^-_{\text{added}}]$ (mmol/L)	3.19	3.37	3.57	4.75	3.57
conductivity (25°C) (μs/cm)	15 450	15 280	15 670	15 620	15 430
pH (before the titration)	1.87	1.9	1.87	1.89	1.9
Titration conditions					
$g(t_{\text{titration}})$	0.9989	0.9989	0.9989	0.9989	0.9989
$[OH_{\text{tot}}\ (t_{\text{titration}})]$ (mol/L)	55.35	55.35	55.35	55.35	55.35
$\epsilon(t_{\text{titration}})$	78.54	78.54	78.54	78.54	78.54
$A(t_{\text{titration}})$	0.51	0.51	0.51	0.51	0.51
ρ(20°C) (ohm.cm)	64.8	65.5	63.9	64.1	64.9
J(20°C) (mmol/L)	296.19	292.64	300.78	299.74	295.77
$J(t_{\text{titration}})$ (mmol/L)	295.85	292.3	300.44	299.39	295.43
$\gamma_1(t_{\text{titration}})$	0.697	0.698	0.696	0.696	0.697
$\gamma_2(t_{\text{titration}})$	0.236	0.237	0.235	0.235	0.236
$K_0(t_{\text{titration}})$ ($\times 10^{16}$)	1.829	1.829	1.829	1.829	1.829
$K_1(t_{\text{titration}})$ ($\times 10^{7}$)	4.452	4.452	4.452	4.452	4.452
$K_2(t_{\text{titration}})$ ($\times 10^{11}$)	4.68	4.68	4.68	4.68	4.68
pH $_{\text{initial}}$	4.51	4.5	4.28	4.5	4.5
$f_{11\ \text{initial}}$	1	1	1	1	1
$f_{12\ \text{initial}}$	1.98	1.98	1.988	1.98	1.98
pH $_{\text{final}}$	8.24	8.3	8.32	8.33	8.25
$f_{11\ \text{final}}$	1	1	1	1	1
$f_{12\ \text{final}}$	0.985	0.981	0.979	0.978	0.985
$[CO_{3_{\text{tot}}}]_{\text{container}}$ (mmol/L)	3.16	3.32	3.46	4.69	3.54
$[CO_{3_{\text{tot}}}]_{\text{sample}}$ (mmol/L)	6.76	6.55	7.32	10.28	6.36
Test conditions					
$g(t_{\text{test}})$	1.0007	1.0007	1.0007	1.0007	1.0007
$[CO_{3_{\text{tot}}}(t_{\text{test}})]$ (mmol/L)	6.77	6.56	7.33	10.3	6.37
$\epsilon(t_{\text{test}})$	81.66	81.66	81.66	81.66	81.66
$A(t_{\text{test}})$	0.5	0.5	0.5	0.5	0.5
$J(t_{\text{test}})$ (mmol/L)	296.39	292.84	300.99	299.95	295.97
$\gamma_1(t_{\text{test}})$	0.701	0.702	0.7	0.7	0.701
$\gamma_2(t_{\text{test}})$	0.241	0.242	0.24	0.24	0.241
$K_1(t_{\text{test}})$ ($\times 10^{7}$)	3.912	3.912	3.912	3.912	3.912
$K_2(t_{\text{test}})$ ($\times 10^{11}$)	3.861	3.861	3.861	3.861	3.861
pH (during the test)	1.88	1.87	1.86	1.86	1.86
d_{32}	0.99996	0.99996	0.99996	0.99996	0.99996
$[CO_2(t_{\text{test}})]$ (mmol/L)	6.77	6.56	7.33	10.3	6.37

sample	**B15**	**B16**	**B17**	**B18**	**B19**
sampling time (s)	900	1 200	1 500	1 800	2 100
t_{test} (°C)	16.5	16.5	16.6	16.5	16.6
$t_{\text{titration}}$ (°C)	25	25	26.6	25.4	25
V_{sample} (mL)	24.64	24.19	24.05	24.37	24.29
titrant used	NaOH	NaOH	NaOH	NaOH	NaOH
n_{H^+}/n_{OH^-} added (mmol)	179.69	221.3	181.03	172.54	139.87
$V_{\text{container}}$ (mL)	50.79	51.09	51.75	51.97	50.19
$[H^+_{\text{added}}]/[OH^-_{\text{added}}]$ (mmol/L)	3.54	4.33	3.5	3.32	2.79
conductivity (25°C) (μs/cm)	15 350	15 300	15 200	15 200	15 060
pH (before the titration)	1.85	1.87	1.86	1.9	1.96
Titration conditions					
g($t_{\text{titration}}$)	0.9989	0.9989	0.9984	0.9988	0.9989
$[OH_{\text{tot}}$ ($t_{\text{titration}}$)] (mol/L)	55.35	55.35	55.32	55.34	55.35
$\epsilon(t_{\text{titration}})$	78.54	78.54	77.96	78.4	78.54
$A(t_{\text{titration}})$	0.51	0.51	0.51	0.51	0.51
ρ(20°C) (ohm.cm)	65.2	65.4	65.9	65.9	66.5
J(20°C) (mmol/L)	294.1	293.05	290.97	290.97	288.05
$J(t_{\text{titration}})$ (mmol/L)	293.76	292.72	290.52	290.61	287.72
$\gamma_1(t_{\text{titration}})$	0.698	0.698	0.698	0.698	0.699
$\gamma_2(t_{\text{titration}})$	0.237	0.237	0.237	0.238	0.239
$K_0(t_{\text{titration}})$ ($\times 10^{16}$)	1.829	1.829	2.066	1.886	1.829
$K_1(t_{\text{titration}})$ ($\times 10^{7}$)	4.452	4.452	4.539	4.474	4.452
$K_2(t_{\text{titration}})$ ($\times 10^{11}$)	4.68	4.68	4.832	4.719	4.68
pH $_{\text{initial}}$	4.46	4.49	4.51	4.55	4.5
$f_{11\ \text{initial}}$	1	1	1	1	1
$f_{12\ \text{initial}}$	1.982	1.981	1.979	1.978	1.98
pH $_{\text{final}}$	8.3	8.36	8.28	8.41	8.23
$f_{11\ \text{final}}$	1	1	1	1	1
$f_{12\ \text{final}}$	0.981	0.976	0.982	0.972	0.986
$[CO_{3_{\text{tot}}}]_{\text{container}}$ (mmol/L)	3.48	4.26	3.46	3.26	2.76
$[CO_{3_{\text{tot}}}]_{\text{sample}}$ (mmol/L)	7.18	9	7.44	6.94	5.7
Test conditions					
g(t_{test})	1.0007	1.0007	1.0007	1.0007	1.0007
$[CO_{3_{\text{tot}}}(t_{\text{test}})]$ (mmol/L)	7.19	9.02	7.46	6.96	5.71
$\epsilon(t_{\text{test}})$	81.66	81.66	81.62	81.66	81.62
$A(t_{\text{test}})$	0.5	0.5	0.5	0.5	0.5
$J(t_{\text{test}})$ (mmol/L)	294.3	293.26	291.16	291.17	288.24
$\gamma_1(t_{\text{test}})$	0.701	0.702	0.702	0.702	0.703
$\gamma_2(t_{\text{test}})$	0.242	0.242	0.243	0.243	0.244
$K_1(t_{\text{test}})$ ($\times 10^{7}$)	3.912	3.912	3.919	3.912	3.919
$K_2(t_{\text{test}})$ ($\times 10^{11}$)	3.861	3.861	3.87	3.861	3.87
pH (during the test)	1.86	1.86	1.86	1.88	1.89
d_{32}	0.99996	0.99996	0.99996	0.99996	0.99996
$[CO_2(t_{\text{test}})]$ (mmol/L)	7.19	9.02	7.46	6.96	5.71

sample	**B20**	**B21**	**B22**	**B23**	**B24**
sampling time (s)	2 400	2 700	3 000	3 300	3 600
t_{test} (°C)	16.6	16.6	16.5	16.6	16.6
$t_{\text{titration}}$ (°C)	23.9	25	25.7	25	25
V_{sample} (mL)	24.33	23.66	23.89	22.52	24.46
titrant used	NaOH	NaOH	NaOH	NaOH	NaOH
n_{H^+}/n_{OH^-} added (mmol)	138.6	120.22	137.19	139.5	144.26
$V_{\text{container}}$ (mL)	50.23	47.66	48.84	46.16	49.96
$[H^+_{\text{added}}]/[OH^-_{\text{added}}]$ (mmol/L)	2.76	2.52	2.81	3.02	2.89
conductivity (25°C) (μs/cm)	15 090	14 980	14 900	14 870	14 850
pH (before the titration)	1.95	1.92	1.91	1.92	1.99
Titration conditions					
$g(t_{\text{titration}})$	0.9991	0.9989	0.9987	0.9989	0.9989
$[OH_{\text{tot}}\ (t_{\text{titration}})]$ (mol/L)	55.36	55.35	55.34	55.35	55.35
$\epsilon(t_{\text{titration}})$	78.94	78.54	78.29	78.54	78.54
$A(t_{\text{titration}})$	0.51	0.51	0.51	0.51	0.51
ρ(20°C) (ohm.cm)	66.3	66.8	67.2	67.3	67.4
J(20°C) (mmol/L)	288.68	286.38	284.72	284.09	283.68
$J(t_{\text{titration}})$ (mmol/L)	288.42	286.05	284.34	283.77	283.35
$\gamma_1(t_{\text{titration}})$	0.699	0.7	0.7	0.7	0.7
$\gamma_2(t_{\text{titration}})$	0.239	0.239	0.24	0.24	0.24
$K_0(t_{\text{titration}})$ ($\times 10^{16}$)	1.68	1.829	1.93	1.829	1.829
$K_1(t_{\text{titration}})$ ($\times 10^{7}$)	4.389	4.452	4.49	4.452	4.452
$K_2(t_{\text{titration}})$ ($\times 10^{11}$)	4.575	4.68	4.747	4.68	4.68
pH $_{\text{initial}}$	4.5	4.31	4.42	4.43	4.45
$f_{11\ \text{initial}}$	1	1	1	1	1
$f_{12\ \text{initial}}$	1.981	1.987	1.983	1.983	1.982
pH $_{\text{final}}$	8.26	8.31	8.22	8.3	8.33
$f_{11\ \text{final}}$	1	1	1	1	1
$f_{12\ \text{final}}$	0.985	0.98	0.987	0.981	0.979
$[CO_{3_{\text{tot}}}]_{\text{container}}$ (mmol/L)	2.72	2.43	2.76	2.96	2.82
$[CO_{3_{\text{tot}}}]_{\text{sample}}$ (mmol/L)	5.62	4.9	5.65	6.07	5.77
Test conditions					
$g(t_{\text{test}})$	1.0007	1.0007	1.0007	1.0007	1.0007
$[CO_{3_{\text{tot}}}(t_{\text{test}})]$ (mmol/L)	5.63	4.91	5.66	6.08	5.78
$\epsilon(t_{\text{test}})$	81.62	81.62	81.66	81.62	81.62
$A(t_{\text{test}})$	0.5	0.5	0.5	0.5	0.5
$J(t_{\text{test}})$ (mmol/L)	288.87	286.58	284.91	284.28	283.87
$\gamma_1(t_{\text{test}})$	0.703	0.703	0.704	0.704	0.704
$\gamma_2(t_{\text{test}})$	0.244	0.244	0.245	0.245	0.245
$K_1(t_{\text{test}})$ ($\times 10^{7}$)	3.919	3.919	3.912	3.919	3.919
$K_2(t_{\text{test}})$ ($\times 10^{11}$)	3.87	3.87	3.861	3.87	3.87
pH (during the test)	1.89	1.89	1.89	1.89	1.9
d_{32}	0.99996	0.99996	0.99996	0.99996	0.99996
$[CO_2(t_{\text{test}})]$ (mmol/L)	5.63	4.91	5.66	6.08	5.78

8.6 Summary of test conditions and results

Table 14: Summary of the conditions and results of all the tests.

	September 2019 small scale	January 2020 small scale	June 2020 large scale
Conditions of the tests			
temperature tracer test (°C)	20.8	14.6	15.1
temperature O_2 test (°C)	23.8	16.2	15.4
temperature CO_2 test **A** (°C)	23.6	17.1	16.1
temperature CO_2 test **B** (°C)	23.6	16.3	16.5
water height (cm)	9.8	7	150
V_R (L)	267.1	408.9	78 400
V_A (L)	22	70.9	24 400
$V_{channel}$ (L)	245.1	338	54 000
Tracer tests			
t_c (s)	227	393	~ 20
t_A (s)	24	130	/
$t_{channel}$ (s)	203	263	/
O_2 transfer tests			
$(k_l a)_R$ outlet of the airlift (s^{-1})	$2.3 \times 10^{-3} \pm 1.3 \times 10^{-5}$	$1.8 \times 10^{-3} \pm 1.2 \times 10^{-5}$	$4.4 \times 10^{-4} \pm 1 \times 10^{-6}$
$(k_l a)_R$ inlet of the airlift (s^{-1})	$1.9 \times 10^{-3} \pm 1.5 \times 10^{-5}$	$1.6 \times 10^{-3} \pm 1.5 \times 10^{-5}$	$4.2 \times 10^{-4} \pm 2.8 \times 10^{-6}$
$(k_l a)_R$ mean (s^{-1})	$2.1 \times 10^{-3} \pm 2 \times 10^{-5}$	$1.7 \times 10^{-3} \pm 1.9 \times 10^{-5}$	$4.3 \times 10^{-4} \pm 3 \times 10^{-6}$
$(k_l a)_A$ model (s^{-1})	2.36×10^{-2}	6.6×10^{-3}	/
$(k_l a)_A$ Equation (3.15) (s^{-1})	2.65×10^{-2}	6.2×10^{-3}	/
$(k_l a)_A$ mean (s^{-1})	2.5×10^{-2}	6.4×10^{-3}	/
$(k_l a)_{channel}$ (s^{-1})	4.1×10^{-5}	8.4×10^{-4}	/
CO_2 transfer tests			
$(k_l a)_R$ test **A** (s^{-1})	/	$1 \times 10^{-3} \pm 1.2 \times 10^{-4}$	/
$(k_l a)_R$ test **B** (s^{-1})	$1.3 \times 10^{-3} \pm 2.1 \times 10^{-4}$	$1.2 \times 10^{-3} \pm 4.6 \times 10^{-4}$	$2.6 \times 10^{-4} \pm 1.4 \times 10^{-4}$
Ratios $(k_l a)_{CO_2} / (k_l a)_{O_2}$			
test **A**	/	0.58 ± 0.08	/
test **B**	0.64 ± 0.11	0.7 ± 0.28	0.6 ± 0.33